THE FRACTURE MECHANICS
OF
BI-MATERIAL SYSTEMS

by

Anuradha Banerjee

A thesis submitted for the degree of
Doctor of Philosophy
to the
Department of Mechanical Engineering
Faculty of Engineering, University of Glasgow

August 2003

ProQuest Number: 10391034

ProQuest 10391034

Acknowledgements

I would like to express sincere appreciation for my supervisor Prof. John Hancock. He has been a great source of inspiration and I am thankful for the encouragement, guidance and support that he has provided towards my development as a researcher. I have thoroughly enjoyed working with him and could not have asked for a more enriching experience. I am also grateful to the University of Glasgow for granting the financial support throughout the course of my study and making it possible.

I am indebted to my friends who made my stay in Glasgow a memorable experience. I will miss the regular lunch hour with Abdul and Puneet who spiced up the lunches with their wit and humour, the coffee meetings and 'muscle tone' sessions with Kate and Maria. It has been a pleasure sharing office with Niall, Moshiur and Feizal and knowing Kirsteen and Julian. I would specially like to thank Bostjan for his cooperation and the enjoyable discussions we had on fracture mechanics.

I would like to thank the administrative staff of the department and the faculty office. They have been most friendly and helpful. I would also like to thank the technical staff, in particular Alec Tory, for his help in conducting the experiments.

I am most appreciative of my husband, Rajesh, who has been a great source of strength. Without his love, inspiration, understanding and continual moral support it would have been impossible for me to undertake and complete this project.

Finally, I would like to dedicate this thesis to my parents who have always been there for me.

Contents

List of Figures

List of Tables

Summary

A stationary crack normal to the boundary between two elastically mismatched solids such that the crack tip is located at the interface is studied analytically and computationally. Eigenvalue expansions establish the first two terms of the asymptotic expansion of the plane strain elastic stress fields for mode I and mode II loading. The second order term was determined as a function of elastic mismatch for a thin cracked film on a substrate and for a thin cracked lamina between two substrates.

Elastic-plastic analysis was performed when one of the solids was fully elastic and the other solid was elastic perfectly-plastic. Analytic and numerical solutions of the asymptotic stress fields were developed in small strain yielding. The angular span at the crack tip was composed of elastic and plastic sectors. Analytic solution of the stresses in plastic sectors was based on slip line theory and the stresses in the elastic sectors were developed using solutions to semi-infinite problems. Numerical solutions obtained using boundary layer formulations were in close agreement with the analytic results. When the crack was located in plastic solid, the elastic solid ahead of the crack develops a logarithmic singularity. The effect of the T-stress on the extent of plasticity on the flanks is determined. Interest is mainly focussed on the case when the crack is in an elastic solid and the material ahead is elastic perfectly-plastic. Solutions are developed at different levels of elastic mismatch, mode mixity and T-stress. Mode I fields are identified to be parameterised by the constraint ahead of the crack tip which depends on the elastic mismatch and the T-stress. The effect of constraint on the competition between interface failure and penetration is discussed.

A crack located in an interfacial zone between two plastically dissimilar solids in which toughness and yield strength were assumed to interpolate linearly across the zone, has been studied both analytically and computationally. The problem is an idealisation of a crack in the heat affected zone between a weld and parent plate in which the mechanical properties are dependent on position or a crack in a solid subject to a non-uniform temperature field.

Due to the gradation in yield strength, even under a remote mode I load the plastic zone shapes are asymmetric about the crack plane resulting in a non-unity plastic mixity at the crack tip. Plane strain asymptotic stress fields under conditions of small scale yielding and non-hardening plasticity have been constructed by assembling elastic and plastic sectors using slip line theory. The numerical solutions using boundary layer formulations are in close agreement with the analytic solutions. From the asymptotic field under assumption of local homogeneity, higher plastic mismatch and compressive T-stress result in higher inclination of the crack extension plane towards the solid of higher yield strength. Failure is also modelled using a weakest link model which allows initiation of cleavage failure within the plastic zone and not necessarily at the crack tip. Mismatch in yield strength and toughness show opposing effects on the crack extension direction, the plastic mismatch favours crack initiation in the softer material while toughness mismatch favours crack initiation in less tough material.

Introduction

Thermal barrier, and wear resistant coatings successfully combine dissimilar materials so that the beneficial properties of the constituents complement each other. A ceramic coating deposited on a steel component significantly increases its thermal shock bearing capacity, allowing the operational temperatures and efficiencies of turbines and internal combustion engines to be increased. The effective combination of metal and ceramic in laminates also provides structures which have high strength (and stiffness) to weight ratios. Manufacturing processes, including soldering, welding and cladding also result in combinations of dissimilar materials. Failure of these systems often results from the failure of the interface between the solids. This may be caused by flaws or defects in the interface or in one of the solids and approaching the interface. Understanding the factors that influence the stress field of such cracks is fundamental to the design, development and life assessment of these composite systems. In the present work, the interest is focussed on a crack normal to the interface between mismatched solids and a crack located in a zone of graded toughness and yield strength.

The thesis starts with a review of elastic and plastic behaviour of materials followed by a summary of the literature in the development of single parameter and two parameter fracture mechanics for both linear elastic and elastic-plastic homogeneous solids. The key studies in the development of fracture mechanics in bi-material systems are then introduced.

In the case of a crack normal to the interface between mismatched solids, the effect of elastic mismatch, the non-singular term and the loading phase angle of the outer elastic field on the elastic plastic crack tip field is determined under plane strain contained yielding conditions. The work firstly establishes the asymptotic elastic field for a crack normal to the interface between mismatched solids. In contained yielding, the non-singular term of the

outer elastic field has been shown to determine the constraint of the homogeneous problem (Betegón and Hancock, 1991; Du and Hancock, 1991; O'Dowd and Shih, 1991) and affect the constraint for an interface crack (Kim et. al, 1997). In Chapter 4, the details of the elastic analysis are presented. The work of Cook and Erdogan (1972) and Chao et al. (1993) for a crack normal to the interface between mismatched solids has been extended by determining the second order term in the asymptotic expansion. The elastic field is then used in the modified boundary layer formulation to perform elastic-plastic analysis under small strain yielding. The work has focussed on the limiting case of plastic mismatch when one of the solids is elastic and the other is elastic-perfectly plastic. The analytic solution establishes the parameters that characterise the crack tip field following which the effect of elastic mismatch, geometric effects due to non-singular terms and loading phase angle on the characterising parameters is determined computationally.

In bi-material systems, interface failure between dissimilar solids may occur as a consequence of abrupt transitions in composition and properties across a well defined interface. To minimise these problems a class of materials known as functionally graded materials (FGMs) has been developed to minimise property mismatch effects by varying the composition gradually from one material to another in a controlled manner. In the interfacial zone of a ceramic-metal composite the composition can be varied by mixing ceramic and metal in different proportions such that the spatial change of properties from ceramic to metal is gradual which results in less severe thermal stress distributions (Choules and Kokini, 1996; Wetherhold et al., 1996). Surface treatments such as laser hardening, carburising or nitriding also induce changes in the composition at the surface which result in a spatial variation of physical properties. The surface being stronger than the substrate and thus more wear resistant.

A spatial variation in properties may also result from manufacturing processes such as welding and cladding. In welding, the thermal cycle results in a heat affected zone which

typically has a higher yield strength than the parent plate. As a result, the yield strength varies from the weld zone to the parent material in a continuous manner. Even homogeneous materials in non-uniform temperature fields may result in a spatial variation in mechanical properties as the yield strength is a function of the temperature. The work concentrates on a crack in an interfacial zone of uniform elastic modulus but graded yield strength. Chapter 7 first develops the plane strain asymptotic stress field in contained yielding both analytically and computationally, followed by a discussion using a statistical approach based on a weakest link analysis on the effect of gradient in yield strength and toughness on the failure probabilities and crack propagation direction.

Fundamental Concepts

The aim of fracture mechanics is to determine the effect of cracks and defects on the integrity and life of engineering structures. In order to establish a framework for the present work, the concepts of continuum mechanics are introduced. This includes the equilibrium equations, stress-strain relations, strain-displacement relations and yield criteria followed by a brief description of plane strain slip line theory. A review of some of the key developments in the application of fracture mechanics starts with the studies based on the assumption of a linear elastic response, the review subsequently develops the critical concepts in elastic-plastic fracture mechanics. The principles of single parameter characterisation are presented for both elastic and plastic crack tip fields with a discussion on their limitations. The recent developments in two-parameter fracture mechanics are then reviewed.

2.1 Constitutive relations

The theory of elastic deformation has been covered in many standard texts such as Timoshenko and Goodier (1970). In a continuum, the stress field gives a measure of the intensity of the internal forces that may arise from the applied surface and body forces. Consider an elemental volume in an orthogonal Cartesian co-ordinate system x_i ($i = 1, 2, 3$) as shown in Fig. 2.1. If an incremental force vector, ΔF_i, acts on an elemental area, ΔA_j, which has a surface normal, n_j, the stress tensor, σ_{ij}, is defined as:

$$\sigma_{ij} = \lim_{\Delta A_j \to 0} \frac{\Delta F_i}{\Delta A_j} \tag{2.1}$$

The complete stress state is described by 9 components. However, rotational equilibrium reduces the number of independent components as $\sigma_{ij} = \sigma_{ji}$. Within a body at equilibrium,

the stress-state may be non-uniform. To maintain equilibrium, every element within it must be in equilibrium under the action of the stresses on the element faces. Equilibrium in the x_i $(i = 1, 2, 3)$ directions is ensured by:

$$\frac{\partial \sigma_{ij}}{\partial x_j} + X_j = 0 \tag{2.2}$$

where, X_j $(j = 1, 2, 3)$ are body forces per unit volume in the Cartesian directions.

Strain is essentially a geometric quantity which depends on the relative displacements of points within a material. For small deformations, the strain components are related to the displacements by the strain-displacement equations:

$$\epsilon_{ij} = \frac{1}{2} \left(\frac{\partial u_i}{\partial x_j} + \frac{\partial u_j}{\partial x_i} \right) \tag{2.3}$$

where, u_i are the components of the displacement vector. Shear strain may be quantified by the tensor definition given in Eq. 2.3, or by an engineering definition in which $\gamma_{ij} = 2\,\epsilon_{ij}$; $(i \neq j)$. The rigid body rotation is:

$$\omega_{ij} = \frac{1}{2} \left(\frac{\partial u_i}{\partial x_j} - \frac{\partial u_j}{\partial x_i} \right) \tag{2.4}$$

The strain-displacement relations express the strains in terms of displacements u_i which gives rise to a set of relations between the strain components. These relations can be established by eliminating the displacements from the 6 strain-displacement equations to develop compatibility relations which have two forms:

$$\frac{\partial^2 \epsilon_{11}}{\partial x_2^2} + \frac{\partial^2 \epsilon_{22}}{\partial x_1^2} = 2 \frac{\partial^2 \epsilon_{12}}{\partial x_1 \partial x_2}, \cdots \cdots \tag{2.5}$$

$$\frac{\partial^2 \epsilon_{11}}{\partial x_2 \partial x_3} = \frac{\partial}{\partial x_1} \left(-\frac{\partial \epsilon_{23}}{\partial x_1} + \frac{\partial \epsilon_{13}}{\partial x_2} - \frac{\partial \epsilon_{12}}{\partial x_3} \right), \cdots \cdots \tag{2.6}$$

The compatibility relations ensure the existence of a unique displacement field related to the strain components. Physically these relations mean that the body remains connected after straining and material is neither created nor destroyed. For a linear elastic, isotropic and homogeneous material the deformation is reversible and independent of the orientation of the body. The deformation is fully characterised by two independent constants Young's modulus, E, and Poisson's ratio, ν. The stresses and the strains for such a material are related by Hooke's law :

$$\epsilon_{ij} = \frac{1}{E}\left[(1+\nu)\sigma_{ij} - \nu\delta_{ij}\sigma_{kk}\right] \tag{2.7}$$

where, δ_{ij} is Kronecker's delta. In the solution of two-dimensional problems, it is convenient to define a stress function, Φ, which is related to the stress field by:

$$\sigma_{11} = \frac{\partial^2 \Phi}{\partial x_2^2} \tag{2.8}$$

$$\sigma_{22} = \frac{\partial^2 \Phi}{\partial x_1^2} \tag{2.9}$$

$$\sigma_{12} = -\frac{\partial^2 \Phi}{\partial x_1 \partial x_2} \tag{2.10}$$

On substituting the stresses in terms of the stress function, the governing equations reduce to the bi-harmonic equation:

$$\nabla^4 \Phi = 0 \tag{2.11}$$

Since the bi-harmonic equation satisfies the equilibrium equations, compatibility equations, its solution with appropriate boundary conditions gives the complete state of stress field.

In uniaxial tension, the material behaviour changes at the yield point, beyond which irreversible non-linear behaviour is exhibited. In uniaxial tension the limit is defined as the yield stress, σ_o, which is a material property.

2.1.1 Yield criteria

The theory of plasticity has been developed in standard text books such as Hill (1950). For a general state of stress the onset of plastic flow is described by a yield criterion which is a function of the invariants of the deviatoric stress tensor, J_2 and J_3, defined as:

$$J_2 = \frac{1}{2} s_{ij} s_{ij} \tag{2.12}$$

$$J_3 = \frac{1}{2} s_{ij} s_{jk} s_{ki} \tag{2.13}$$

where, $s_{ij} = \sigma_{ij} - \delta_{ij} \sigma_{kk}/3$ are the stress deviators. The two most widely used criteria in metals are the Tresca and von Mises yield criterion (Hill, 1950). If σ_1, σ_2 and σ_3 are the principal stresses such that $\sigma_1 > \sigma_2 > \sigma_3$, the Tresca yield criterion suggests yielding occurs when the maximum shear stress, τ_{max}, developed in the material reaches a critical value:

$$\tau_{max} = \frac{\sigma_1 - \sigma_3}{2} = \frac{\sigma_o}{2} \tag{2.14}$$

The disadvantage of using Tresca criterion is that it requires a knowledge of the maximum and the minimum principal stresses. The von Mises yield criterion suggests that yielding occurs when J_2 attains a critical value which can be expressed either in terms of the yield stress in uni-axial tension, σ_o, or the yield stress in shear, k:

$$\frac{1}{2} s_{ij} s_{ij} = k^2 = \frac{\sigma_o^2}{3} \tag{2.15}$$

2.1.2 Stress-strain relation in the plastic range

To relate the stresses and strains during plastic deformation, it is convenient to introduce an equivalent stress, $\overline{\sigma}_e$, and the equivalent plastic strain increment, $\overline{d\epsilon}^p$:

$$\overline{\sigma}_e = \sqrt{\frac{3}{2} s_{ij} s_{ij}} \tag{2.16}$$

$$\overline{d\epsilon}^p = \sqrt{\frac{2}{3}d\epsilon_{ij}^p d\epsilon_{ij}^p} \tag{2.17}$$

The plastic stress-strain relation can be derived from a plastic potential, $g(J_2, J_3)$, which defines the ratios of components of the plastic strain increment by a flow rule:

$$d\epsilon_{ij}^p = d\lambda \frac{\partial g}{\partial \sigma_{ij}} \tag{2.18}$$

where, $d\lambda$ is a positive scalar. For the plastic potential, $g = J_2 = s_{ij}s_{ij}/2$, the associated flow rule gives the increment of plastic strains:

$$d\epsilon_{ij}^p = d\lambda s_{ij} \tag{2.19}$$

where, $d\lambda = 3\overline{d\epsilon}^p/2\overline{\sigma}_e$. Thus, the total strain increment which has elastic and plastic components can be expressed as:

$$\begin{aligned} d\epsilon_{ij} &= d\epsilon_{ij}^e + d\epsilon_{ij}^p \\ &= \frac{1}{E}\left[(1+\nu)d\sigma_{ij} - \nu\delta_{ij}d\sigma_{kk}\right] + d\lambda\left(\sigma_{ij} - \frac{1}{3}\sigma_{kk}\delta_{ij}\right) \end{aligned} \tag{2.20}$$

The elastic increments depend only on the stress increments while the plastic strain increments depend on the entire stress-strain path.

2.1.3　Slip line fields

Metal forming processes such as rolling or drawing involve extensive plastic flow. In such situations it is reasonable to neglect the elastic component of the total strain and assume the material to be rigid perfectly-plastic. Rigidity implies zero elastic strains and perfect-plasticity implies the absence of strain or work hardening. Slip line theory has been extensively used for solving this class of problems under plane strain and plane stress conditions

(Hill, 1950). More recently it has been used to describe the crack tip fields in elastic-plastic fracture mechanics (Rice, 1968; McClintock, 1971).

The theory can be developed from the basic governing equations: equilibrium equation, plastic stress-strain relations and the yield criterion in both plane strain and plane stress. Right handed Cartesian axes x, y, z, are used and interest is focussed on plane strain in the z-direction which requires that $\epsilon_{xz} = \epsilon_{yz} = \epsilon_{zz} = \sigma_{xz} = \sigma_{yz} = 0$, and that all the stress and strain components are independent of z, implying $\frac{\partial}{\partial z} = 0$. The equilibrium equations subsequently reduce to:

$$\frac{\partial \sigma_{xx}}{\partial x} + \frac{\partial \sigma_{xy}}{\partial y} = 0 \tag{2.21}$$

$$\frac{\partial \sigma_{xy}}{\partial x} + \frac{\partial \sigma_{yy}}{\partial y} = 0 \tag{2.22}$$

Neglecting the elastic strain components, and using the plane strain condition $\mathrm{d}\epsilon^p_{zz} = 0$ in the plastic stress-strain relations gives:

$$\sigma_{zz} = \frac{1}{2}(\sigma_{xx} + \sigma_{yy}) \tag{2.23}$$

The out-of-plane stress, σ_{zz}, is necessarily a principal stress since $\sigma_{xz} = \sigma_{yz} = 0$. In plane strain under incompressible deformation, the von Mises yield criterion for plane strain reduces to:

$$\frac{1}{4}(\sigma_{xx} - \sigma_{yy})^2 + \sigma^2_{xy} = k^2 \tag{2.24}$$

where, k is the yield stress in shear. The stress state in a material in yield can be described graphically using Mohr's circle as illustrated in Fig. 2.2. The orientation of the plane of maximum principal stress , σ_1, is defined by an angle taken anti-clockwise from x-axis, and denoted ϕ. There are two planes where the magnitude of shear stress is maximum, the first

plane is inclined at $45°$ clockwise from the the plane of maximum principal stress and the second is at $90°$ anti-clockwise from the first shear plane. The orientation of the planes of maximum and minimum shear stress define a set of curvilinear axes denoted $\alpha - \beta$ such that the principal stresses lie in the first and third quadrants of the $\alpha - \beta$ axes. The slip lines comprise two orthogonal families of curves whose tangent at every point coincides with the orientation of the planes of maximum shear. The curves along the first shear plane are termed α-lines while in the second shear plane, β-lines, as illustrated in Fig. 2.3.

Mohr's circle (Fig. 2.2) allows the principal stresses to be expressed in terms of the mean or hydrostatic stress, $\sigma_m = \frac{\sigma_{kk}}{3}$:

$$\sigma_1 = \sigma_m + k$$
$$\sigma_2 = \sigma_m \tag{2.25}$$
$$\sigma_3 = \sigma_m - k$$

Also,

$$\tan 2\phi = \frac{2\sigma_{xy}}{(\sigma_{xx} - \sigma_{yy})} \tag{2.26}$$

$$\tan 2\theta' = \frac{(\sigma_{yy} - \sigma_{xx})}{2\sigma_{xy}} \tag{2.27}$$

where, θ' is the angle made by the first shear line with the x-axis. The stresses expressed in $\alpha - \beta$ axes adopt a simple form:

$$\sigma_{\alpha\alpha} = \sigma_{\beta\beta} = \sigma_m \tag{2.28}$$

$$\sigma_{\alpha\beta} = \pm k \tag{2.29}$$

The state of stress in Cartesian co-ordinates then can be expressed in terms of two independent quantities, σ_m and θ' as:

$$\sigma_{xx} = \sigma_m - k \sin 2\theta'$$
$$\sigma_{yy} = \sigma_m + k \sin 2\theta' \tag{2.30}$$
$$\sigma_{xy} = k \cos 2\theta'$$

In curvilinear $(\alpha - \beta)$ axes the equilibrium equations reduce to a simple form known as Hencky's equations (Hill, 1950):

$$\frac{\sigma_m}{2k} - \theta' = C_1 \text{ along the } \alpha \text{ curve} \tag{2.31}$$

$$\frac{\sigma_m}{2k} + \theta' = C_2 \text{ along the } \beta \text{ curve} \tag{2.32}$$

Two common plane strain slip lines are fields illustrated in Fig. 2.4. Fig. 2.4(a) shows a constant stress region comprising orthogonal straight lines. Along the straight α and β lines, the angle (θ') remains constant and Hencky's equations indicate that σ_m remains constant, representing a uniform stress field. Fig. 2.4(b) shows a centred fan, which has straight radial lines and concentric circular arcs. The angle (θ') along the radial lines is constant, but along the arcs the angle varies linearly with the polar angle (θ). Therefore, σ_m is constant along the radial lines but varies linearly with the distance along the arcs.

While Hencky's equation ensure equilibrium in the curvilinear co-ordinates, the compatibility of displacements is secured by Geiringer's equations (Hill, 1950):

$$du - vd\theta' = 0$$
$$dv - ud\theta' = 0 \tag{2.33}$$

where u and v are the displacements along the α and β axes.

2.2   Single parameter fracture mechanics

Fracture mechanics is founded on the energetics of crack advance and the characterisation of asymptotic crack tip fields. In this section, the energy balance approach of Griffiths (1920) and eigenvalue expansion method developed by Williams (1957) are introduced. This establishes a basis for fracture mechanics using the stress intensity factor (K) for largely linear elastic materials. Finally, the development of the crack tip opening displacement and J-integral (J) is introduced to deal with non-linear response.

2.2.1   The energy criterion

The energetics of crack extension were developed by Griffiths (1920) who considered a through thickness plane stress crack in an infinitely wide plate Fig. 2.5. Griffiths postulated that the extension of the crack is accompanied by a reduction in the potential energy of the system. The crack extends only when the decrease in potential energy due to crack growth is greater or equal to the energy required to create the crack surfaces such that:

$$-\frac{d\Pi}{dA} \geq \frac{dW_s}{dA}$$
(2.34)

where, Π is the potential energy of the system and W_s is the work required to create new surfaces. For the crack shown in Fig. 2.5 the potential energy is given by:

$$\Pi = \Pi_o - \frac{\pi \sigma^2 a^2 B}{E'}$$
(2.35)

where $E' = E$ for plane stress and for plane strain $E' = E/(1 - \nu^2)$ and Π_o is the potential energy of the uncracked plate and B is the thickness of the plate.

$$W_s = 4aB\gamma_s$$
(2.36)

γ_s being the surface energy of the material. Substituting in Eq. 2.35 the fracture stress is obtained as:

$$\sigma_f = \left[\frac{2E'\gamma_s}{\pi a}\right]^{\frac{1}{2}} \tag{2.37}$$

Irwin (1957) introduced the concept of the potential energy release rate, G, within the context of energy balance approach:

$$G = -\frac{d\Pi}{dA} \tag{2.38}$$

such that crack extends when

$$G \geq G_c \tag{2.39}$$

The critical potential energy, G_c, is a material property which defines the resistance to crack propagation, or toughness, of the material. For a crack extending under fixed displacements at the boundary the force-displacement diagram is shown in Fig. 2.6(b) where P and Δ denote the force load and extension. The compliance of the system, C, is defined as:

$$C = \frac{\Delta}{P} \tag{2.40}$$

The change in potential energy of the system due to crack extension under fixed displacement condition is given by:

$$d\Pi = \frac{1}{2}P\Delta - \frac{1}{2}P_o\Delta = \frac{1}{2}\Delta dP \tag{2.41}$$

$$\frac{d\Pi}{da}\Big|_\Delta = \frac{\Delta}{2}\frac{dP}{da}\Big|_\Delta \tag{2.42}$$

Using Eq. 2.40:

$$\frac{dP}{da}\Big|_\Delta = -\frac{\Delta}{C^2}\frac{dC}{da}\Big|_\Delta \tag{2.43}$$

implying,

$$\frac{d\Pi}{da}\Big|_{\Delta} = -\frac{\Delta^2}{C^2}\frac{dC}{da}\Big|_{\Delta} = -\frac{P^2}{2}\frac{dC}{da}\Big|_{\Delta} \tag{2.44}$$

For a system subjected to a constant load, the force-displacement diagram is as shown in Fig. 2.6(a). The change in potential energy due to crack extension under constant load is given by:

$$d\Pi = \frac{1}{2}P\Delta_f - \frac{1}{2}P\Delta_o - P(\Delta_f - \Delta_o) = -\frac{1}{2}Pd\Delta \tag{2.45}$$

$$\frac{d\Pi}{da}\Big|_{P} = -\frac{P}{2}\frac{d\Delta}{da}\Big|_{P} \tag{2.46}$$

From Eq. 2.40:

$$\frac{d\Delta}{da}\Big|_{P} = P\frac{dC}{da}\Big|_{P} \tag{2.47}$$

Substituting in Eq. 2.46:

$$\frac{d\Pi}{da}\Big|_{P} = -\frac{P^2}{2}\frac{dC}{da}\Big|_{P} \tag{2.48}$$

Since compliance C is a geometric property $\frac{dC}{da}\Big|_{\Delta} = \frac{dC}{da}\Big|_{P}$. Therefore, the rate of change in potential energy due to crack extension is the same regardless of whether extension occurs under constant load or displacement. The energy release rate can be determined from compliance measurements.

2.2.2 Asymptotic fields at the crack tip

In order to determine the stress field near the tip of a crack in a homogeneous, isotropic, elastic solid Williams (1957) assumed a variable separable form of the stress function as the

solution of the bi-harmonic equation, Eq. 2.11. If Cartesian and polar co-ordinate systems are located at the crack tip such that the crack is along the negative x-axis as shown in Fig. 2.7, the stress function is assumed to be of the form:

$$\Phi(r,\theta) = r^{\lambda+1}F(\theta) \tag{2.49}$$

where, $F(\theta) = [A\sin(\lambda+1)\theta + B\cos(\lambda+1)\theta + C\sin(\lambda-1)\theta + D\cos(\lambda-1)\theta]$ and A, B, C and D are constants which depend on λ and the type of loading. Traction free crack flanks require the boundary conditions are:

$$\sigma_{\theta\theta}(\pi) = 0$$
$$\sigma_{r\theta}(\pi) = 0$$

$$\tag{2.50}$$

$$\sigma_{\theta\theta}(-\pi) = 0$$
$$\sigma_{r\theta}(-\pi) = 0$$

These conditions give rise to a set of 4 homogeneous equations:

$$\begin{bmatrix} \sin\pi\lambda & \cos\pi\lambda & \sin\pi\lambda & \cos\pi\lambda \\ -\sin\pi\lambda & \cos\pi\lambda & -\sin\pi\lambda & \cos\pi\lambda \\ (\lambda+1)\cos\pi\lambda & -(\lambda+1)\sin\pi\lambda & (\lambda-1)\cos\pi\lambda & -(\lambda-1)\sin\pi\lambda \\ (\lambda+1)\cos\pi\lambda & +(\lambda+1)\sin\pi\lambda & (\lambda-1)\cos\pi\lambda & +(\lambda-1)\sin\pi\lambda \end{bmatrix} \begin{bmatrix} A \\ B \\ C \\ D \end{bmatrix} = 0 \tag{2.51}$$

The condition for a non-trivial solution of these homogeneous equations gives rise to the eigen-equation:

$$\sin 2\lambda\pi = 0 \tag{2.52}$$

A series of eigenvalues (λ) are obtained from the solution of the eigen-equation. For finite strain energy density around the crack tip only the positive roots are considered such that $\lambda = n/2, n = 1, 2, 3 \cdots$. The crack tip stress field is thus an asymptotic expansion:

$$\sigma_{ij} = C_a r^{-\frac{1}{2}} a_{ij}(\theta) + C_b r^0 b_{ij}(\theta) + C_c r^{\frac{1}{2}} c_{ij}(\theta) + \cdots \tag{2.53}$$

where, C_a, C_b, $C_c \cdots$ are the intensities and $a_{ij}(\theta)$, $b_{ij}(\theta)$, $c_{ij}(\theta) \cdots$ angular functions of the terms. Linear elastic fracture mechanics is based on the leading term in the expansion which is singular in r. Higher order terms are ignored as they either vanish or become finite at the crack tip ($r \rightarrow 0$). This allows the asymptotic stress field to be expressed as:

$$\sigma_{ij} = \frac{K}{\sqrt{2\pi r}} \tilde{\sigma}_{ij}(\theta) \tag{2.54}$$

where $\tilde{\sigma}_{ij}(\theta)$ are angular functions and K is the stress intensity factor which is a function of the load and geometry. Three different modes of fracture: opening, shearing and tearing denoted by mode I, mode II and mode III are shown in Fig. 2.8. In general a crack may be subjected to a combination of these modes. The stress field is then a superposition of the individual contribution from each type of loading:

$$\sigma_{ij} = \frac{K_I}{\sqrt{2\pi r}} \tilde{\sigma}_{ij}^I(\theta) + \frac{K_{II}}{\sqrt{2\pi r}} \tilde{\sigma}_{ij}^{II}(\theta) + \frac{K_{III}}{\sqrt{2\pi r}} \tilde{\sigma}_{ij}^{III}(\theta) \tag{2.55}$$

In the present work, the interest is focused on mode I and mode II failure modes. The leading terms of stresses under mixed mode (I/II) loading are:

$$[\sigma] = \frac{K_I}{\sqrt{2\pi r}} \cos \frac{\theta}{2} \begin{bmatrix} 1 - \sin \frac{\theta}{2} \sin \frac{3\theta}{2} & \sin \frac{\theta}{2} \cos \frac{3\theta}{2} \\ \sin \frac{\theta}{2} \cos \frac{3\theta}{2} & 1 + \sin \frac{\theta}{2} \sin \frac{3\theta}{2} \end{bmatrix}$$

$$+\frac{K_{II}}{\sqrt{2\pi r}}\begin{bmatrix} \sin\frac{\theta}{2}\left[2+\cos\frac{\theta}{2}\cos\frac{3\theta}{2}\right] & \cos\frac{\theta}{2}\left[1-\sin\frac{\theta}{2}\sin\frac{3\theta}{2}\right] \\ \cos\frac{\theta}{2}\left[1-\sin\frac{\theta}{2}\sin\frac{3\theta}{2}\right] & \sin\frac{\theta}{2}\cos\frac{\theta}{2}\cos\frac{3\theta}{2} \end{bmatrix} \qquad (2.56)$$

For a mode I crack, the stress intensity factor is related to the energy release rate by the relation:

$$G = \frac{K_I^2}{E'} \qquad (2.57)$$

where $E' = E$ for plane stress and for plane strain $E' = E/(1 - \nu^2)$. A dimensional argument shows that the stress intensity factor can be expressed as a function of the remote stress, σ^∞, and a characteristic dimension of the cracked body such as the crack length, a:

$$K = K_o \sigma^\infty \sqrt{\pi a} \qquad (2.58)$$

where K_o is a non-dimensional function of geometry. A wide range of stress intensity factors have been determined and tabulated by Rooke and Cartwright (1976) and Murakami (1987). Since the stress intensity factor describes the stress field completely a failure is taken to occur when:

$$K \geq K_c \qquad (2.59)$$

where K_c is the critical value of K. The toughness (K_c) decreases with increasing thickness and saturates to a minimum for large thicknesses where plane strain conditions apply (Irwin et. al, 1958). The critical stress intensity factor under plane strain, K_{Ic}, is referred to as the fracture toughness of the material. For ferritic steels K_{Ic} and the fracture mode depend on temperature as shown qualitatively in Fig. 2.9 (Ritchie et. al, 1973). At high temperatures the failure occurs as a result of void growth and coalescence and mode of failure is ductile

tearing. In ductile tearing there is stable crack growth and considerable plastic deformation. For lower temperatures, the crack initially grows in a ductile manner followed by rapid crack growth by cleavage failure. At low temperatures the mode of failure is cleavage. Cleavage fracture is a low energy failure mode involving the separation of crystallographic planes that results in rapid transgranular crack growth, thus considered most dangerous mode of failure. An important feature of cleavage failure is the scatter in the experimental data, which may be explained by the fact that the micro-structure of real materials is not homogeneous and that microcracks or defects are distributed throughout the material. A statistical model based on a weakest link approach has been reviewed later in Chapter 7 before developing the model for materials which have graded properties. In Fig. 2.9 with increasing temperature the mode of failure changes from cleavage to ductile tearing correspondingly the toughness increases, implying increase in resistance to crack growth. At low temperatures the plasticity is small enough for the failure process to be described under assumption of linear elasticity (LEFM).

The plastic zone is a function of the applied load and yield stress. The Mises stress near the crack tip has a square root singularity: $\sigma_{mises} \sim K/\sqrt{r}$. On the boundary of the plastic zone $r = r_y$, $\sigma_{mises} = \sigma_o$, where σ_o is the uniaxial yield stress. Implying:

$$\frac{K}{\sqrt{r_y}} \sim \sigma_o \tag{2.60}$$

$$r_y \sim \left(\frac{K}{\sigma_o}\right)^2 \tag{2.61}$$

Linear elastic fracture mechanics can be applied usefully as long as crack tip plasticity is a minor perturbation of a largely elastic stress field. This condition is ensured if the plastic zone size, r_y, is very small compared with any of the specimen dimensions: crack length, a, the width of the specimen, W, the remaining ligament, $W - a$ or the thickness B. The requirement given by ASTM (1983) are:

$$a \geq 2.5 \left(\frac{K_{Ic}}{\sigma_o}\right)^2$$

$$B \geq 2.5 \left(\frac{K_{Ic}}{\sigma_o} \right)^2 \tag{2.62}$$

$$W \geq 5.0 \left(\frac{K_{Ic}}{\sigma_o} \right)^2$$

where, σ_o is the uniaxial yield stress. Under conditions of appreciable crack tip plasticity compared to the specimen dimensions as prescribed in Eq. 2.63, characterisation through the stress intensity factor is no longer valid. This problem is addressed by elastic-plastic fracture mechanics which extends the applicability of fracture mechanics by including a non-linear response. The parameters which have been widely used to describe elastic-plastic crack tip fields and toughness are the crack tip opening displacement (CTOD) and J-integral.

2.2.3   Crack tip opening displacement: CTOD

Wells (1961) observed that plastic deformation caused the crack tip to blunt prior to fracture. The degree of crack blunting prior to crack extension increased with the toughness of the material. This led to a proposal that the crack tip opening could be used as a measure of toughness. In the limit of small scale yielding the CTOD can be related to the stress intensity factor. In plane stress conditions the plastic zone radius is given by:

$$r_y = \frac{1}{2\pi} \left(\frac{K_I}{\sigma_o} \right)^2 \tag{2.63}$$

Irwin (1961) showed that crack tip plasticity makes the effective crack length $a_{eff} = a + r_y$. In this case the actual crack tip is located at a distance r_y distance behind the effective crack tip and the displacement normal to the crack flanks can be approximated as:

$$u_y = \left(\frac{\kappa + 1}{2\mu} \right) K_I \sqrt{\frac{r_y}{2\pi}} = \frac{4}{E} K_I \sqrt{\frac{r_y}{2\pi}} \tag{2.64}$$

The crack tip opening displacement, δ, can be related to the stress intensity factor, K, and energy release rate, G, as:

$$\delta = 2u_y = \frac{4K_I^2}{\sigma_o E} = \frac{4G}{\sigma_o} \qquad (2.65)$$

This relation is based on a plane stress state and non-hardening plasticity, however, more generally:

$$\delta = \frac{K_I^2}{m\sigma_o E'} = \frac{G}{m\sigma_o} \qquad (2.66)$$

where, m is a dimensionless constant that depends on the state of stress. In numerical studies the crack tip opening displacement is taken to be the vertical displacement between the points where a 90 degree angle intercepts the crack flanks (Kumar et. al, 1981).

2.2.4 J-integral

For a crack in a non-linear elastic solid Rice (1968a) identified a path independent line integral referred as the J-integral:

$$J = \int_\Gamma W \, dy - \left[P_x \frac{\partial u_x}{\partial x} + P_y \frac{\partial u_y}{\partial y} \right] ds \qquad (2.67)$$

where Γ is an arbitrary contour surrounding the crack tip. In the first term, $W = \int \sigma_{ij} d\epsilon_{ij}$ is the strain energy density. The second term in Eq. 2.67 is the work done by the traction at the boundary, traction and displacement vectors at the boundary being P and u. The J-integral is path independent and under non-linear elastic conditions it quantifies the potential energy release rate as the crack advances:

$$J = -\frac{d\Pi}{dA} \qquad (2.68)$$

where Π is the potential energy and A is the crack area. Consider a crack in a non-linear elastic solid such that the stress-strain relation is described by the Ramberg-Osgood equation:

$$\frac{\epsilon}{\epsilon_o} = \frac{\sigma}{\sigma_o} + \alpha \left(\frac{\sigma}{\sigma_o} \right)^n \tag{2.69}$$

where, ϵ_o, σ_o and α are material constants and n is the strain hardening exponent. The first term in Eq. 2.69 is the elastic component of the total strain. At the crack tip the plastic strains are much larger compared to the elastic strains. Ignoring the elastic component the stress-strain reduces the relation to a power law: $\epsilon/\epsilon_o = \alpha(\sigma/\sigma_o)^n$. Hutchinson (1968a) and Rice and Rosengren (1968) (HRR henceforth) demonstrate that the leading term of the asymptotic stress and strain fields for a crack in a non-linear elastic solid are characterised through J:

$$\sigma_{ij} = \sigma_o \left[\frac{J}{\epsilon_o \sigma_o \alpha I_n r} \right]^{\frac{1}{1+n}} \tilde{\sigma}_{ij}(\theta, n) \tag{2.70}$$

$$\epsilon_{ij} = \frac{\sigma_o \alpha}{E} \left[\frac{J}{\epsilon_o \sigma_o \alpha I_n r} \right]^{\frac{n}{1+n}} \tilde{\epsilon}_{ij}(\theta, n) \tag{2.71}$$

where, I_n is an integration constant that depends on n and $\tilde{\sigma}_{ij}(\theta, n)$ and $\tilde{\epsilon}_{ij}(\theta, n)$ are non-dimensional angular functions tabulated by Shih (1983). The J-integral and the crack tip opening are uniquely related to each other by the relation (Shih, 1981):

$$\delta = \frac{d_n J}{\sigma_o} \tag{2.72}$$

where, d_n is a constant which has a strong dependence on the strain hardening exponent and it also depends weakly on $\alpha \sigma_o / E$. Both J and CTOD have been used widely to characterise the stress field in elastic-plastic fracture mechanics. The HRR field is a small geometry change solution which does not take into account the effects of finite geometry changes associated with crack tip blunting. McMeeking and Parks (1979) established that the blunting effect vanishes for distances greater than 2δ. Thus, at distances when $r < \frac{2J}{\sigma_o}$ use of the HRR

field is inaccurate. The ability of a single parameter, such as J, δ or K, to characterise the elastic-plastic crack tip field is limited. McClintock (1968) showed that cracks in different geometries under mode I loading can have completely different plane strain slip line fields. Figs. 2.10-2.13 show the mode I slip line fields of a centre-cracked panel, deep and shallow cracked bars and Prandtl field for deeply double edge cracked bar. These fields show that the slip line fields are not unique and depend on geometry as well requiring two parameter representation. Shih and German (1981) proposed a criterion for identifying J-dominant fields: the stress field at a distance $r\sigma_o/J = 2$ ahead of a crack tip must be within 10 percent of the HRR field. J-dominance can be expressed through a controlling parameter c that has dimensions of length such that for single parameter representation:

$$c > \frac{\mu J}{\sigma_o} \tag{2.73}$$

where, μ is a non-dimensional constant. For deeply cracked plane strain centre cracked panels, the controlling parameter is the width of the uncracked ligament and μ is approximately 200. In bars with deeply cracked edge, the controlling parameter is again the uncracked ligament width and $\mu = 25$. In the case of shallow edge cracked bars the controlling parameter is the crack length and J-dominance is valid when $a > 200\ J/\sigma_o$. To incorporate the effect of geometry in the local stress field two parameter fracture mechanics is required. The effect of geometry is expressed through the T-stress of the elastic field or the Q-parameter of the elastic-plastic field.

2.3   Two parameter fracture mechanics

2.3.1 T-stress

The second order term in Williams expansion for the homogeneous crack tip field is independent of distance and corresponds to a uni-axial stress, parallel to the crack flanks such

that in the Cartesian co-ordinates the field can be expressed as:

$$[\sigma] = \frac{K}{\sqrt{2\pi r}}[\tilde{\sigma}](\theta) + T\begin{bmatrix} 1 & 0 \\ 0 & 0 \end{bmatrix} + \text{higher order terms} \qquad (2.74)$$

where, T has the dimensions of stress and depends on the remote load and geometry. The other higher order terms in the Williams expansion tend to zero at the crack tip. On the crack flanks, $\theta = \pm\pi$ plane, the angular function $\tilde{\sigma}_{11}(\pm\pi) = 0$, which allows the T-stress to be evaluated directly from finite element analysis as:

$$T = \lim_{r \to 0} \sigma_{11}(r, \theta = \pi) \qquad (2.75)$$

The T-stress can also be expressed in terms of a bi-axiality parameter $\beta = T\sqrt{\pi a}/K$. The T-stress has been determined for a range of geometries and tabulated by Leevers and Radon (1983), Sham (1991), Sherry et. al (1995). Larsson and Carlsson (1975) demonstrated that the T-stress affects the shape and size of plastic zone that develops near the crack tip, as illustrated in Fig. 2.14 following Du and Hancock (1991). Compressive T-stresses increase the plastic zone size and swing the plastic zone forward while tensile T-stresses decrease the plastic zone size and swing it backwards to the flanks. Bilby et. al (1986) and Betegón and Hancock (1991) using finite element analysis showed the effect of the non-singular term on the elastic-plastic crack tip field for a range of finite specimens. For negative T, the crack tip stresses are less than the HRR solution which is within 5 percent of small scale yielding ($T = 0$), necessitating the introduction of a second parameter in the stress equation which depends on the T of the outer field. On the plane ahead of the crack tip the hoop stress is (Betegón and Hancock, 1991):

$$\frac{\sigma_{\theta\theta}(r, T)}{\sigma_o} - \frac{\sigma_{\theta\theta}(r, T = 0)}{\sigma_o} + 0.64\left(\frac{T}{\sigma_o}\right) - 0.4\left(\frac{T}{\sigma_o}\right)^2 \qquad n = 13, \ \frac{T}{\sigma_o} \le 0 \qquad (2.76)$$

$$\frac{\sigma_{\theta\theta}(r, T)}{\sigma_o} = \frac{\sigma_{\theta\theta}(r, T = 0)}{\sigma_o} + 0.6\left(\frac{T}{\sigma_o}\right) - 0.75\left(\frac{T}{\sigma_o}\right)^2 \qquad n = \infty, \ \frac{T}{\sigma_o} \le 0 \qquad (2.77)$$

For positive T the stresses approach the HRR field and a single parameter characterisation is valid, but for negative T a two parameter representation is required, to take into account the associated loss of constraint. Du and Hancock (1991) identified that in the asymptotic slip line field plasticity encompasses the crack tip only under conditions in which T is positive. When T is negative, there is incomplete plasticity at the crack tip as an elastic wedge appears at the crack flank and there is loss of constraint ahead of the crack tip.

2.3.2 Q-parameter

In the non-linear elastic field the leading term in the stress expansion is the HRR field. O'-Dowd and Shih (1991) express the higher order solution in the form:

$$\frac{[\sigma]}{\sigma_o} = \left(\frac{J}{\alpha\epsilon_o\sigma_o I_n r}\right)^{\frac{1}{n+1}} [\tilde{\sigma}_J(\theta,n)] + Q\left(\frac{r\sigma_o}{J}\right)^t [\tilde{\sigma}_Q(\theta,n)] + \cdots \tag{2.78}$$

For low hardening rates, when $t \to 0$, Eq. 2.78 can be simplified as:

$$\frac{[\sigma]}{\sigma_o} = \frac{[\sigma^{ref}]}{\sigma_o} + Q\begin{bmatrix} 1 & 0 \\ 0 & 1 \end{bmatrix} \tag{2.79}$$

where $[\sigma^{ref}]$ is taken as the reference field, HRR field or small scale yielding. Comparing Eqs. 2.76-2.77, the second order term of the outer elastic field: the T-stress and the second order term of the elastic-plastic field at the crack tip Q-parameter may be related to each other as:

$$Q = 0.64\left(\frac{T}{\sigma_o}\right) - 0.4\left(\frac{T}{\sigma_o}\right)^2 \qquad n = 13, \; \frac{T}{\sigma_o} \le 0 \tag{2.80}$$

$$Q = 0.6\left(\frac{T}{\sigma_o}\right) - 0.75\left(\frac{T}{\sigma_o}\right)^2 \qquad n = \infty, \; \frac{T}{\sigma_o} \le 0 \tag{2.81}$$

the implication being that in contained yielding conditions either T or Q can be used to characterise the constraint effects on the elastic-plastic crack tip fields.

2.3.3 $J - Q$ or T **toughness locus**

Classical fracture mechanics predicts failure on the assumption that the fracture toughness is a material constant that is independent of geometry. The assumption that failure can be characterised by a single parameter is however valid only in a limited range of geometries and loadings. For wider applicability of elastic-plastic fracture mechanics it is necessary to include the constraint effects by expressing the toughness as a function of the Q-parameter or T-stress:

$$J_c = J_c(Q \text{ or } T) \tag{2.82}$$

Thus, fracture toughness is dependent on the geometry through the second order term. Betegón and Hancock (1991) and Sumpter and Hancock (1994) examined different geometrics and determined the critical value of toughness, J_c, for cleavage failure at different levels of constraint. Centre cracked panels and shallow edge cracked bars that develop the most negative T-stresses were tougher than deeply cracked edge bars which develop positive T-stress. Figs. 2.15 shows the J_c-T locus determined by Sumpter (1993) and the corresponding J_c-Q locus is shown in Fig. 2.16. The figures indicate that the toughness (J_c) increases as Q or T become more negative. Hancock, Reuter and Parks (1993) examined stable ductile tearing in A710 pressure vessel steel. The measured CTOD is shown in Fig. 2.17 as a function of T for crack extensions Δa= 0, 200 μm and 400 μm. Initiation toughness was taken to be the critical value of J from Δa= 200 μm. For geometries with compressive T-stress (centre cracked panel), the initiation toughness was approximately 4 times greater than that of deeply cracked bend bars and compact tension specimens. The effect of constraint was even more significant for higher crack extensions.

Loss of constraint results in increased toughness for both cleavage failure and ductile tearing while highly constrained geometries exhibit constraint independent toughness. The toughness locus that represents the toughness as a function of constraint for a material is used

to predict failure by comparing the driving force curve with the toughness locus. Failure is predicted to occur when:

$$J(Q \text{ or } T) \geq J_c(Q \text{ or } T) \tag{2.83}$$
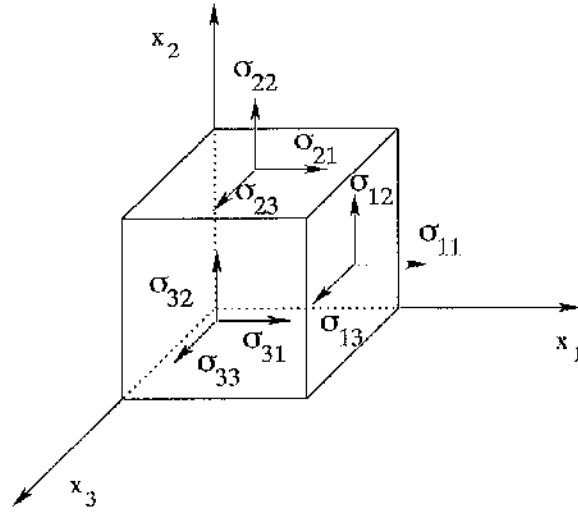
Fig 2.1: Stress components referred to Cartesian coordinates.
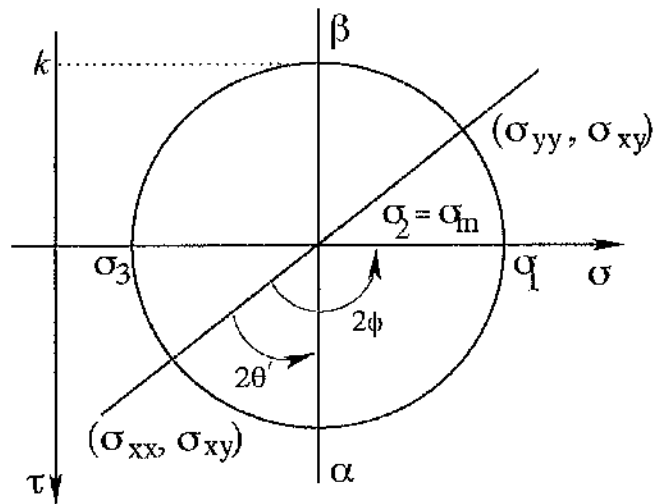
Fig 2.2: Mohr's circle.
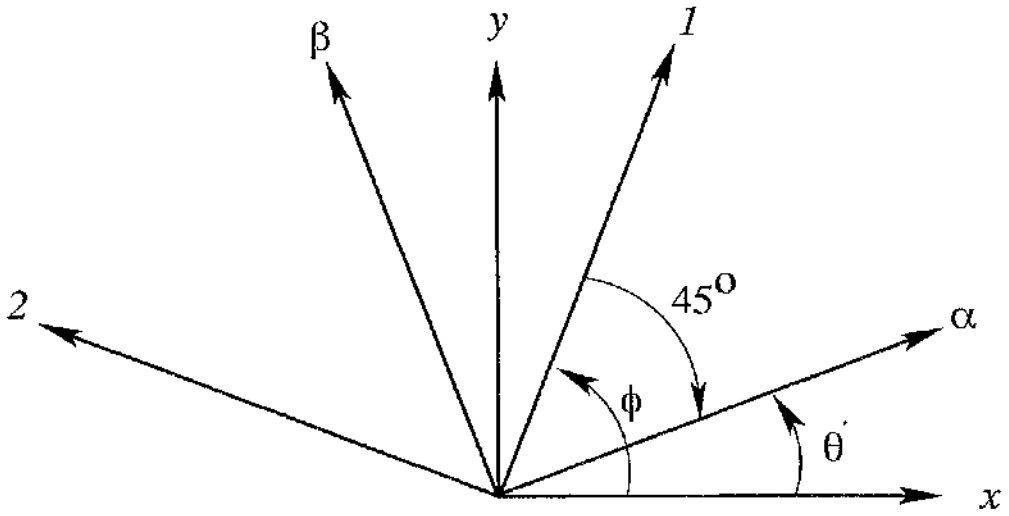
Fig 2.3: Direction of planes.
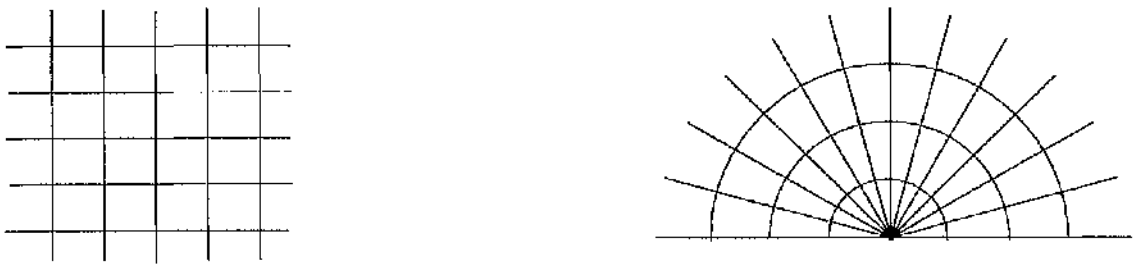
Fig 2.4: Constant stress and centred fan slip lines.
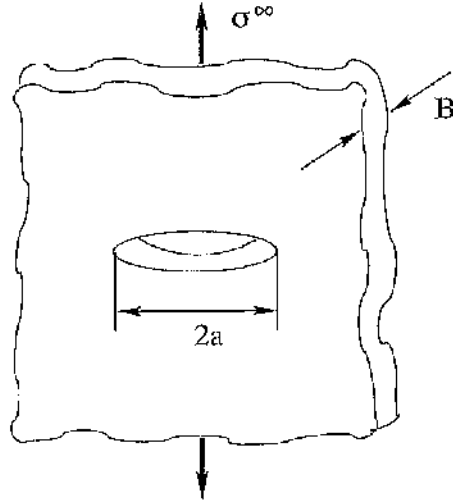
Fig 2.5: Centre cracked panel.

(a)   (b)
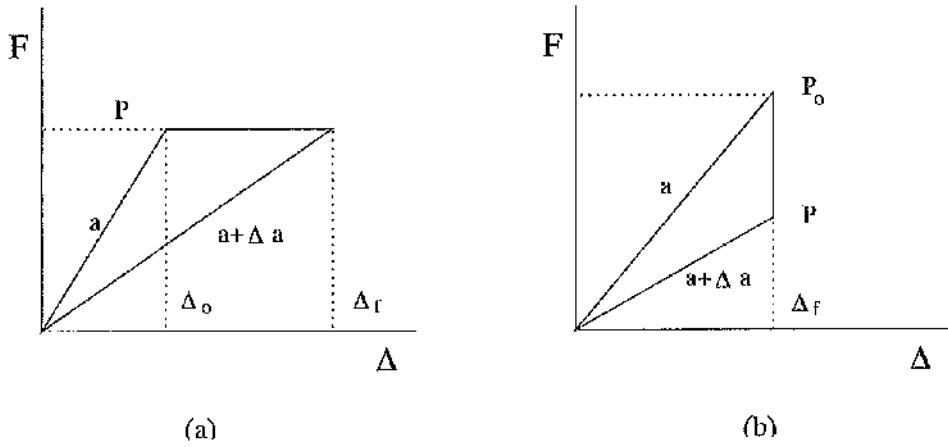
Fig 2.6: Force-displacement diagrams.
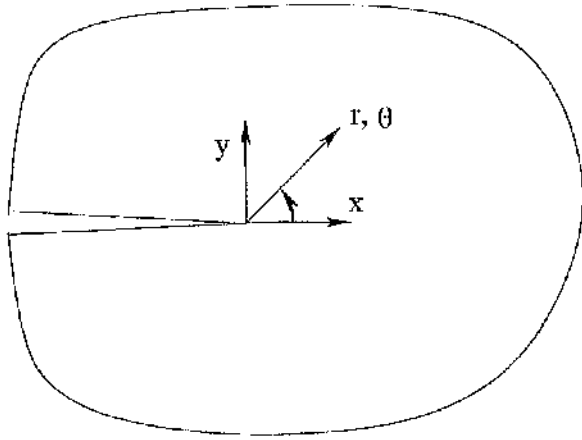
Fig 2.7: Crack in a homogeneous solid.

Mode I   Mode II   Mode III
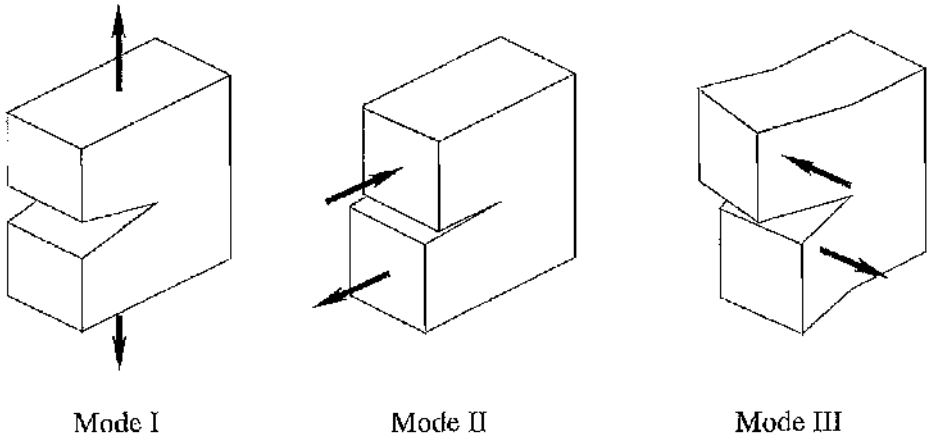
Fig 2.8: Fracture modes: Mode I, Mode II and Mode III.
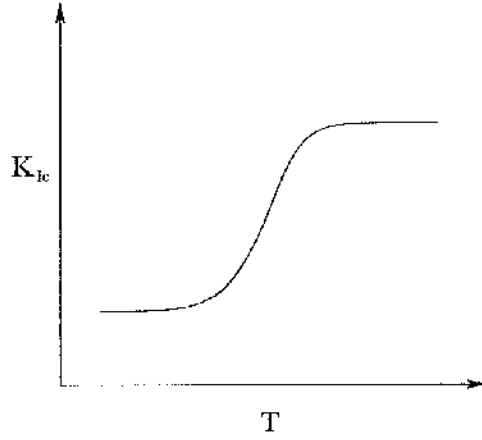
Fig 2.9: Dependence of fracture toughness, K_{Ic}, on temperature.
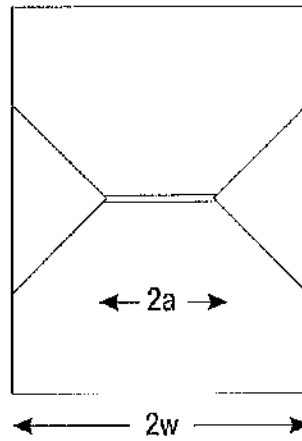
Fig 2.10: The slip line field for a centre-cracked tension panel.
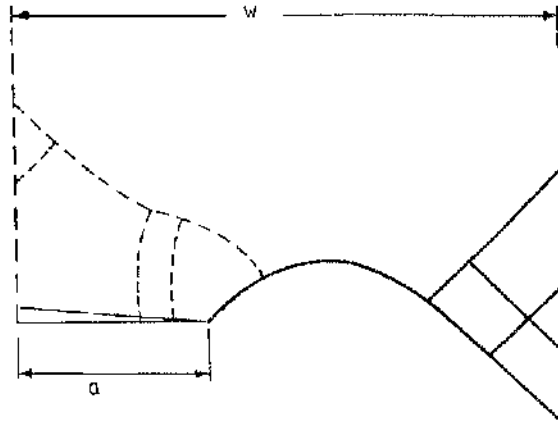
Fig 2.11: The slip line field for deep and shallow-cracked bars in bending after Ewing (1968) and Green (1953).
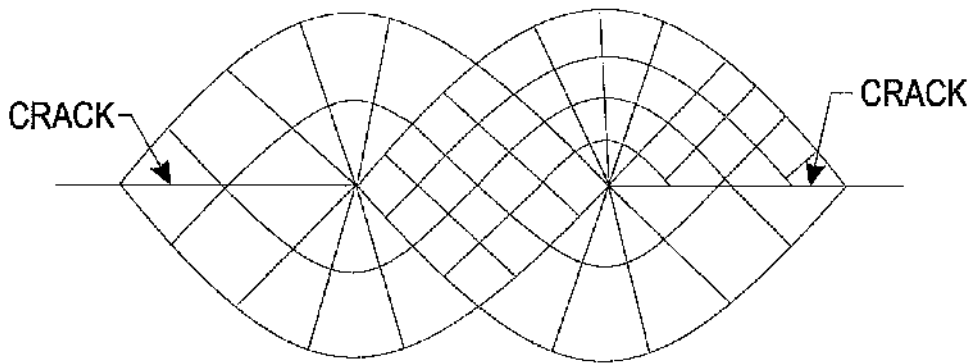
Fig 2.12: Prandtl field for a deeply double edge cracked bar
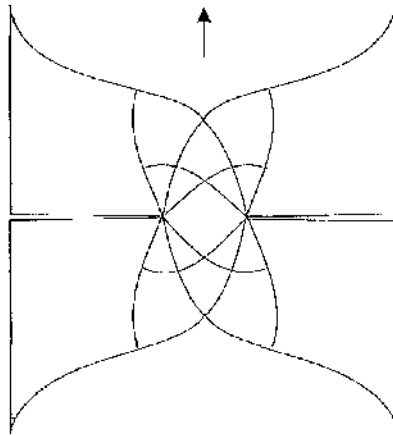
Fig 2.13: Slip line field for a shallow double edge cracked bar, after Ewing and Hill (1967)
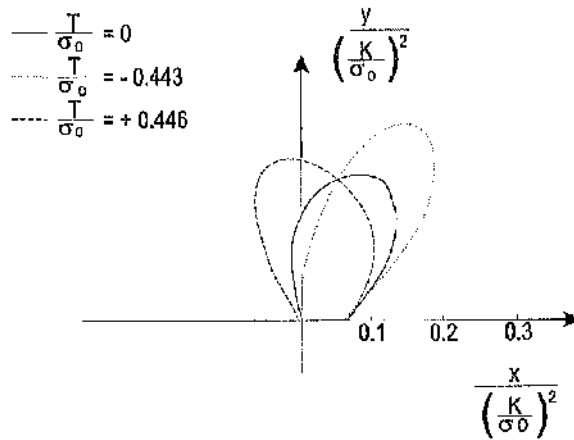
Fig 2.14: The effect of the T-stress on the plastic zone shape and size after Du and Hancock (1991).
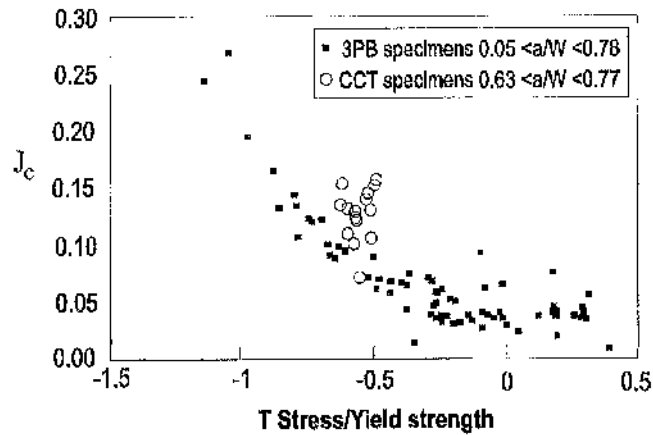
Fig 2.15: Critical value of J as a function of T/σ_o for 3PB and CCT specimens, low-grade mild steel at -50°C, Sumpter (1993)
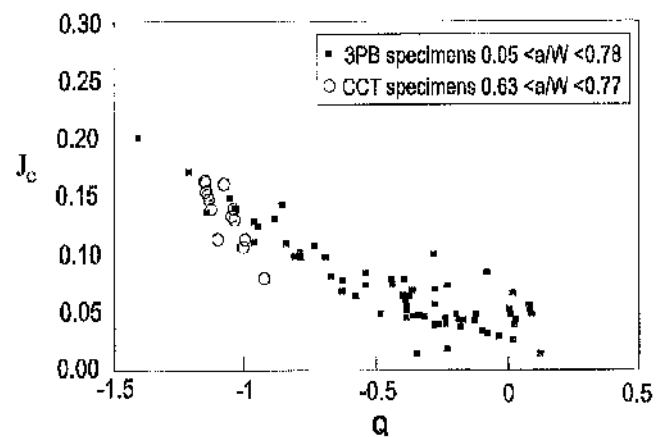
Fig 2.16: Critical value of J as a function of Q-parameter for 3PB and CCT specimens, low-grade mild steel at -50°C, Sumpter and Hancock (1994)
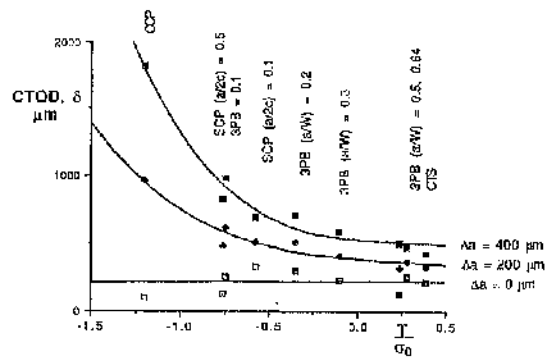
Fig 2.17: The CTOD as a function of T at crack extensions of 0, 200 and 400 μm, after Hancock, Reuter and Parks (1991).

Fracture Mechanics of Mismatched Bi-Material Systems

The structural integrity of bi-material systems such as thermal barrier coatings, ceramic laminates or cladding in pressure vessels may be compromised by cracks in the interface or which terminate at the interface between the constituting solids (Kokini and Takeuchi, 1994; He et. al, 1993; Evans and Marshall, 1989). Interest is largely focused on the factors that determine the crack tip field with the objective of improving the performance and reliability of bi-material systems. This chapter reviews the literature on: a crack located in a sharp interface across which material properties change abruptly, a crack located in an interfacial zone of graded properties between two dissimilar solids, and a crack normal to the interface between mismatched solids. For each case, the results obtained from linear elastic fracture mechanics are presented followed by solutions for small scale yielding.

3.1 Interface cracks

In one of the first studies of cracks in dissimilar materials Williams (1959) considered the plane problem of two isotropic, homogeneous, elastic dissimilar materials with a semi-infinite crack located in the interface as shown in Fig. 3.1. The crack flanks were taken to be traction free. Cartesian (x, y) and cylindrical (r, θ) coordinate systems are used, such that the origins lie at the crack tip and the crack is located along the negative x-axis ($\theta = \pi$). Material 1 is the solid above the interface ($y > 0$) and material 2 ($y < 0$) below. $E^{(k)}$, $\nu^{(k)}$ and $G^{(k)}$ ($k = 1,2$) are the Young's moduli, Poisson's ratios and the shear moduli of the two materials. Let $\kappa^{(k)} = 3 - 4\nu^{(k)}$ for plane strain and $\kappa^{(k)} = (3 - \nu^{(k)})/(1 + \nu^{(k)})$ for plane stress. In studies of mismatched systems, the Dundurs parameters (Dundurs , 1969) α and β

are widely used:

$$\alpha = \frac{G^{(1)}(\kappa^{(2)}+1) - G^{(2)}(\kappa^{(1)}+1)}{G^{(1)}(\kappa^{(2)}+1) + G^{(2)}(\kappa^{(1)}+1)} \tag{3.1}$$

$$\beta = \frac{G^{(1)}(\kappa^{(2)}-1) - G^{(2)}(\kappa^{(1)}-1)}{G^{(1)}(\kappa^{(2)}+1) + G^{(2)}(\kappa^{(1)}-1)} \tag{3.2}$$

Using eigenvalue expansions Williams (1959) established the singularity of the leading term, starting with stress functions, $\Phi^{(k)}(r,\theta)$, for both materials that satisfy the equilibrium and compatibility equations:

$$\Phi^{(k)}(r,\theta) = r^{\lambda+1} F^{(k)}(\theta) \tag{3.3}$$

where $F^{(k)}(\theta) = \left[A^{(k)} \sin(\lambda+1)\theta + B^{(k)} \cos(\lambda+1)\theta + C^{(k)} \sin(\lambda-1)\theta + D^{(k)} \cos(\lambda-1)\theta \right]$ and $A^{(k)}$, $B^{(k)}$, $C^{(k)}$ and $D^{(k)}$ are constants. The application of boundary conditions corresponding to traction free crack faces combined with traction and displacement continuity at the interface gives rise to a set of eight equations:

$$\sigma_{\theta\theta}^{(1)}(\pi) = 0$$

$$\sigma_{r\theta}^{(1)}(\pi) = 0$$

$$\sigma_{\theta\theta}^{(2)}(-\pi) = 0$$

$$\sigma_{r\theta}^{(2)}(-\pi) = 0$$

$$\sigma_{\theta\theta}^{(1)}(0) = \sigma_{\theta\theta}^{(2)}(0) \tag{3.4}$$

$$\sigma_{r\theta}^{(1)}(0) = \sigma_{r\theta}^{(2)}(0)$$

$$u_r^{(1)}(0) = u_r^{(2)}(0)$$

$$u_\theta^{(1)}(0) = u_\theta^{(2)}(0)$$

For non-trivial solutions of these equation the following characteristic equation needs to be satisfied:

$$\cos^2 \lambda\pi + \left[\frac{2\Omega(1 - \zeta^{(2)}) - 2(1 - \zeta^{(1)}) - (\Omega - 1)}{2\Omega(1 - \zeta^{(2)}) + 2(1 - \zeta^{(1)})} \right]^2 = 0 \tag{3.5}$$

where, $\zeta^{(k)} = \nu^{(k)}/(1 + \nu^{(k)})$. An infinite number of λ values satisfy the characteristic equation. The dominant complex eigenvalue is $\lambda = 1/2 + i\epsilon$. Where ϵ is a function of Dundur's parameter, β:

$$\epsilon = \frac{1}{2\pi} \ln \left(\frac{1 - \beta}{1 + \beta} \right) \tag{3.6}$$

For any plane problem, in which the crack flanks of the interface crack are traction free, the dominant stress singularity is of the form:

$$[\sigma] = \frac{1}{\sqrt{2\pi r}} \left(\mathrm{Re}\left(K r^{i\epsilon} \right) \left[\tilde{\sigma}^I(\theta, \epsilon) \right] + \mathrm{Im}\left(K r^{i\epsilon} \right) \left[\tilde{\sigma}^{II}(\theta, \epsilon) \right] \right) \tag{3.7}$$

where $i = \sqrt{-1}$ and $K = K_1 + iK_2$ is the complex stress intensity factor. Quantitatively, $K_j (j = 1, 2)$ depend on the loading and geometry. The stresses on the interface directly ahead of crack tip are given by:

$$\sigma_{yy} + i\sigma_{xy} = \frac{(K_1 + iK_2)}{\sqrt{2\pi r}} r^{i\epsilon} \tag{3.8}$$

where

$$r^{i\epsilon} = e^{i\epsilon \ln r} = \cos(\epsilon \ln r) + i\sin(\epsilon \ln r) \tag{3.9}$$

Substituting in Eq. 3.8,

$$\sigma_{yy} + i\sigma_{xy} = \frac{(K_1 + iK_2)(\cos(\epsilon \ln r) + i\sin(\epsilon \ln r))}{\sqrt{2\pi r}} \tag{3.10}$$

Implying,

$$\sigma_{yy} = \frac{K_1 \cos(\epsilon \ln r) - K_2 \sin(\epsilon \ln r)}{\sqrt{2\pi r}} \tag{3.11}$$

and

$$\sigma_{xy} = \frac{K_2 \cos(\epsilon \ln r) + K_1 \sin(\epsilon \ln r)}{\sqrt{2\pi r}} \tag{3.12}$$

Both σ_{yy} and σ_{xy}, directly ahead of the crack depend on K_1 and K_2 in an inherently coupled manner. The singular behaviour of the stresses retains the square root singularity of homogeneous solids. However, the stresses possess a pronounced oscillatory nature of the type:

$$\sigma \sim r^{-\frac{1}{2}} \; \begin{array}{c} \sin \\ \text{or} \\ \cos \end{array} \; (\epsilon \ln r) \tag{3.13}$$

Using the central features of the asymptotic field of interface cracks established by the eigenfunction expansion in the complex variable approach, Rice and Sih (1965) developed complete solutions for some specific problems. For the problem of a central crack of length $2a$, lying in the interface between two semi-infinite blocks subject to remote stresses σ_{yy}^{∞} and σ_{xy}^{∞}, the complex stress intensity factor at the right tip is:

$$
\begin{aligned}
K_1 + iK_2 &= (\sigma_{yy}^{\infty} + i\sigma_{xy}^{\infty})(1 + 2i\epsilon)\sqrt{\pi a}(2a)^{i\epsilon} \\
&= \sqrt{\pi a}(\sigma_{yy}^{\infty} + i\sigma_{xy}^{\infty})(1 + 2i\epsilon)e^{-i\epsilon \ln(2a)} \\
&= \sqrt{\pi a}(\sigma_{yy}^{\infty} + i\sigma_{xy}^{\infty})(1 + 2i\epsilon)(\cos(\epsilon \ln 2a) - i\sin(\epsilon \ln 2a))
\end{aligned} \tag{3.14}
$$

Implying,

$$\frac{K_1}{\sqrt{\pi a}} = (\sigma_{yy}^\infty - 2\epsilon\sigma_{xy}^\infty)\cos(\epsilon \ln 2a) + (\sigma_{xy}^\infty + 2\epsilon\sigma_{yy}^\infty)\sin(\epsilon \ln 2a) \tag{3.15}$$

$$\frac{K_2}{\sqrt{\pi a}} = (\sigma_{xy}^\infty + 2\epsilon\sigma_{yy}^\infty)\cos(\epsilon \ln 2a) - (\sigma_{yy}^\infty - 2\epsilon\sigma_{xy}^\infty)\sin(\epsilon \ln 2a) \tag{3.16}$$

In bi-material problems, in the expressions for K_1 and K_2 both the symmetric and skew-symmetric loadings are inherently coupled. As a result K_2 and thus σ_{xy} directly ahead of crack is non-zero even when the remote loading is symmetric ($\sigma_{xy}^\infty = 0$). The energy release rate for crack advance in the interface is:

$$G = \frac{(1 - \beta^2)}{E_*}(K_1^2 + K_2^2) \tag{3.17}$$

where

$$\frac{1}{E_*} = \frac{1}{2}\left(\frac{1}{\tilde{E}^{(1)}} + \frac{1}{\tilde{E}^{(2)}}\right) \tag{3.18}$$

and $\tilde{E}^{(k)} = E^{(k)}/(1 - (\nu^{(k)})^2)$ in plane strain and $\tilde{E}_i = E_i$ in plane stress. For incompressible solids ($\nu^{(1)} = \nu^{(2)} = 0.5$), Dundur's parameter $\beta = 0$ which implies a bi-material constant $\epsilon = 0$. As a result, the stresses lose the oscillatory nature and the normal and shear stresses are decoupled such that the stresses ahead of the crack become:

$$(\sigma_{yy}, \sigma_{xy}) = (K_1, K_2)\frac{1}{\sqrt{2\pi r}} \tag{3.19}$$

The interface stress intensity factors K_1 and K_2 now play similar roles to their counterparts for a crack in a homogeneous isotropic solid. However, for non-zero β, normal and shear components remain inherently coupled. The mode mixity can be generalised following Rice (1988) by introducing a phase angle parameter, ψ:

$$\psi = \tan^{-1}\left(\frac{Im(Kl^{i\epsilon})}{Re(Kl^{i\epsilon})}\right) = \tan^{-1}\left(\frac{\sigma_{xy}}{\sigma_{yy}}\right)_{r=l} \tag{3.20}$$

where K is the complex stress intensity factor and l is a reference length. England (1965) noted that for a crack with traction free crack flanks the solutions of the displacements of the crack flanks oscillate and predict inter-penetration. The crack flank displacements, $\delta_i = u_i^{(1)}(r, \theta = \pi) - u_i^{(2)}(r, \theta = -\pi)$, $i = 1, 2$, are:

$$\delta_2 + i\delta_1 = \frac{8(K_1 + iK_2)}{E_*(1 + 2i\epsilon)\cosh(\pi\epsilon)}\sqrt{\frac{r}{2\pi}}r^{i\epsilon} \tag{3.21}$$

Inter-penetration is however physically impossible leading Comninou (1977,1978) to propose a contact zone model which allowed closure of the crack flanks. On this basis the leading term solution of the crack tip field becomes:

$$\left\{ \begin{array}{c} \sigma_{rr} \\ \sigma_{\theta\theta} \\ \sigma_{r\theta} \end{array} \right\} = -\frac{K_{II}^c}{4\sqrt{2r}}\left\{ \begin{array}{c} 5(1+\beta)\sin\frac{\theta}{2} - (3-\beta)\sin\frac{5\theta}{2} \\ 3(1+\beta)\sin\frac{\theta}{2} + (3-\beta)\sin\frac{5\theta}{2} \\ (1+\beta)\cos\frac{\theta}{2} + (3-\beta)\cos\frac{5\theta}{2} \end{array} \right\} \tag{3.22}$$

where K_{II}^c is the stress intensity factor for the interface crack tip field given frictionless contact of the crack flanks. On the plane ahead of the crack tip ($\theta = 0$) and the crack flanks both the radial stress and the hoop stress are zero while the shear stress is singular. As a result the crack tip field is mode II like. Comninou (1978) concluded that the oscillation zone was very small compared to the fracture process zone or the plastic zone in the case of tensile loading but may be significant for predominantly shear loading situations. Any plasticity at the crack tip would further reduce the effect of the oscillation zone which allows the use of model with traction free crack flanks for predominantly remote tensile loadings.

3.1.1 Crack paths in homogeneous and bi-material systems

A crack in a homogeneous solid subject to mode I loading continues to propagate in the plane of the initial crack. However, under mixed mode loading, in brittle fracture of steels,

poly-crystalline alumina the crack propagates at an angle to the initial crack plane (Maccagno and Knott, 1991; Suresh and Shih, 1991). The criteria used to predict the deviation in crack path due to mixed mode loading are based on the direction of maximum hoop stress (Erdogan and Sih, 1963), the direction of maximum energy release rate (Cotterell, 1965) and direction of vanishing K_{II} stress intensity factor (Cotterell and Rice, 1980). The kink directions predicted by these criterions are in close agreement for kink angles less than 40°. To determine the kink angle using the criterion based on vanishing K_{II} stress intensity factor an infinitesimal crack at an angle, ϕ, clockwise from the initial plane is considered. The mode I, mode II stress intensity factors in terms of the stress intensity factors of the initial crack can be expressed in the form:

$$K_I^* = C_{11}(\phi)K_I + C_{12}(\phi)K_{II} \tag{3.23}$$

$$K_{II}^* = C_{21}(\phi)K_I + C_{22}(\phi)K_{II} \tag{3.24}$$

where, C_{ij} are coefficients determined by a method described by Lo (1978). The extension angle is the angle for which K_{II}^* vanishes.

For an interface crack, the stress intensity factors of the kinked crack depends on the kink length (Δa). He and Hutchinson (1989) using a dimensional argument relate the complex stress intensity factor of the kinked crack, K^*, to the interface crack complex stress intensity factor, K, as:

$$K^* = c(\phi, \alpha, \beta)K(\Delta a)^{i\epsilon} + \bar{d}((\phi, \alpha, \beta)\bar{K}(\Delta a)^{-i\epsilon} \tag{3.25}$$

where functions c and d are complex valued. Since the stress intensity factor, K^*, is a strong function of the kink length, the kink length is viewed as a bi-material property. Kinking is favoured when the ratio between the energy release rate for the crack to kink into one of the materials and the rate for crack to extend in the interface is greater than the ratio of the toughness between the material and the interface.

3.1.2   Elastic-plastic interfacial crack tip fields

Zywicz and Parks (1989, 1992) and Shih and co-workers (1988,1991) have examined elastic-plastic interfacial crack tip fields for two elastically mismatched solids using the singular term of the Williams expansion to define the outer elastic field. Zywicz and Parks (1989) expressed their results in terms of a load phase angle, ζ_o:

$$\zeta_o = \angle K + \epsilon \ln(r_P) = \angle K + \epsilon \ln\left[\frac{K\overline{K}}{\sigma_o^2 \pi \cosh^2(\pi\epsilon)}\right] \tag{3.26}$$

where, $\angle K$ is the phase angle of the complex stress intensity factor ($\angle K = \tan^{-1}(K_1/K_2)$) and r_P is the approximate plastic zone radius. The near-tip slip line fields are shown as a function of the loading phase parameter, ζ_o, for an elastic-perfectly plastic material bonded to an elastic or rigid substrate in Fig. 3.2.

For $\zeta_o < 0$, fully plastic fields which consist of a fan and (quasi-) constant state sectors encompass the crack tip. In the (quasi-) constant state sectors the slip lines have small but finite curvatures which allow modest stress gradients. However, over small radial distances the angular stress distribution in conventional constant state sectors accurately represents the stress states within the (quasi-) constant state sectors. In the range $-30^o < \zeta_o < 0$ the unique sectoral composition gives rise to an extremely high interfacial triaxiality ($\sigma_{kk}/3\sigma_o = 3.29$), which is extremely conducive to crack extension by ductile void nucleation, growth and coalescence as well as cleavage fracture. The slip line fields for $\zeta_o > 0$ are composed of both elastic and plastic sectors and exhibit modest interface normal tractions.

Extending these investigations based on the leading singular term of the Williams expansion, Kim et. al (1997) considered the effect of the second order term, T-stress, on the interfacial crack tip fields. The effect of plastic mismatch ($M = \sigma_o^{(2)}/\sigma_o^{(1)}$) and T-stress ($\tau = T/\sigma_o^{(1)}$) is illustrated by the slip line fields shown in Fig. 3.3 for elastically matched but plastically mismatched solids.

Starting with plastically matched solids and looking at the upper half ($0 \geq \theta \geq \pi$), the slip line field consists of an elastic sector at the flank ($\sim 50^\circ$) and a constant stress sector ahead of the crack tip making an angle, $\psi_1 = 45^\circ$, as shown in the figure. As the plastic mismatch is increased, ψ_1 decreases till it becomes zero for $M \geq 1.8$, however, the elastic sector remains unchanged. As a result, for high plastic mismatches the slip line field is composed of an elastic sector at the flank followed by a centred fan sector extending up to the interface such that $\sigma_m(0) = 3.20\sigma_o^{(1)}$ and $\sigma_{r\theta}(0) = \sigma_o^{(1)}/\sqrt{3}$. The phase angle, ψ_1, is approximated in terms of the plastic mismatch as:

$$\psi_1(M) = \begin{cases} -0.314\pi(M-1) + 0.25\pi; & \text{for } 1 \leq M \leq 1.8 \\ \\ 0 & \text{for } 1.8 < M \end{cases} \tag{3.27}$$

The stresses at the interface can be expressed in terms of ψ_1 and thus of M as:

$$\sigma_m(0) = \left(1 + \frac{13}{9}\pi - 2\psi_1\right)\frac{\sigma_o^{(1)}}{\sqrt{3}}$$

$$\sigma_{\theta\theta}(0) = \sigma_m(0) + \cos\left(\frac{\pi}{2} - 2\psi_1\right)\frac{\sigma_o^{(1)}}{\sqrt{3}} \tag{3.28}$$

$$\sigma_{r\theta}(0) = \sin\left(\frac{\pi}{2} - 2\psi_1\right)\frac{\sigma_o^{(1)}}{\sqrt{3}}$$

For homogeneous systems ($M = 1$), $\sigma_m(0) = 2.29\sigma_o^{(1)}$, $\sigma_{\theta\theta}(0) = 2.87\sigma_o^{(1)}$ and $\sigma_{r\theta}(0) = 0$. While for all plastic strength mismatches greater than 1.8, $\sigma_m(0) = 3.20\sigma_o^{(1)}$ and $\sigma_{r\theta}(0) = \sigma_o^{(1)}/\sqrt{3}$. Increasing the plastic mismatch leads to higher crack tip constraint and mode mixities. Fig. 3.3 also shows the effect of the T-stress for the limiting case of plastic mismatch, $M = \infty$. Under positive T-stress plasticity fully surrounds the crack tip and the fan extends to the interface. The stresses in this field are the highest possible for interfacial cracks in

bimaterial systems:

$$\sigma_m = \sigma_{\theta\theta} = \sigma_{rr} = 3.30\sigma_o^{(1)} \tag{3.29}$$

$$\sigma_{r\theta} = \frac{\sigma_o^{(1)}}{\sqrt{3}} \tag{3.30}$$

The effect of negative T-stresses ($\tau = T/\sigma_o^{(1)}$) on the mean stress and hoop stress ahead of crack can be summarised as:

$$\sigma_m(0) = \left(3.20 + 0.56\tau - 1.97\tau^2\right)\sigma_o^{(1)} \tag{3.31}$$

$$\sigma_{\theta\theta}(0) = \left(3.20 + 0.29\tau - 1.60\tau^2\right)\sigma_o^{(1)} \tag{3.32}$$

Kim et. al (1997) also show the effect of elastic mismatch on interfacial crack tip constraint. For an interface crack between elastically mismatched solids the first two terms of the stress field can be written as:

$$\sigma_{ij}^{(k)} = \frac{Kr^{i\epsilon}}{\sqrt{2\pi r}}\tilde{\sigma}_{ij}^{(k)} + T^{(k)}\delta_{1i}\delta_{2j}; \quad (k = 1, 2) \tag{3.33}$$

where, $T^{(1)} = (1 + \alpha)T$ and $T^{(2)} = (1 - \alpha)T$, α being the Dundur's parameter defined in Eq. 3.1. Fig. 3.4 shows that elastic mismatch through α significantly affects the interfacial crack tip constraint, $\sigma_m(0)$, at compressive T-stress. The effect is most pronounced for positive values of α. For tensile T-stresses, the crack tip is fully surrounded by plasticity and the effect of elastic mismatch disappears.

Sham et. al (1999) considered an interface crack between yield strength mismatched solids under general mixed mode loadings. The asymptotic crack tip stress fields are characterised by the strength mismatch (y) and a phase angle, ϕ, such that $\sigma_{\theta\theta}\sin\phi(\theta = 0) = \sigma_{r\theta}(\theta = 0)\cos\phi$. The slip line fields for strength mismatches $y = 1.25$ and 1.5 are drawn in

Fig. 3.5. Depending on the mode mixity of the remote load and the plastic mismatch, a set of distinct configurations denoted B, C, E, G are obtained. A critical mismatch $y_{cr} = 1.408$ is identified that classifies crack tip fields into sub-critical, critical and super critical when locally near mode I conditions apply. The near mode I field saturates at a phase angle $\phi_{sat} = 9.9^o$ when the configuration in the softer material consists of a 45°-constant stress sector on the crack flank leading to a 135° centred fan sector. Saturation implies that the stress field in the soft material is independent of yield strength mismatch when $y \geq y_{cr}$. Strength mismatched systems were also investigated in hardening materials (Li, 1998). The plane of maximum principal stress is located in the harder material and rotates as the mode II component increases. On these planes the stress profiles are parallel and deviatorically similar and differ only by a hydrostatic term. The constraint parameter in the plane of maximum principal stress, $Q = (\sigma_m - \sigma_m^{SSY})/\sigma_o$, is shown in Fig. 3.6 to decrease with increasing mode II component.

Burstow et. al (1998) studied a two-material idealisation of welded joints containing cracks by considering the crack to be centrally located within the weld material and parallel to the interface with the base material. The materials were elastically matched but differed in their plastic strength ($\sigma_{y,weld}$, $\sigma_{y,base}$). The obtained crack tip stress fields were symmetric about the crack plane. Self similarity of stress fields at the same level of plastic mismatch was obtained by identifying a loading parameter, $J/(h\sigma_{y,weld})$, which describes the size of plastic zone relative to the width of the weld material, h. Crack tip constraint was identified to depend on both the plastic mismatch between the two materials as well as the T-stress of the outer field. Over-matching ($\sigma_{y,weld} > \sigma_{y,base}$) resulted in loss of constraint while under-matching ($\sigma_{y,weld} < \sigma_{y,base}$) increased constraint. The effect of T-stress was similar to the effect of the T-stress term in the homogeneous case: compressive T-stress lowered the constraint while tensile T-stresses raised the level of constraint till it saturated. However, in under-matched specimens the T-stress had little or no effect.

3.1.3   Crack in a zone of graded properties

The bi-material crack tip fields discussed so far consider an interface which features a step change in material properties across a sharply defined interface. However, interfaces in structures such as welded joints and functionally graded systems, the variation in properties from one material to the other material is gradual. Work addressing the problem of a crack in a zone of graded yield strength is presented in chapter 6. The results of which can also be applied to a crack in a homogeneous solid under a non-uniform temperature field. Amongst the first studies to gain insight into the effect of crack like defects within a zone of graded properties, Delale and Erdogan (1983) studied a crack located in a solid with a spatial variation of elastic modulus. If the properties are considered to be piecewise continuous the crack tip singularity is identical to that of a homogeneous crack, the near crack-tip field being of the form:

$$\sigma_{ij} = \frac{K_I}{\sqrt{2\pi r}} f_{ij}^I(\theta) + \frac{K_{II}}{\sqrt{2\pi r}} f_{ij}^{II}(\theta) \tag{3.34}$$

where, K_I and K_{II} are the stress intensity factors which depend on the remote loading and the elastic gradient, and $f_{ij}^I(\theta)$ and $f_{ij}^{II}(\theta)$ are the universal angular functions. Unlike homogeneous systems, both K_I and K_{II} depend on the remote opening and shearing loads, implying that even for a remote pure tensile load the local field is mixed mode.

Gu and Asaro (1997) studied small crack deflection in brittle functionally graded materials. A crack located centrally in a functionally graded inter-layer between two elastically dissimilar solids is considered. Under the assumption of local homogeneity the toughness is taken to be independent of direction; as a result, the gradient in elastic modulus only affects the failure mode through the crack tip mixity and the crack path is predicted along the direction of maximum energy release rate or the direction which gives a vanishing mode II stress intensity factor. Under remote mode I load the crack is predicted to kink towards the elastically compliant material. Experiments by Rousseau and Tippur (2000) on compositionally

graded particulate composites consisting of glass spheres dispersed in an epoxy matrix veri-
fied that a crack normal to the elastic gradient subjected to mode I loading exhibits a mixed
mode failure. The mixity caused the crack to propagate at an angle to the initial direction
towards the less stiff solid. The assumption of local homogeneity is true if fracture initiates
at the crack tip, however, inhomogeneity in material may lead to fracture which is initiated
at a region which differs in strength from the crack tip. Becker et. al (2002) allow a dis-
tributed strength described by Weibull statistics in their recent analyses on fracture initiation
near a crack tip in functionally graded elastic materials. The probability of failure based on
a weakest link model was assumed to be of the form:

$$P = 1 - \exp\left[-\sum_n \frac{V_i}{V_o} \left(\frac{\sigma_i}{\sigma_u} \right)^m \right] \tag{3.35}$$

where the Weibull parameters, σ_u and m are material constants, V_o is the reference volume
and V_i is the volume subject to stress σ_i within the stressed zone. Gradients in the Weibull
scaling stress, σ_u, were found to lead to dramatic decrease in initiation toughness and the
crack was predicted to grow towards the material of lower Weibull scaling stress. In func-
tionally graded systems in which the elastic modulus has a gradient in the direction normal
to the crack plane, the Weibull modulus, m, plays a significant role. At high m when the
strength has less scatter, the average crack initiation angle is the same as the crack in a homo-
geneous solid having the same remote phase angle, $\psi = \tan^{-1} K_{II}/K_I$, implying initiation
in the material of lower elastic moduli which agrees with the predictions of Gu and Asaro
(1997). However, in case of lower m, the far field stresses drive the crack back towards the
elastically stiffer material. Thus, at high values of m, the near crack tip stress field dominates
the failure probabilities while for lower m the far field stresses also become significant.

Rashid and Tvergaard (2003) analyse the effect of a gradient in plastic properties com-
putationally using exclusion region theory. They consider a crack in a thin layer between
two elastically similar but plastically dissimilar solids such that the yield strength of the

inter-layer is a linear interpolation. The fracture criterion is specified such that a *separation function*, Φ, does not exceed a critical value Φ_c. The advance of the crack occurs in the direction which maximises the separation function. For nine different locations within the interlayer the crack grows towards the plastically stronger material. The energy dissipation per unit area for a crack in a graded layer is even higher than for a crack in a homogeneous solid of the more ductile material. The energy dissipation profile remains well above that for a homogeneous material until large crack extensions have occurred such that the crack is well within the more brittle material.

The present work is motivated to study the effect of a gradient in plastic strength on the asymptotic field of a crack located in an interfacial zone between elastically matched but plastically different solids. The discussion is then developed using a statistical approach to find the effect of a gradient in fracture toughness and plastic strength on the failure probabilities and crack extension direction.

3.2 Crack normal to an interface

The first studies of a crack normal to an interface between two homogeneous, isotropic, elastically mismatched solids (Zak and Williams, 1963; Cook and Erdogan, 1972) focused on the asymptotic elastic field in mode I loading. Using cylindrical co-ordinates (r, θ) centred at the crack tip, the stress field, σ_{ij}, can be expressed in the form:

$$\sigma_{ij}(r, \theta) = K(2\pi r)^{\lambda - 1}\tilde{\sigma}_{ij}(\theta) \tag{3.36}$$

The strength of the singularity is defined by the exponent $(\lambda - 1)$ such that the well known $r^{-\frac{1}{2}}$ singularity is recovered for elastically matched solids. λ can be determined from the characteristic equation:

$$-\cos(\pi\lambda) - 2\left(\frac{\alpha - \beta}{1 - \beta}\right)\lambda^2 + \frac{\alpha - \beta^2}{1 - \beta^2} = 0 \tag{3.37}$$

where α and β are the Dundur's parameters. The amplitude of the singularity is described by a stress intensity factor, K, and the angular variation of stress is given by universal angular functions, $\tilde{\sigma}_{ij}(\theta)$, which depend on the elastic mismatch. The present work determines the second order term in the expansion of the crack tip elastic field, and considers its significance. The details of the determination of the elastic field are developed in Chapter 4.

In a study of the general non-linear elastic problem Chao et al. (1993) the stress-strain relation is taken to be of the form:

$$\frac{\epsilon}{\epsilon_l} = \alpha \left(\frac{\sigma}{\sigma_l}\right)^{1/N} \tag{3.38}$$

where ϵ_l, σ_l and α are material constants. The stresses are expressed in a separable form as a product of a power of the radial distance and a function of the polar angle, θ:

$$\sigma_{ij}^{(k)} = r^\lambda \tilde{\sigma}_{ij}^{(k)}(\theta) \tag{3.39}$$

where the superscript $k = 1, 2$ denotes the two materials. The crack was located in material 2 and the material ahead of crack was taken as material 1. The discussion is largely focused on materials with the same hardening exponent. Eigenvalues and angular functions were determined for a range of β_{ch} defined as the ratio of the material constants: $\sigma_l^{(1)}/\sigma_l^{(2)}$ and the hardening exponent N as shown in Fig. 3.7. λ becomes less singular for increasing β_{ch}, and very weakly dependent on β_{ch} when $\beta_{ch} > 5$. The stress fields are most singular for $N = 1$ and become less singular as N decreases. In the limit as $N \to 0$, the materials tend towards the ideally plastic response and the stress singularity vanishes. When $N^{(1)} > N^{(2)}$, the singularity depends only on $N^{(2)}$. The effect of non-linear behaviour on the leading singularity was identified such that the results of Cook and Erdogan (1972) were recovered in the limit of linear behaviour. Although non-linear elasticity indicates the effect of crack tip plasticity, such solutions do not involve a yield criterion. As non-linear behaviour is taken to occur at all angles around the crack tip, non-linear elastic solutions are equivalent to

assuming that deformation plasticity occurs at all angles around the tip. As a result, the crack tip stress field depends only on plastic properties and there is no effect of elastic mismatch.

3.2.1 Elastic-plastic solutions for a crack normal to an interface

Sugimura et. al (1995) consider a crack approaching an interface between elastically similar but plastically dissimilar materials. The crack tip is at a distance, L, from the interface. One material is taken to be fully elastic while the other is strain hardening. The J- integral is path independent in the two domains: in the crack tip region $r < L$ and in the remote region $r > R_p$, R_p being the plastic zone radius. J_{tip} is calculated along any contour lying within the crack tip region and J_{app} is calculated for a remote contour as indicated in Fig. 3.8. When the crack is within the plastically weaker material and approaches the bi-material interface, the effective J-integral at the crack tip is smaller than the remotely applied J. When the crack approaches the interface from the elastic solid, the near tip J is higher than the applied J indicating amplification of the driving force. However, this approach is not valid for a crack tip that is very near the interface ($L \to 0$) as J_{tip} does not remain path-independent.

He et. al (1992) and Stahle and Shih (1992) obtain the nature of the crack tip fields for a crack normal to the interface between elastically and plastically mismatched solids using an elastic perfectly-plastic response, which allows the use of slip line theory (Hill, 1950). The elastic singular field was used as the boundary condition in a boundary layer formulation to obtain small scale yielding asymptotic solutions. In the limit of plastic mismatch when one solid is elastic and the other is elastic perfectly-plastic, the slip line fields are shown in Fig. 3.9. The crack may be located in either solid giving rise to two configurations. When the crack is located in the elastic perfectly-plastic solid, the asymptotic stresses in the yielded material are:

$$\sigma_{rr} = k(1 + \cos 2\theta)$$

$$\sigma_{\theta\theta} = k(1 - \cos 2\theta) \qquad (3\pi/4 \le \theta \le \pi) \qquad (3.40)$$

$$\sigma_{r\theta} = -k \sin 2\theta$$

The stresses in the centred fan adjoining the constant stress sector are:

$$\sigma_{rr} = \sigma_{\theta\theta} = \sigma_m - 2k \left[\frac{1}{2} + \frac{3\pi}{4} - \theta \right]$$

$$\sigma_{r\theta} = k \qquad (\pi/2 \le \theta \le 3\pi/4) \qquad (3.41)$$

He et. al (1992) give the asymptotic solution for the stresses in the elastic material ahead of the crack tip without proof as:

$$\sigma_{\theta\theta} = -\frac{4k \cos \theta}{\pi} \left[\cos \theta \left(\log \frac{r}{r_o} + \frac{1}{2} \right) - \theta \sin \theta \right] + \left(1 + \frac{\pi}{2} \right) k \sin^2 \theta$$

$$\sigma_{rr} = \frac{2k}{\pi} \left[-2 \sin^2 \theta \log \frac{r}{r_o} + \cos^2 \theta - \theta \sin 2\theta \right] + \left(1 + \frac{\pi}{2} \right) k \cos^2 \theta \qquad (3.42)$$

$$\sigma_{r\theta} = -\frac{2k}{\pi} \left[\sin 2\theta \left(\log \frac{r}{r_o} + \frac{1}{2} \right) + \theta \cos 2\theta \right] - \left(1 + \frac{\pi}{2} \right) k \sin \theta \cos \theta$$

The stresses in the material ahead is postulated to have a logarithmic singularity which emphasises the limitation of the assumption that the dependence on radial distance is always described by the Eq. 3.39. r_o is a constant that has dimensions of length. The present work verifies the form of the stresses and identifies its dependence on loading. The asymptotic solution in the material behind ($\pi \ge \theta \ge \pi/2$) is determined assuming plasticity at all angles as shown in Fig. 3.9(a). The present work will argue that plasticity at all angles occurs only as a special case: the details being presented in Chapter 4 and 5.

When the crack is located in the elastic solid the slip line field as in Fig 3.9(b) is similar to that of a homogeneous mode I crack. However, the radial stresses are discontinuous across the interface due to the mismatch in properties. The asymptotic field can be fully expressed in terms of the hoop stress at the interface, $\sigma_{\theta\theta}(\pi/2)$. In the perfectly plastic region:

$$\sigma_{\theta\theta} = \sigma_{\theta\theta}(\pi/2) + \frac{k\pi}{2} + k\cos 2\theta$$

$$\sigma_{rr} = \sigma_{\theta\theta}(\pi/2) + \frac{k\pi}{2} - k\cos 2\theta \tag{3.43}$$

$$\sigma_{r\theta} = k\sin 2\theta$$

The constraint (hydrostatic stress) ahead of the crack tip is a function of the elastic mismatch as shown in Fig. 3.10 through the Dundur's parameter, α.
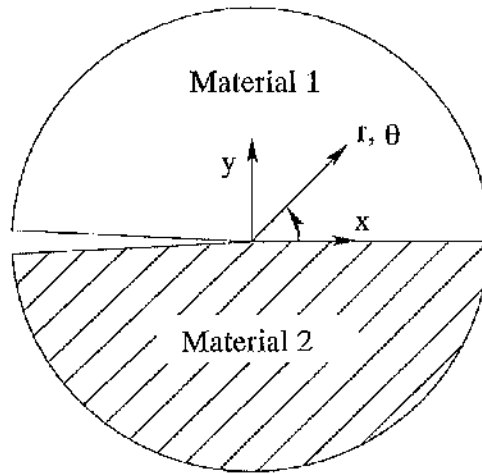
Fig 3.1: Semi-infinite crack between dissimilar solids.
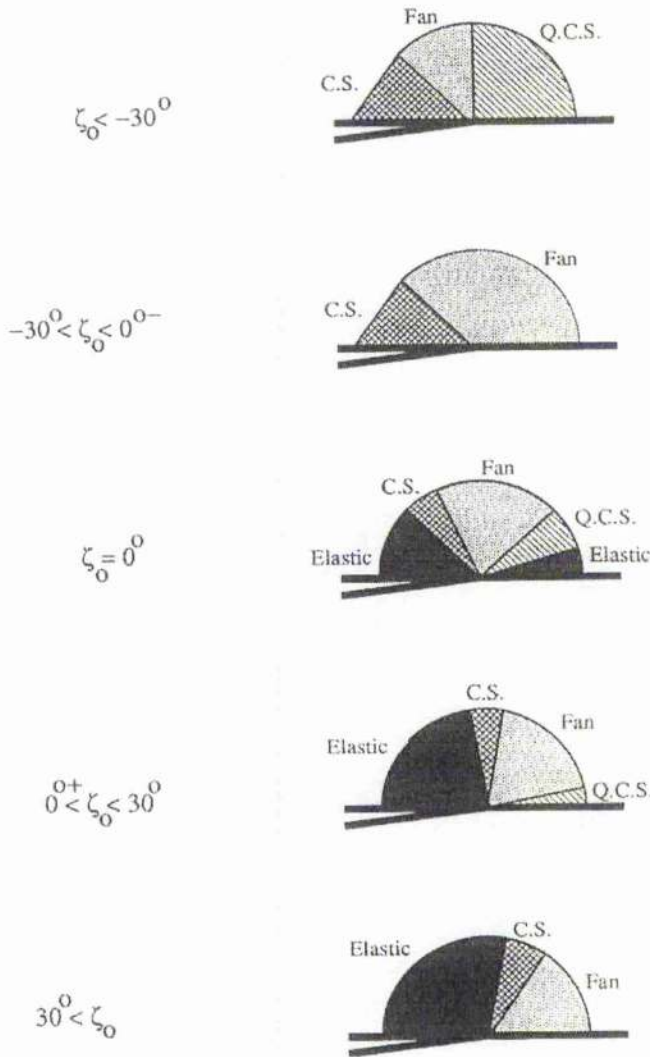
Fig 3.2: Slip lines are based on solutions with $\epsilon = 0.07796$ for cases with $\zeta_o > 0$ and with $\epsilon = -0.07923$ for cases with $\zeta_o \leq 0$ (Zywicz and Parks, 1992).
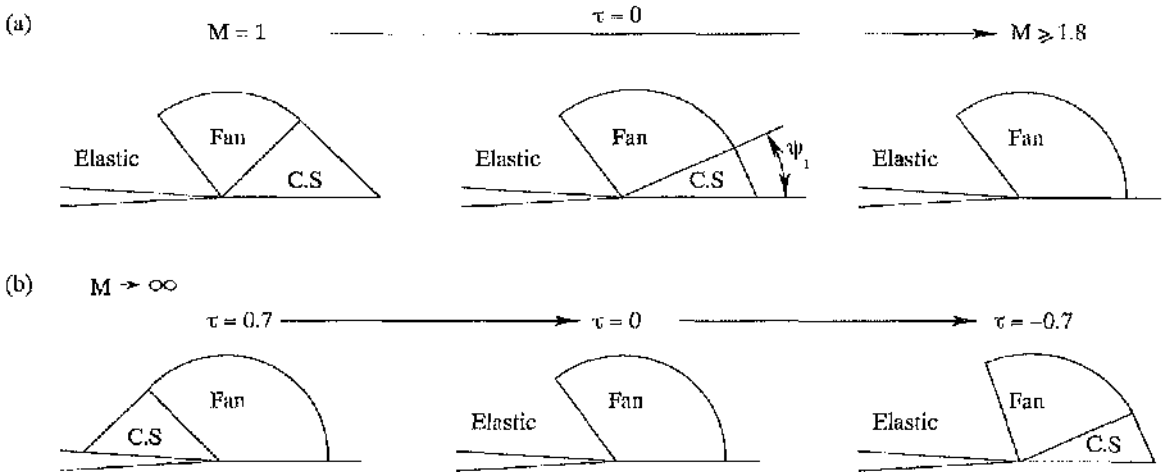
Fig 3.3: Slip line fields for an interface crack between elastically matched but plastically mismatched solids, showing the effect of (a) strength mismatch, M, and (b) normalized second order term $\tau = T/\sigma_o^{(1)}$ (Kim et. al, 1997).
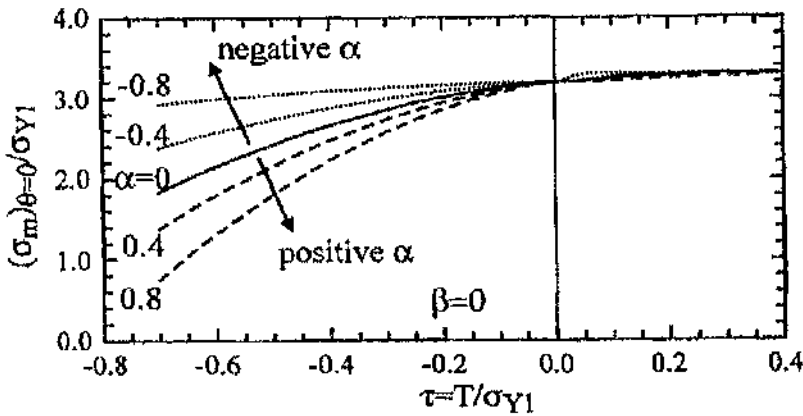
Fig 3.4: Effect of the non singular term (T-stress) on interfacial crack tip constraint, $\sigma_m(0)/\sigma_o^{(1)}$ (Kim et. al, 1997).
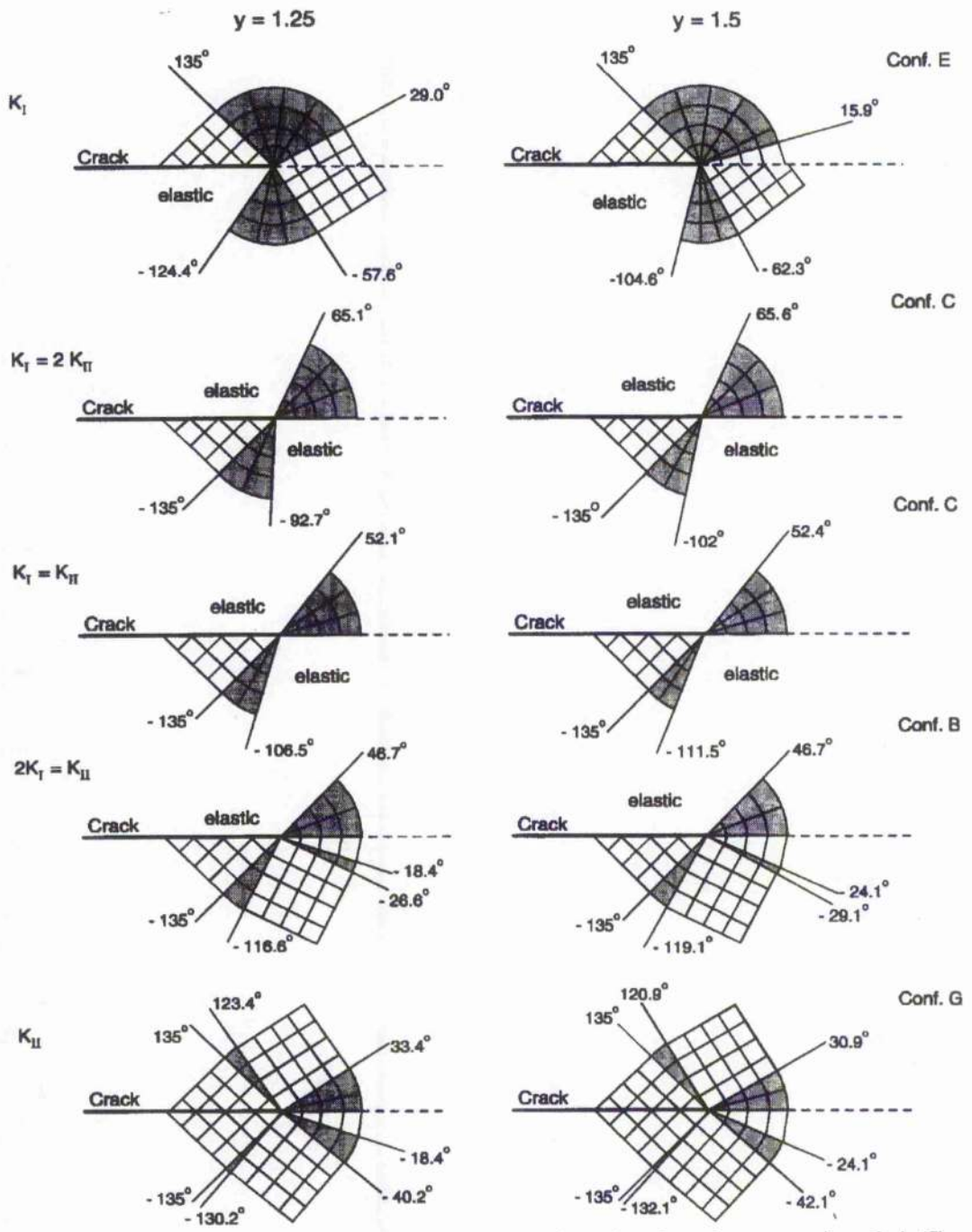
Fig 3.5: Slip line fields for interfacial crack tip in strength mismatched solids (Sham et. al, 1999).
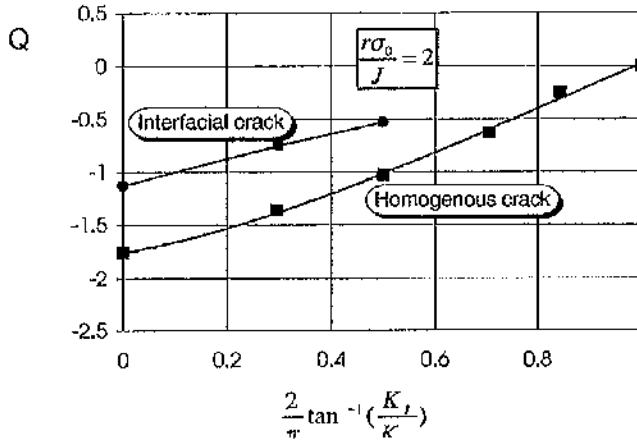
Fig 3.6: Effect of remote load mode mixity on the constraint parameter in the plane of maximum principal stress (Li, 1998).
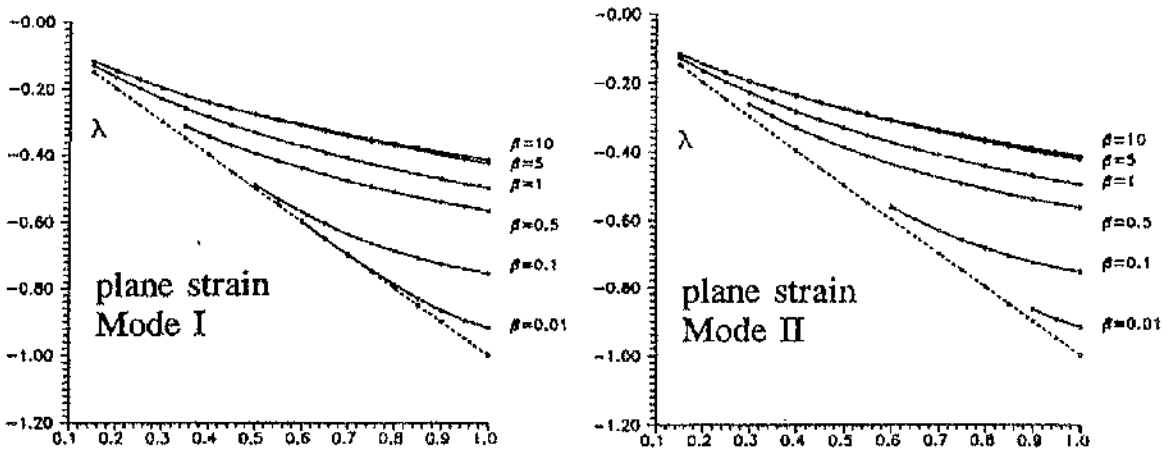
Fig 3.7: Dependence of singularity on β_{chao} and N (Chao et al., 1993).
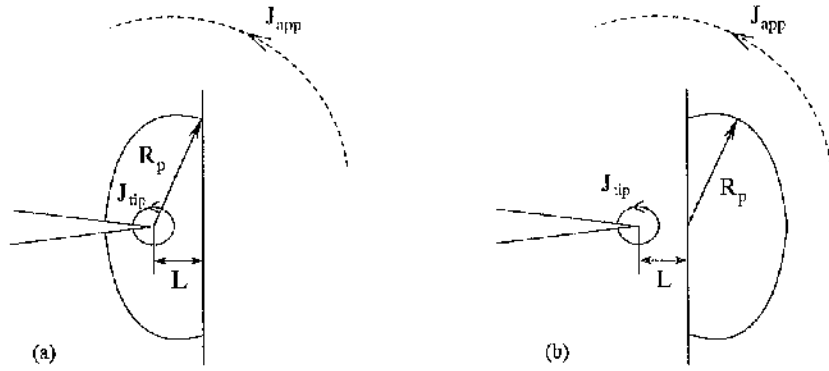
Fig 3.8: Crack approaching an interface between elastically similar but plastically dissimilar materials when crack is in (a) a plastic solid, approaching an elastic solid and (b) an elastic solid, approaching a plastic solid.
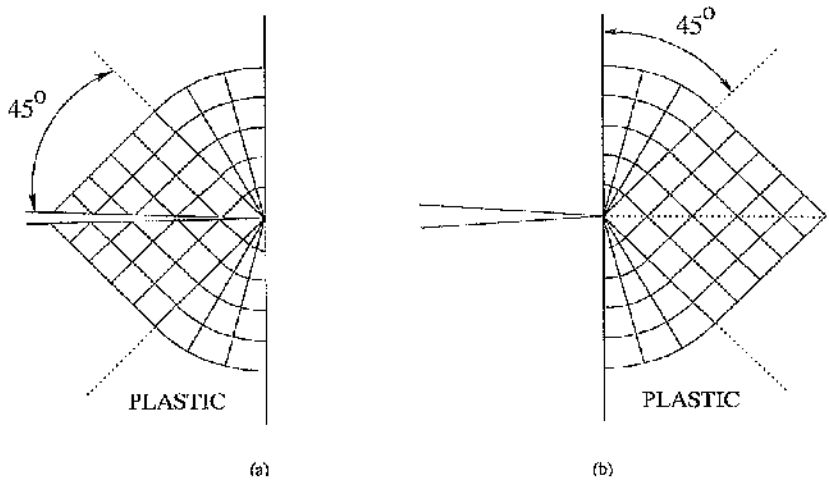
Fig 3.9: Slip line fields when crack is in (a) a plastic solid and (b) an elastic solid (He et. al, 1992; Stahle and Shih , 1992).
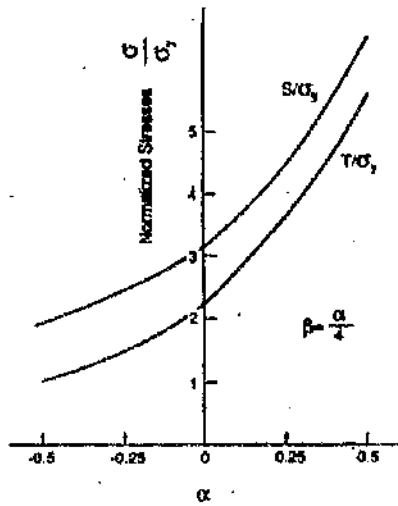
Fig 3.10: Hydrostatic stress, S, and radial stress T ahead of crack (He et. al, 1992).

Elastic Analysis of a Crack Normal to an Interface

In contained yielding, the non-singular term of the outer elastic field has been shown to determine the constraint of the homogeneous problem (Betegón and Hancock, 1991; Du and Hancock, 1991; O'Dowd and Shih, 1991) and affect the constraint for an interface crack (Kim et. al, 1997). In order to determine the constraint effects for a crack normal to the interface between mismatched solids in contained yielding, the first two terms of the linear elastic stress field are developed using eigenvalue expansions. The strength of the singularity of the leading term is determined as a function of the elastic mismatch. The associated angular functions and the second order term in the asymptotic expansion are obtained for symmetric (mode I) and anti-symmetric (mode II) loading. Full field analysis is performed to obtain the second order non-singular term for two geometries of technological significance. The geometries include a thin cracked film on a substrate and a thin cracked film between two substrates.

4.1 Asymptotic analysis

A crack normal to the interface between two elastically mismatched homogeneous, isotropic solids is considered. The bonded materials are represented by superscript, k, ($k = 1$, 2), such that $G^{(k)}$ and $\nu^{(k)}$ are the elastic constants shear modulus and Poisson's ratio respectively. The ratio of the shear modulii ($G^{(1)}/G^{(2)}$) is denoted by Ω. The geometry is defined using both Cartesian (x, y) and polar (r, θ) co-ordinate systems with the origin located at the crack tip as shown in Fig. 4.1. The material interface lies along the plane $\theta = \pm\pi/2$ and the crack lies normal to the interface along the plane $\theta = \pm\pi$ such that material 1 is divided into two

disconnected regions by the crack. Without loss of generality the upper half ($0 \leq \theta \leq \pi$) of the geometry can be considered, allowing the solution to be extended to the lower half, symmetrically or anti-symmetrically about the $\theta - 0$ plane. In order to determine the crack tip stress field, following the eigenvalue expansion method described by Williams (1957) the solution of the bi-harmonic equations in each material is taken to be:

$$\Phi^{(k)}(r, \theta) = r^{\lambda+1} F^{(k)}(\theta) \tag{4.1}$$

where

$$
\begin{aligned}
F^{(k)}(\theta) \quad = \quad & \Big[A^{(k)} \sin(\lambda + 1)\theta + B^{(k)} \cos(\lambda + 1)\theta \\
& + C^{(k)} \sin(\lambda - 1)\theta + D^{(k)} \cos(\lambda - 1)\theta \Big]
\end{aligned}
\tag{4.2}
$$

and $A^{(k)}$, $B^{(k)}$, $C^{(k)}$ and $D^{(k)}$ are constants which depend on λ and the type of loading. For mode I, symmetry about $\theta = 0$ requires that $\Phi^{(2)}$ is an even function of θ. As a result $A^{(2)}$ and $C^{(2)}$ are zero. For mode II loading, $B^{(2)}$ and $D^{(2)}$ are zero such that $\Phi^{(2)}$ is antisymmetric. In both case there are 6 unknown coefficients.

To ensure continuity of tractions along the interface, at all radial distances both $\Phi^{(1)}$ and $\Phi^{(2)}$ are taken to be the same function of r. The stress fields in cylindrical co-ordinates can then be written as:

$$\sigma_{rr}^{(k)} = r^{\lambda-1} \left[\frac{\partial^2 F^{(k)}}{\partial \theta^2} + (\lambda + 1) F^{(k)}(\theta) \right] = r^{\lambda-1} \tilde{\sigma}_{rr}^{(k)}(\theta) \tag{4.3}$$

$$\sigma_{\theta\theta}^{(k)} = r^{\lambda-1} \left[\lambda(\lambda + 1) F^{(k)}(\theta) \right] = r^{\lambda-1} \tilde{\sigma}_{\theta\theta}^{(k)}(\theta) \tag{4.4}$$

$$\sigma_{r\theta}^{(k)} = r^{\lambda-1} \left[-\lambda \frac{\partial F^{(k)}}{\partial \theta} \right] = r^{\lambda-1} \tilde{\sigma}_{r\theta}^{(k)}(\theta) \tag{4.5}$$

In plane strain, the radial and hoop displacement, $u_r^{(k)}$ and $u_\theta^{(k)}$, become:

$$u_r^{(k)} = \frac{r^\lambda}{2G^{(k)}} \quad \left[-(\lambda+1)F^{(k)}(\theta) \right.$$
$$\left. +4(1-\nu^{(k)})\left(C^{(k)}\sin(\lambda-1)\theta + D^{(k)}\cos(\lambda-1)\theta\right) \right] \qquad (4.6)$$

$$u_\theta^{(k)} = \frac{r^\lambda}{2G^{(k)}} \quad \left[-\frac{\partial F^{(k)}}{\partial\theta} \right.$$
$$\left. -4(1-\nu^{(k)})\left(C^{(k)}\cos(\lambda-1)\theta - D^{(k)}\sin(\lambda-1)\theta\right) \right] \qquad (4.7)$$

The boundary conditions of a traction free crack surface combined with continuity of tractions across the interface give rise to a set of 6 homogeneous equations for both mode I and mode II loading:

$$\sigma_{\theta\theta}^{(1)}(\pi) = 0 \qquad (4.8)$$

$$\sigma_{r\theta}^{(1)}(\pi) = 0 \qquad (4.9)$$

$$\sigma_{\theta\theta}^{(1)}(\pi/2) = \sigma_{\theta\theta}^{(2)}(\pi/2) \qquad (4.10)$$

$$\sigma_{r\theta}^{(1)}(\pi/2) = \sigma_{r\theta}^{(2)}(\pi/2) \qquad (4.11)$$

$$u_r^{(1)}(\pi/2) = u_r^{(2)}(\pi/2) \qquad (4.12)$$

$$u_\theta^{(1)}(\pi/2) = u_\theta^{(2)}(\pi/2) \qquad (4.13)$$

4.1.1   Structure of the mode I crack tip field

For mode I loading, symmetry about $\theta = 0$ requires that Φ_2 should be an even function of θ. As a result A_2 and C_2 are zero. Applying the boundary conditions to Eqs. (4.3)-(4.7) gives a

set of 6 homogeneous equations:

$$\left[C^I\right] \left[A^{(1)}\ B^{(1)}\ C^{(1)}\ D^{(1)}\ B^{(2)}\ D^{(2)}\right]^T = 0 \tag{4.14}$$

where,

$$C^I = \left\{ \begin{array}{l} \begin{bmatrix} \sin \pi\lambda & \cos \pi\lambda & \sin \pi\lambda \\[2mm] -(\lambda+1)\cos \pi\lambda & (\lambda+1)\sin \pi\lambda & -(\lambda-1)\cos \pi\lambda \\[2mm] \cos \frac{\pi\lambda}{2} & -\sin \frac{\pi\lambda}{2} & -\cos \frac{\pi\lambda}{2} \\[2mm] -(\lambda+1)\sin \frac{\pi\lambda}{2} & -(\lambda+1)\cos \frac{\pi\lambda}{2} & (\lambda-1)\sin \frac{\pi\lambda}{2} \\[2mm] (\lambda+1)\sin \frac{\pi\lambda}{2} & (\lambda+1)\cos \frac{\pi\lambda}{2} & -(P+(\lambda-1))\sin \frac{\pi\lambda}{2} \\[2mm] (\lambda+1)\cos \frac{\pi\lambda}{2} & (\lambda+1))\sin \frac{\pi\lambda}{2} & -(P-(\lambda+1))\cos \frac{\pi\lambda}{2} \end{bmatrix} \cdots \\[20mm] \cdots \begin{bmatrix} \cos \pi\lambda & 0 & 0 \\[2mm] (\lambda-1)\sin \pi\lambda & 0 & 0 \\[2mm] \sin \frac{\pi\lambda}{2} & \sin \frac{\pi\lambda}{2} & -\sin \frac{\pi\lambda}{2} \\[2mm] (\lambda-1)\cos \frac{\pi\lambda}{2} & (\lambda+1)\cos \frac{\pi\lambda}{2} & -(\lambda-1)\cos \frac{\pi\lambda}{2} \\[2mm] -(P+(\lambda-1))\cos \frac{\pi\lambda}{2} & -\Omega(\lambda+1)\cos \frac{\pi\lambda}{2} & \Omega(Q+(\lambda-1))\cos \frac{\pi\lambda}{2} \\[2mm] (P-(\lambda+1))\sin \frac{\pi\lambda}{2} & -\Omega(\lambda+1)\sin \frac{\pi\lambda}{2} & -\Omega(Q-(\lambda+1))\sin \frac{\pi\lambda}{2} \end{bmatrix} \end{array} \right. \tag{4.15}$$

and $P = 4(1 - \nu^{(1)})$ and $Q = 4(1 - \nu^{(2)})$. For a non-trivial solution $Det\left[C^I\right] = 0$ which gives rise to a characteristic equation. In the present work elastic deformation of both the materials is taken to be incompressible ($\nu^{(1)} = \nu^{(2)} = 0.5$) which simplifies the characteristic

equation to:

$$\left[(\Omega - 1)(2\lambda^2 - 1) + (\Omega + 1)\cos(\pi\lambda)\right]\sin(\pi\lambda) = 0 \qquad (4.16)$$

The solution gives a series of eigenvalues, λ. The strain energy of the region at the crack tip enclosed within radius r is given by:

$$S.E = \int_0^r w.2\pi r \, dr \qquad (4.17)$$

where the strain energy density, $w = \int_0^\epsilon \sigma_{ij} \, d\epsilon_{ij}$. The r-dependence of strain energy density thus can be described as:

$$w \sim r^{2(\lambda - 1)} \qquad (4.18)$$

Substituting in the expression for strain energy:

$$S.E \sim \int_0^r r^{2(\lambda-1)} r \, dr$$

$$\sim r^{2\lambda} \qquad (4.19)$$

Thus, for strain energy at the crack tip to be finite, positive eigenvalues ($\lambda > 0$) are considered. Singular terms arise when $\lambda < 1$ while terms for which $\lambda \geq 1$ are finite or disappear at the crack tip. The smallest positive value of λ depends on the ratio of the shear modulii of the two materials, Ω, as shown in Fig. 4.2. Substituting valid value of λ and solving the Eq. (4.14), gives the corresponding unknown coefficients. The coefficients for mode 1 loading are presented in Tables. 4.1-4.3 which allow $F_k(\theta)$ to be determined in terms of an arbitrary constant. The angular functions ($\tilde{\sigma}_{rr}(\theta)$, $\tilde{\sigma}_{\theta\theta}(\theta)$ and $\tilde{\sigma}_{r\theta}(\theta)$) can be determined by Eqs. (4.3)-(4.5). These angular functions are shown graphically in Figs. 4.3 and 4.4.

Ω	λ	A	B	C	D
0.05	0.589	0.257	0.0617	-0.0814	0.5484
0.1	0.584	0.247	0.0777	-0.0728	0.569
0.25	0.568	0.215	0.125	-0.050	0.636
0.5	0.543	0.153	0.201	-0.021	0.753
1	0.5	0	0.333	0	1
2	0.433	-0.361	0.516	-0.065	1.486
4	0.350	-1.094	0.647	-0.400	2.297
10	0.244	-2.820	0.410	-1.600	3.836
20	0.178	-4.774	-0.292	-3.247	5.320

Table 4.1: Coefficients for the material in the angular span $\pi/2 \geq \theta \geq \pi$.

Ω	λ	A	B	C	D
0.05	0.589	0	0.2585	0	1
0.1	0.584	0	0.263	0	1
0.25	0.568	0	0.275	0	1
0.5	0.543	0	0.296	0	1
1	0.5	0	0.333	0	1
2	0.433	0	0.395	0	1
4	0.350	0	0.481	0	1
10	0.244	0	0.608	0	1
20	0.178	0	0.697	0	1

Table 4.2: Coefficients for the material in the angular span $-\pi/2 \geq \theta \geq \pi/2$.

4.1.2 Structure of the mode II crack tip field

The antisymmetry of mode II loading about $\theta = 0$ requires $B^{(2)}$ and $D^{(2)}$ to be zero such that $\Phi^{(2)}$ is antisymmetric. Applying the boundary conditions described by Eqs. (4.8)-(4.13). A

Ω	λ	A	B	C	D
0.05	0.589	-0.257	0.0617	0.0814	0.5484
0.1	0.584	-0.247	0.0777	0.0728	0.569
0.25	0.568	-0.215	0.125	0.050	0.636
0.5	0.543	-0.153	0.201	0.021	0.753
1	0.5	0	0.333	0	1
2	0.433	0.361	0.516	0.065	1.486
4	0.350	1.094	0.647	0.400	2.297
10	0.244	2.820	0.410	1.600	3.836
20	0.178	4.774	-0.292	3.247	5.320

Table 4.3: Coefficients for the material in the angular span $-\pi \geq \theta \geq -\pi/2$.

system of 6 homogeneous equations is obtained:

$$\left[C^{II} \right] \left[A^{(1)}\ B^{(1)}\ C^{(1)}\ D^{(1)}\ A^{(2)}\ C^{(2)} \right]^{T} = 0 \qquad (4.20)$$

where

$$
C^{II} = \begin{bmatrix}
\sin \pi\lambda & \cos \pi\lambda & \sin \pi\lambda & \cos \pi\lambda & 0 & 0 \\[4pt]
-(\lambda+1)\cos \pi\lambda & (\lambda+1)\sin \pi\lambda & -(\lambda-1)\cos \pi\lambda & (\lambda-1)\sin \pi\lambda & 0 & 0 \\[4pt]
\cos \tfrac{\pi\lambda}{2} & -\sin \tfrac{\pi\lambda}{2} & -\cos \tfrac{\pi\lambda}{2} & \sin \tfrac{\pi\lambda}{2} & -\cos \tfrac{\pi\lambda}{2} & \cos \tfrac{\pi\lambda}{2} \\[4pt]
-(\lambda+1)\sin \tfrac{\pi\lambda}{2} & -(\lambda+1)\cos \tfrac{\pi\lambda}{2} & (\lambda-1)\sin \tfrac{\pi\lambda}{2} & (\lambda-1)\cos \tfrac{\pi\lambda}{2} & (\lambda+1)\sin \tfrac{\pi\lambda}{2} & -(\lambda-1)\sin \tfrac{\pi\lambda}{2} \\[4pt]
(\lambda+1)\sin \tfrac{\pi\lambda}{2} & (\lambda+1)\cos \tfrac{\pi\lambda}{2} & -(P+(\lambda-1))\sin \tfrac{\pi\lambda}{2} & -(P+(\lambda-1))\cos \tfrac{\pi\lambda}{2} & -\Omega(\lambda+1)\sin \tfrac{\pi\lambda}{2} & \Omega(Q+(\lambda-1))\sin \tfrac{\pi\lambda}{2} \\[4pt]
-(\lambda+1)\cos \tfrac{\pi\lambda}{2} & (\lambda+1))\sin \tfrac{\pi\lambda}{2} & -(P-(\lambda+1))\cos \tfrac{\pi\lambda}{2} & (P-(\lambda+1))\sin \tfrac{\pi\lambda}{2} & \Omega(\lambda+1)\cos \tfrac{\pi\lambda}{2} & \Omega(Q-(\lambda+1))\cos \tfrac{\pi\lambda}{2}
\end{bmatrix}
\tag{4.21}
$$

Non-trivial solution of the Eq. 4.20 requires that $Det\left[C^{II}\right] = 0$, and gives rise to the same characteristic equation as obtained for analysis of mode I field. Hence, the same singularity (Fig. 4.2) can be applied to mode II. For the smallest valid value of λ the corresponding unknown coefficients and hence the angular functions can be obtained using equations summarised in Eq. (4.20). The coefficients for mode II loading are tabulated in Tables. 4.4-4.5. The angular functions are shown in Figs. 4.5-4.6 for elastic mismatch of 0.1 and 10.

Ω	λ	A	B	C	D
0.05	0.589	-0.548	-0.081	0.239	-0.994
0.1	0.584	-0.569	-0.073	0.296	-0.942
0.25	0.568	-0.636	-0.050	0.454	-0.783
0.5	0.543	-0.753	-0.021	0.679	-0.517
1	0.5	-1	0	1	0
2	0.433	-1.486	-0.065	1.305	0.913
4	0.350	-2.297	-0.400	1.345	2.275
10	0.244	-3.836	-1.598	0.674	4.637
20	0.178	-5.320	-3.247	-0.418	6.844

Table 4.4: Coefficients for the material in the angular span $\pi/2 \geq \theta \geq \pi$.

4.1.3 Stress function of the distance independent term under mode 1 and mode II loading

The next and only other eigenvalue for which the stresses are non-zero at the crack tip is $\lambda = 1$. In contrast to the leading eigenvalue, this eigenvalue is independent of elastic mismatch, and gives rise to a second order term in stresses which is independent of distance. Substituting $\lambda = 1$, equation. 4.14 becomes:

$$
\begin{bmatrix}
0 & -1 & 0 & -1 & 0 & 0 \\
2 & 0 & 0 & 0 & 0 & 0 \\
0 & -1 & 0 & 1 & 1 & -1 \\
-2 & 0 & 0 & 0 & 0 & 0 \\
2 & 0 & -P & 0 & 0 & 0 \\
0 & 2 & 0 & P-2 & -2\Omega & -\Omega(Q-2)
\end{bmatrix}
\begin{bmatrix}
A^{(1)} \\
B^{(1)} \\
C^{(1)} \\
D^{(1)} \\
B^{(2)} \\
D^{(2)}
\end{bmatrix} = 0
\qquad (4.22)
$$

Ω	λ	A	B	C	D
0.05	0.589	-1	0	1	0
0.1	0.584	-1	0	1	0
0.25	0.568	-1	0	1	0
0.5	0.543	-1	0	1	0
1	0.5	-1	0	1	0
2	0.433	-1	0	1	0
4	0.350	-1	0	1	0
10	0.244	-1	0	1	0
20	0.178	-1	0	1	0

Table 4.5: Coefficients for the material in the angular span $-\pi/2 \geq \theta \geq \pi/2$.

The corresponding mode I stress functions for the distance independent term can be derived from the boundary conditions to be:

$$
\Phi^I_T =
\begin{cases}
Dr^2 \left[\left(\frac{(\Omega - \nu^{(1)}) - 2\Omega(1 - \nu^{(2)})}{\Omega - \nu^{(1)}} \right) \cos 2\theta + 1 \right]; & 0 \leq \theta \leq \pi/2, \\[2ex]
Dr^2 \Omega \left(\frac{1 - \nu^{(2)}}{\Omega - \nu^{(1)}} \right) [1 - \cos 2\theta]; & \pi/2 \leq \theta \leq \pi
\end{cases}
\tag{4.23}
$$

where D is an arbitrary constant. To determine the stress function for the distance independent term under mode II loading $\lambda = 1$ is substituted in Eq. (4.20) giving:

$$
\begin{bmatrix}
0 & -1 & 0 & -1 & 0 & 0 \\
2 & 0 & 0 & 0 & 0 & 0 \\
0 & -1 & 0 & 1 & 0 & 0 \\
-2 & 0 & 0 & 0 & 2 & 0 \\
2 & 0 & -P & 0 & -2\Omega & Q\Omega \\
0 & 2 & 0 & P-2 & 0 & 0
\end{bmatrix}
\begin{bmatrix}
A^{(1)} \\
B^{(1)} \\
C^{(1)} \\
D^{(1)} \\
A^{(2)} \\
C^{(2)}
\end{bmatrix}
= 0
\tag{4.24}
$$

Ω	λ	A	B	C	D
0.05	0.589	0.548	-0.081	-0.239	-0.994
0.1	0.584	0.569	-0.073	-0.296	-0.942
0.25	0.568	0.636	-0.050	-0.454	-0.783
0.5	0.543	0.753	-0.021	-0.679	-0.517
1	0.5	1	0	-1	0
2	0.433	1.486	-0.065	-1.305	0.913
4	0.350	2.297	-0.400	-1.345	2.275
10	0.244	3.836	-1.598	-0.674	4.637
20	0.178	5.320	-3.247	0.418	6.844

Table 4.6: Coefficients for the material in the angular span $-\pi \geq \theta \geq -\pi/2$.

The solution of these equations simplifies to give the stress function for the second order term to be:

$$\Phi_T^{II} = 0; \quad 0 \leq \theta \leq \pi \tag{4.25}$$

The angular functions can be obtained from the stress functions. Using the Cartesian coordinate system distance independent stresses can be written as:

$$[\sigma_T] = \begin{cases} T \begin{bmatrix} 1 & 0 \\ 0 & \eta \end{bmatrix} & 0 \leq \theta \leq \pi/2, \\[3mm] T \begin{bmatrix} 1 & 0 \\ 0 & 0 \end{bmatrix} & \pi/2 \leq \theta \leq \pi, \end{cases} \tag{4.26}$$

where,

$$\eta = \frac{\Omega \nu^{(2)} - \nu^{(1)}}{\Omega(1 - \nu^{(2)})} \tag{4.27}$$

and T is an arbitrary constant with the dimensions of stress. ϵ_T ensures the compatibility condition at $\theta = \pi/2$:

$$\epsilon_{yy}^{(1)} = \epsilon_{yy}^{(2)} \tag{4.28}$$

In material 1, the second order term is a simple uniaxial stress parallel to the crack flanks. However, in material 2 the stress system is bi-axial, the y-component being related to the x-component by a factor η. For a homogeneous material ($\Omega = 1$), η becomes zero and the higher order term reduces to the second term in the Williams expansion (Williams, 1957) which Rice (1974) has denoted the T-stress. The Cartesian strain field corresponding to the distance independent stresses can be written as:

$$\epsilon_{xx} = \begin{cases} \frac{1}{2G^{(2)}}\left((1-\nu^{(2)})\sigma_{xx} - \nu^{(2)}\sigma_{yy}\right) = \frac{T}{2G^{(2)}}\left((1-\nu^{(2)}) - \nu^{(2)}\eta\right) & 0 \le \theta \le \pi/2, \\ \frac{1}{2G^{(1)}}(1-\nu^{(1)})\sigma_{xx} = \frac{T}{2G^{(1)}}(1-\nu^{(1)}) & \pi/2 \le \theta \le \pi \end{cases} \tag{4.29}$$

$$\epsilon_{yy} = \begin{cases} \frac{1}{2G_2}\left((1-\nu_2)\sigma_{yy} - \nu_2\sigma_{xx}\right) = -\frac{\nu_1 T}{2G_1} & 0 \le \theta \le \pi/2, \\ \frac{1}{2G_1}(-\nu_1\sigma_{xx}) = -\frac{\nu_1 T}{2G_2\Omega} & \pi/2 \le \theta \le \pi \end{cases} \tag{4.30}$$

Using the strain-displacement relations the Cartesian displacement field can be derived from Eqn. 4.26 to be:

$$u_x^T = \begin{cases} (T/2G^{(2)})\left[1 - \nu^{(2)}(1+\eta)\right]r\cos\theta & 0 \le \theta \le \pi/2, \\ (T/2G^{(1)})(1-\nu^{(1)})r\cos\theta & \pi/2 \le \theta \le \pi \end{cases} \tag{4.31}$$

$$u_y^T = \begin{cases} (T/2G^{(2)})\left[\eta - \nu^{(2)}(1+\eta)\right]r\sin\theta & 0 \le \theta \le \pi/2, \\ (T/2G^{(1)})(-\nu^{(1)})r\sin\theta & \pi/2 \le \theta \le \pi \end{cases} \tag{4.32}$$

In the general case of mixed mode loading, the contribution from mode I and mode II components of the load can be combined and the first two terms of the elastic stress field can be written as:

$$[\sigma] = (2\pi r)^{\lambda-1} \left(K^{I} \left[\tilde{\sigma}^{I}(\theta) \right] + K^{II} \left[\tilde{\sigma}^{II}(\theta) \right] \right) + r^{0} T \left[\tilde{\sigma}_{T}^{I} \right] \tag{4.33}$$

where $\left[\tilde{\sigma}^{I} \right]$ and $\left[\tilde{\sigma}^{II} \right]$ are angular functions of the stress components corresponding to mode I and mode II loading respectively. $\left[\tilde{\sigma}_{T}^{I} \right]$ is the angular function of the higher order term for mode I and mode II loading. K^{I}, K^{II} and T are arbitrary constants. For a homogeneous material ($\Omega = 1$), K^{I} and K^{II} become the linear elastic stress intensity factors (K_{I}, K_{II}) in mode I and mode II loadings.

4.2   Full field analysis

In order to determine the effect of elastic mismatch on the second order term in the crack tip elastic field, full field analysis was performed for two technologically important geometries. The configuration of a thin thermal barrier coating containing a surface crack on a thick substrate was represented by modelling a cracked thin film on a substrate as shown in Fig. 4.7. The figure also shows the second geometry that of a thin cracked lamina between two thick substrates which represents the practical situation of a cracked lamina in a ceramic laminate under plane strain conditions. The axi-symmetric version of the problem represents a cracked fibre embedded in a matrix. The ratio of the thickness of the coating to the thickness of the substrate is 1 : 30 and the ratio of the radius of the fibre to that of the thickness of the matrix is also 1 : 30. The finite element mesh for the cracked coating geometry consists of 980 isoparametric 8-noded elements as shown in Fig. 4.8. The mesh is refined near the crack tip such that the ratio between the size of the first element to the crack size is $3/10^{6}$. The same mesh is used for modelling the laminate geometry by enforcing symmetry about the left edge of the model. Analysis is performed for elastic mismatches in the range 0 to 10

for tensile loading represented by a remote uniform displacement. The stress intensity factor was determined using the radial stress on the crack flanks ($\theta = \pi$):

$$K^I = \lim_{r \to 0} \frac{\sigma_{rr}(r, \pi)}{(2\pi r)^{\lambda-1} \tilde{\sigma}_{rr}(\pi)} \qquad (4.34)$$

Table. 4.7 gives the stress intensity factors normalised by the remote tensile stress, σ^∞, and the crack length, a, as a function of elastic mismatch, Ω.

Ω	λ	$\frac{K(\pi a)^{\lambda-1}}{\sigma^\infty}$ (coating)	$\frac{K(\pi a)^{\lambda-1}}{\sigma^\infty}$ (lamina)
0.05	0.589	0.069	0.036
0.5	0.543	0.575	0.492
1	0.500	1.11	0.995
2	0.433	1.88	1.78
4	0.350	2.90	3.03
10	0.244	5.29	5.68

Table 4.7: The effect of elastic mismatch, Ω, on the stress intensity factor, K.

The non-singular higher order term, T, was also determined numerically from the radial stress on the crack flanks using:

$$T = \lim_{r \to 0} \left[\sigma_{rr}(r, \pi) - K^I (2\pi r)^{\lambda-1} \tilde{\sigma}_{rr}(\pi) \right] \qquad (4.35)$$

At low elastic mismatches both geometries have negative T-stresses as shown in Fig. 4.9, but at large elastic mismatches, T remains compressive in the laminate but becomes positive for the coating. Close approximations to the well known results for an edge crack in a semi-infinite homogeneous solid: $T = -0.51\sigma^\infty$ (Harlin and Willis, 1988) and the centre crack

panel: $T = -\sigma^\infty$ (Inglis, 1913) are recovered for elastically matched solids, $\Omega = 1$. The effect of the second order term on the hoop stress ahead of the crack is shown in Fig. 4.10 as the ratio between the first term and the first two terms. For lower elastic mismatches the effect of the second order term becomes apparent at smaller distance from the crack tip. The effect of the non-singular term on the elastic-plastic crack tip fields is similar to that in homogeneous materials as is shown next in Chapter 5.

4.3 Conclusions

The first two terms in the asymptotic elastic crack tip fields of technologically significant bi-material systems have been obtained using analytical and computational methods. For the leading term, the strength of the singularity and the angular functions depend on mismatch. The second order term is distance independent for all elastic mismatches although the angular functions depend on mismatch. The amplitudes of both the terms depend on loading and geometry. In general the second order term in the stress field in material 2 is biaxial. The biaxiality depends on the elastic mismatch and vanishes for elastically matched solids when the uniaxial second order term in the Williams expansion is recovered. The distance over which the leading term dominates the second order term increases with increasing mismatch (Ω).
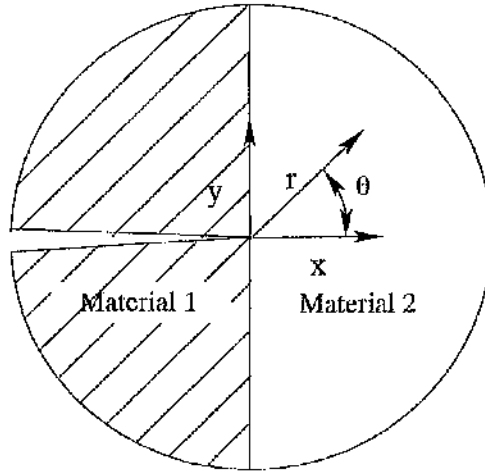
Fig 4.1: Bi-material system.
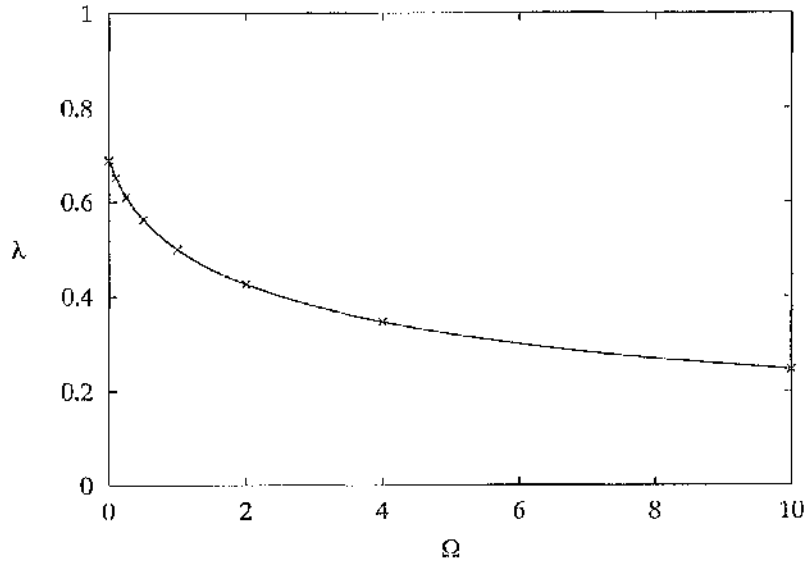
Fig 4.2: The strength of the singularity of the leading term as a function of mismatch.
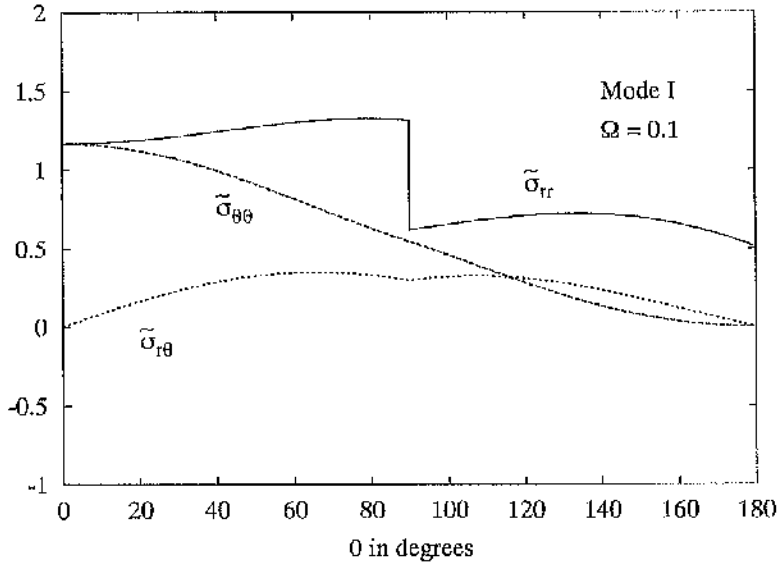
Fig 4.3: Angular functions, $\tilde{\sigma}_{\theta\theta}$, $\tilde{\sigma}_{rr}$ and $\tilde{\sigma}_{r\theta}$ for an elastic mismatch of 0.1
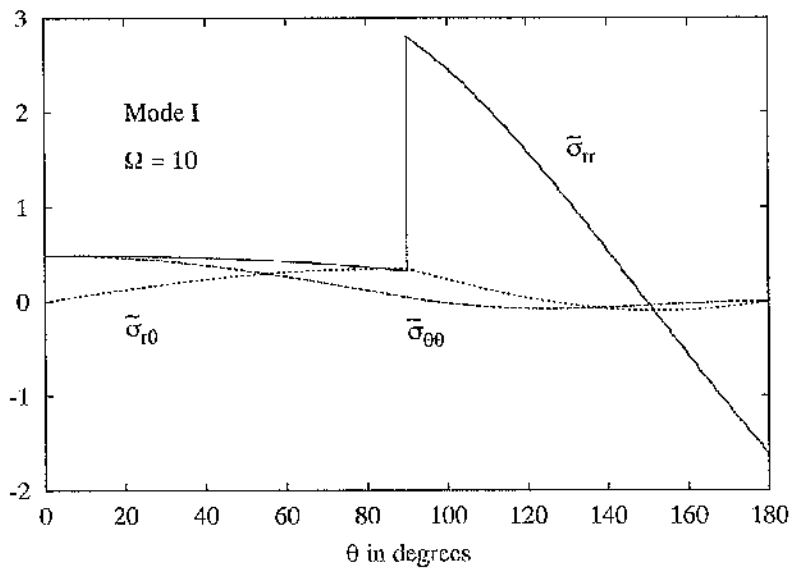
Fig 4.4: Angular functions, $\tilde{\sigma}_{\theta\theta}$, $\tilde{\sigma}_{rr}$ and $\tilde{\sigma}_{r\theta}$ for an elastic mismatch of 10.
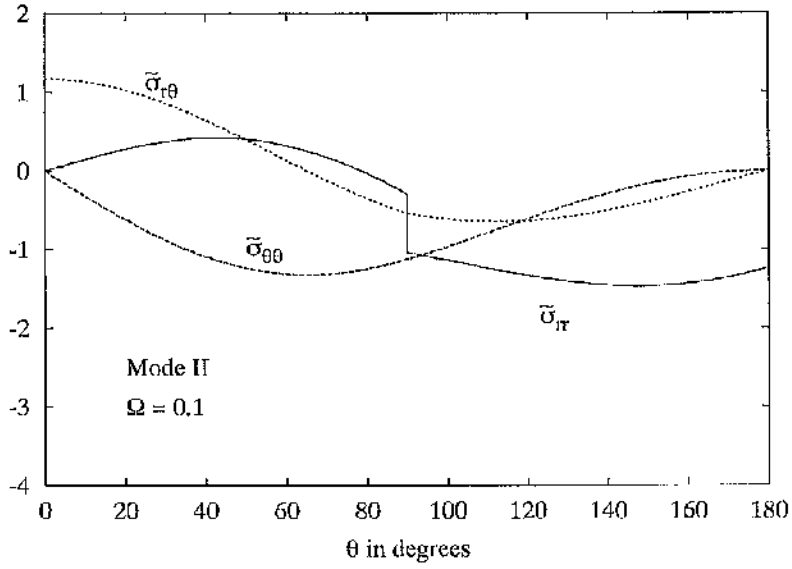
Fig 4.5: Angular functions, $\tilde{\sigma}_{\theta\theta}$, $\tilde{\sigma}_{rr}$ and $\tilde{\sigma}_{r\theta}$ for an elastic mismatch of 0.1

Fig 4.6: Angular functions, $\tilde{\sigma}_{\theta\theta}$, $\tilde{\sigma}_{rr}$ and $\tilde{\sigma}_{r\theta}$ for an elastic mismatch of 10.

(a) Cracked Film   (b) Cracked Lamina
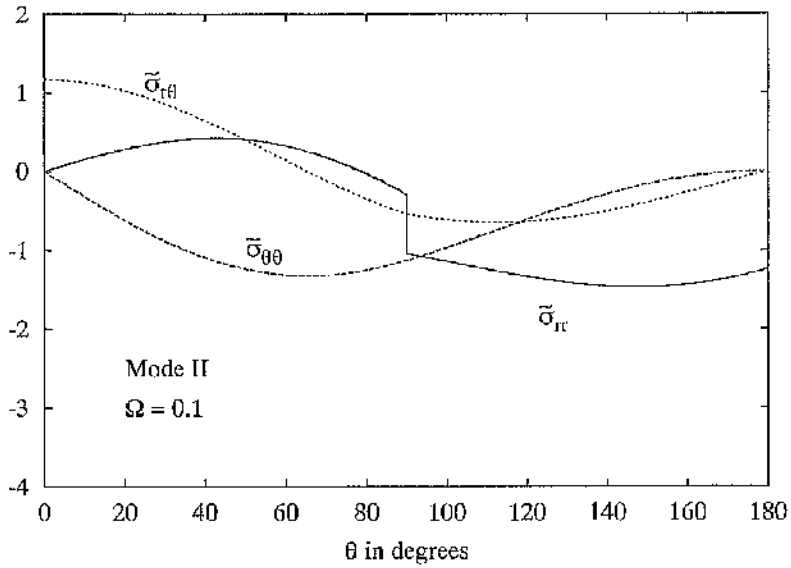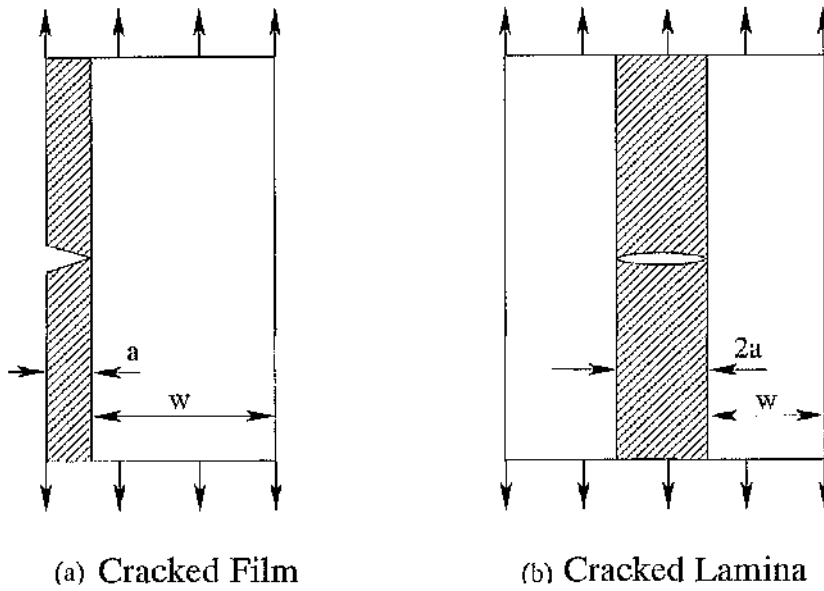
Fig 4.7: Schematic diagrams of the full field geometrics, $w/a - 30$ subjected to remote tensile displacement load.
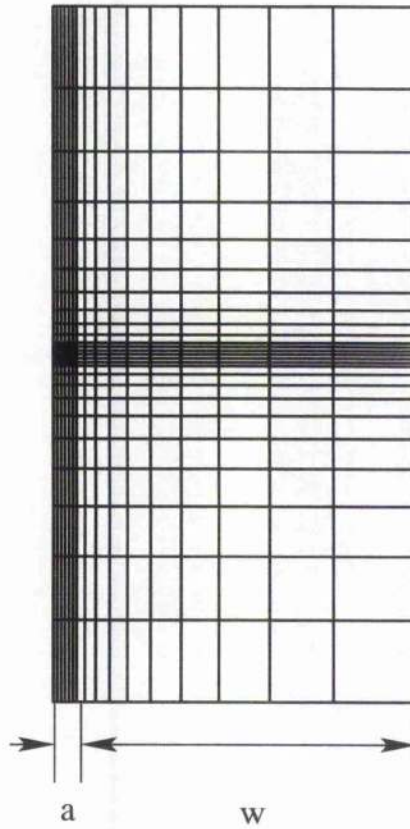
Fig 4.8: Fullfield mesh used for modelling a cracked thin film on a substrate and a lamina between two substrates.
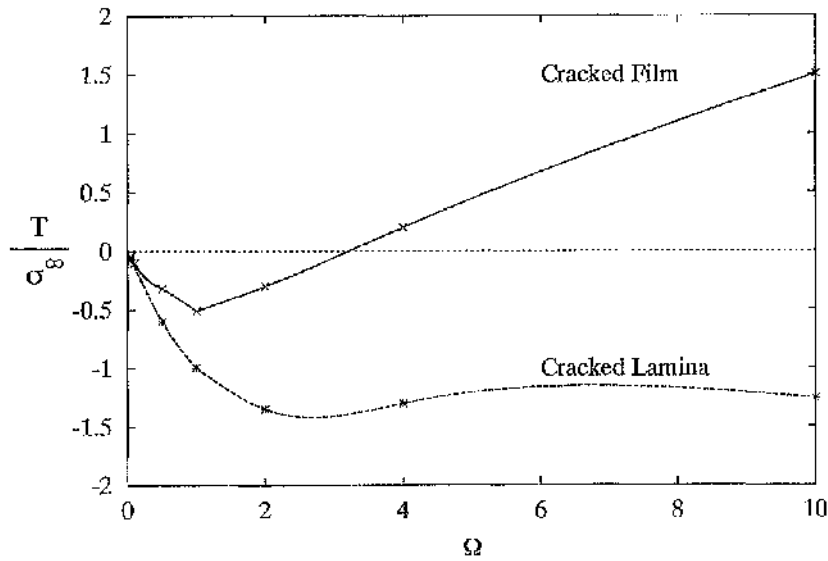
Fig 4.9: The T-stress normalised by the remotely applied stress, σ_{yy}^{∞}, as a function of elastic mismatch.
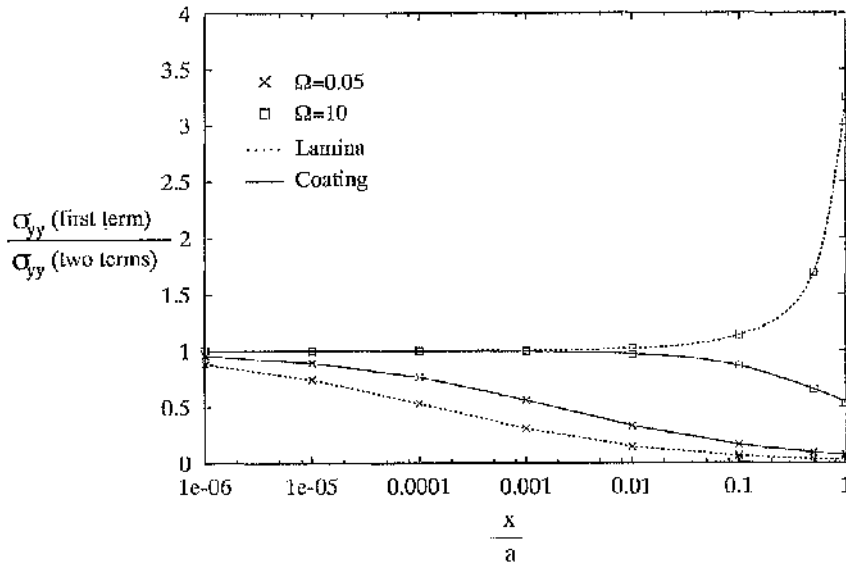
Fig 4.10: The comparative effect of leading term over distances ahead of the crack tip.

A Crack Normal to an Interface: Elastic-Plastic Analytic Solution

Understanding of the mechanism of fracture normal to the interface is essential for failure analysis and design of composite systems. Although the elastic analysis gives a useful description, for larger levels of plasticity elastic-plastic analysis is required. In bi-material systems like hard coatings or laminates which have significant plastic mismatch, insight into the elastic-plastic field can be obtained by taking one of the material as elastic perfectly-plastic while the other is fully elastic. Initially the configuration in which a crack is located in an elastic perfectly-plastic solid (referred as problem A in Fig. 5.1) is considered followed by the case in which the crack is located in a fully elastic material and the material ahead of the crack is elastic perfectly-plastic (problem B). Analytic solution of the elastic-plastic field is developed by representing the angular span at the crack tip as a combination of elastic and plastic sectors using slip line theory.

5.1 Plastic sectors

Within the plastic sectors, slip line field theory (Hill, 1950) allows the stresses to be written in terms of the mean stress σ_m, and ψ, the angle between the positive α slip line direction and the positive x direction:

$$\sigma_{rr} = \sigma_m + k\sin(2\theta - 2\psi)$$

$$\sigma_{\theta\theta} = \sigma_m - k\sin(2\theta - 2\psi) \qquad (5.1)$$

$$\sigma_{r\theta} = k\cos(2\theta - 2\psi)$$

where k is the yield stress in shear. In general both σ_m and ψ are functions of θ. For incompressible deformation $\nu = 1/2$, the yield criterion for plane strain can be simplified to:

$$\frac{3}{4}(\sigma_{\theta\theta} - \sigma_{rr})^2 + 3\sigma_{r\theta}^2 = \sigma_o^2 \tag{5.2}$$

The two dimensional equilibrium equations in cylindrical co-ordinates (r, θ) are:

$$\frac{\partial \sigma_{rr}}{\partial r} + \frac{1}{r}\frac{\partial \sigma_{r\theta}}{\partial \theta} + \frac{\sigma_{rr} - \sigma_{\theta\theta}}{r} = 0 \tag{5.3}$$

$$\frac{\partial \sigma_{r\theta}}{\partial r} + \frac{1}{r}\frac{\partial \sigma_{\theta\theta}}{\partial \theta} + 2\frac{\sigma_{r\theta}}{r} = 0 \tag{5.4}$$

Following an argument of Rice (1982), for finite crack tip stresses, as $r \to 0$, the equilibrium equations reduce to:

$$\sigma_{\theta\theta} - \sigma_{rr} = \frac{\partial \sigma_{r\theta}}{\partial \theta} \tag{5.5}$$

$$\frac{\partial \sigma_{\theta\theta}}{\partial \theta} = -2\sigma_{r\theta} \tag{5.6}$$

Differentiating the yield criterion described in Eq. 5.2 with respect to angle, θ, gives:

$$\frac{3}{2}(\sigma_{\theta\theta} - \sigma_{rr})\frac{\partial}{\partial \theta}(\sigma_{\theta\theta} - \sigma_{rr}) + 6\sigma_{r\theta}\frac{\partial \sigma_{r\theta}}{\partial \theta} = 0 \tag{5.7}$$

Substituting $(\sigma_{\theta\theta} - \sigma_{rr})$ and $\sigma_{r\theta}$ from Eq. 5.5-5.6 gives rise to the condition:

$$-\frac{3}{2}\frac{\partial \sigma_{r\theta}}{\partial \theta}\frac{\partial}{\partial \theta}(\sigma_{\theta\theta} + \sigma_{rr}) = 0 \tag{5.8}$$

In two possible situations the condition in Eq. 5.8 can be satisfied non-trivially:

$$\frac{\partial \sigma_{r\theta}}{\partial \theta} = 0; \qquad \frac{\partial \sigma_m}{\partial \theta} \neq 0 \tag{5.9}$$

$$\frac{\partial \sigma_m}{\partial \theta} = 0; \qquad \frac{\partial \sigma_{r\theta}}{\partial \theta} \neq 0 \tag{5.10}$$

In the first case, substituting $\frac{\partial \sigma_{r\theta}}{\partial \theta} = 0$ in Eq. 5.5 gives:

$$\sigma_{\theta\theta} = \sigma_{rr} \tag{5.11}$$

which reduces the yield criterion to:

$$\sigma_{r\theta}^2 - k^2 = 0 \tag{5.12}$$

Thus, the shear stress component, $\sigma_{r\theta} = +k$. The other stress components can be determined from Eq. 5.6:

$$\frac{\partial \sigma_{\theta\theta}}{\partial \theta} = -2\sigma_{r\theta} = \mp 2k \tag{5.13}$$

which on integration with respect to θ gives:

$$\sigma_{\theta\theta} = \mp 2k\theta + B \tag{5.14}$$

This type of sector which is denoted a centred fan, features a constant shear stress, $\sigma_{r\theta}$, while the mean stress is a linear function of angle, θ. The direction of an α-plane can be radial or tangential. The stresses corresponding to Fig. 5.2(a) are:

$$\begin{aligned}
\sigma_m &= \sigma_m' + 2k(\theta - \theta') \\
\psi &= \frac{\pi}{2} + \theta
\end{aligned} \tag{5.15}$$

or corresponding to Fig. 5.2(b):

$$\begin{aligned}
\sigma_m &= \sigma_m' + 2k(\theta' - \theta) \\
\psi &= \theta
\end{aligned} \tag{5.16}$$

where, $\sigma_m{}'$ and θ' are constants. In the second case, the mean stress is independent of θ and the slip lines are straight giving rise to a constant stress sector, the stresses being described by:

$$\sigma_m, \sigma_{xx}, \sigma_{yy}, \sigma_{zz} = \text{constant}$$

$$\psi = \text{constant} \tag{5.17}$$

5.2   Elastic sector

Elastic sectors adjoining plastic sectors under certain restrictions have finite stresses at the crack tip subject to certain restrictions (Sham et. al, 1999). In the elastic sectors compatibility must be satisfied along with the plane strain equilibrium equations:

$$\left(\frac{\partial^2}{\partial r^2} + \frac{1}{r}\frac{\partial}{\partial r} + \frac{1}{r^2}\frac{\partial^2}{\partial \theta^2} \right)(\sigma_{rr} + \sigma_{\theta\theta}) = 0 \tag{5.18}$$

For finite crack tip stresses at asymptotic distance, $r \to 0$, the compatibility equation reduces to:

$$\frac{\partial^2 \sigma_{rr}}{\partial \theta^2} + \frac{\partial^2 \sigma_{\theta\theta}}{\partial \theta^2} = 0 \tag{5.19}$$

Integrating with respect to θ twice gives:

$$\sigma_{\theta\theta} = E_3\theta + E_4 - \sigma_{rr} \tag{5.20}$$

Substituting in Eq. 5.5 and 5.6 gives:

$$\frac{\partial \sigma_{r\theta}}{\partial \theta} + 2\sigma_{rr} - E_3\theta - E_4 = 0 \tag{5.21}$$

and

$$E_3 - \frac{\partial \sigma_{rr}}{\partial \theta} + 2\sigma_{r\theta} = 0 \tag{5.22}$$

Eliminating $\sigma_{r\theta}$ gives a partial differential equation:

$$\frac{\partial^2 \sigma_{rr}}{\partial \theta^2} + 4\sigma_{rr} - 2E_3\theta - 2E_4 = 0 \tag{5.23}$$

The homogeneous part of the differential equation is:

$$\frac{\partial^2 \sigma_{rr}}{\partial \theta^2} + 4\sigma_{rr} = 0 \tag{5.24}$$

which has the homogeneous solution:

$$\sigma_{rr} = E_1 \sin 2\theta + E_2 \cos 2\theta \tag{5.25}$$

and the particular solution:

$$\sigma_{rr} = \frac{1}{2}(E_3\theta + E_4) \tag{5.26}$$

The general solution is the sum of the homogeneous and particular solutions:

$$\sigma_{rr} = E_1 \sin 2\theta + E_2 \cos 2\theta + \frac{1}{2}(E_3\theta + E_4) \tag{5.27}$$

The other stress components can be obtained in a similar way. The stresses in the elastic sector are:

$$\sigma_{rr} = E_1 \sin 2\theta + E_2 \cos 2\theta + \frac{1}{2}(E_3\theta + E_4) \tag{5.28}$$

$$\sigma_{\theta\theta} = -E_1 \sin 2\theta - E_2 \cos 2\theta + \frac{1}{2}(E_3\theta + E_4) \tag{5.29}$$

$$\sigma_{r\theta} = E_1 \cos 2\theta - E_2 \sin 2\theta - \frac{E_3}{4} \tag{5.30}$$

where E_1, E_2, E_3 and E_4 are determined from the appropriate boundary conditions. In elastic-plastic crack tip fields elastic sectors usually appear at the crack flank as shown in

Fig. 5.3. If the angular span of the elastic sector is ϕ_o, applying the boundary condition of a traction free crack face $(\sigma_{rr}(\pi) = \sigma_{r\theta}(\pi) = 0)$ reduces the stress equations to:

$$\sigma_{rr} = C(2\theta - 2\pi + \sin 2\theta) + D(1 + \cos 2\theta) \tag{5.31}$$

$$\sigma_{\theta\theta} = C(2\theta - 2\pi - \sin 2\theta) + D(1 - \cos 2\theta) \tag{5.32}$$

$$\sigma_{r\theta} = C(\cos 2\theta - 1) - D \sin 2\theta \qquad (\pi - \phi_o \leq \theta \leq \pi) \tag{5.33}$$

where the coefficients C and D can be be determined using the tractions, $\sigma_{\theta\theta} = H$ and $\sigma_{r\theta} = K$, at the wedge surface, $\theta = \pi - \phi_o$:

$$C = \frac{H \sin 2\phi_o - K(1 - \cos 2\phi_o)}{2(1 - \cos 2\phi_o - \phi_o \sin 2\phi_o)} \tag{5.34}$$

and

$$D = \frac{H(1 - \cos 2\phi_o) + K(\sin 2\phi_o - 2\phi_o)}{2(1 - \cos 2\phi_o - \phi_o \sin 2\phi_o)} \tag{5.35}$$

The elastic and plastic sectors can be assembled subject to the requirement of traction free crack flanks and traction continuity across the sector boundaries. Continuity of tractions does not necessarily imply continuity of stresses as jumps in radial stress may be permitted by the equilibrium equations. Analytic solutions are presented for both situations when the crack is located in the elastic perfectly-plastic solid and when it is in a fully elastic solid.

5.3 A crack located in a plastically deforming solid: problem A

In this configuration, plastic deformation is allowed only in the angular region, $-\pi \leq \theta \leq -\pi/2$ and $\pi/2 \leq \theta \leq \pi$ while the material ahead of the crack is fully elastic. In the

limiting case when the angular region in which plastic deformation is allowed is fully plastic at the crack tip, the mode I slip line field comprises a centred fan starting at the interface and extending to $\theta = 3\pi/4$, complemented by a constant stress sector at the crack flank as identified by He et. al (1992) and Stahle and Shih (1992) shown in the Fig. 5.4(a). The stresses in the constant stress sector are:

$$\sigma_{rr} = k(1 + \cos 2\theta) \tag{5.36}$$

$$\sigma_{\theta\theta} = k(1 - \cos 2\theta) \tag{5.37}$$

$$\sigma_{r\theta} = -k \sin 2\theta \qquad (3\pi/4 \le \theta \le \pi) \tag{5.38}$$

The stresses in the centred fan adjoining the constant stress sector are:

$$\sigma_{rr} - \sigma_{\theta\theta} = \sigma_m = 2k \left[\frac{1}{2} + \frac{3\pi}{4} - \theta \right] \tag{5.39}$$

$$\sigma_{r\theta} = k \qquad (\pi/2 \le \theta \le 3\pi/4) \tag{5.40}$$

However, He et. al (1992) and Stahle and Shih (1992) failed to recognise that complete plasticity behind the interface is only a limiting case, which occurs only for tensile T-stresses. In general an elastic wedge adjoins the centred fan sector. However in the presentwork it is established that in the case of elastically matched solids ($\Omega = 1$, $T = 0$), the elastic wedge extends from the crack flank to an angle, $\phi_o = 60.5°$, as shown in Fig. 5.4(b). In the elastic sector at the crack flank the stresses are:

$$\sigma_{rr} = C(2\theta - 2\pi + \sin 2\theta) + D(1 + \cos 2\theta) \tag{5.41}$$

$$\sigma_{\theta\theta} = C(2\theta - 2\pi - \sin 2\theta) + D(1 - \cos 2\theta) \tag{5.42}$$

$$\sigma_{r\theta} = C(\cos 2\theta - 1) - D\sin 2\theta \qquad\qquad (\pi - \phi_o \le \theta \le \pi) \qquad\qquad (5.43)$$

where,

$$C = \frac{k\cos 2\phi_o}{1 - \cos 2\phi_o} \qquad\qquad (5.44)$$

and

$$D = \frac{k\sin 2\phi_o}{1 - \cos 2\phi_o} \qquad\qquad (5.45)$$

The stresses in the centred fan sector are:

$$\sigma_{rr} = \sigma_{\theta\theta} = \sigma_m = P + k(\pi - 2\theta) \qquad\qquad (5.46)$$

$$\sigma_{r\theta} = k \qquad\qquad (\pi/2 \le \theta \le \pi - \phi_o) \qquad\qquad (5.47)$$

where P is the hoop stress at the interface which depends on ϕ_o as:

$$P = k\left[\frac{\sin 2\phi_o - 2\phi_o}{1 - \cos 2\phi_o} + \pi\right] \qquad\qquad (5.48)$$

In the elastic region ahead of the crack the crack tip stresses from the numerical solution are singular. The Eqs. 5.28 developed for an elastic sector cannot be applied as the assumption of finite crack tip stresses does not hold. It is useful to start with a stress function given by Timoshenko and Goodier (1970) for a semi-infinite plate subjected to shear loading on a half-plane as shown in Fig. 5.5:

$$\Phi = \frac{s}{\pi}\left[\frac{y^2}{2}\ln(x^2 + y^2) + xy\tan^{-1}\frac{y}{x} - y^2\right] \qquad\qquad (5.49)$$

The stress function can be modified taking into account the co-ordinate system and boundary conditions as idealised in Fig. 5.6. An arbitrary constant, r_o, with the dimensions of length is introduced such that the stress function is dimensionally consistent:

$$\Phi = -\frac{2k}{\pi}\left[\frac{x^2}{2}\ln\frac{(x^2 - y^2)}{r_o^2} + xy\left(\tan^{-1}\frac{x}{y} - \frac{\pi}{2}\right) - x^2 + Py^2\right] \tag{5.50}$$

The Cartesian stress field corresponding to this stress function features a logarithmic singularity:

$$\sigma_{xx} = \frac{k}{\pi}(1 + \cos 2\theta) - P \tag{5.51}$$

$$\sigma_{yy} = \frac{k}{\pi}\left[4\ln\frac{r}{r_o} + (1 + \cos 2\theta)\right] \tag{5.52}$$

$$\sigma_{xy} = \frac{k}{\pi}\left[\sin 2\theta - 2\theta\right] \tag{5.53}$$

In the limiting case, in which plasticity fully surrounds the crack tip in the angular regions $-\pi \le \theta \le -\pi/2$ and $\pi/2 \le \theta \le \pi$, the hoop stress at the interface, P is $k(1 + \pi/2)$. This recovers the stress fields reported without derivation by He et. al (1992) and Stahle and Shih (1992) in which the nature of the constant, r_o, was left undetermined. The nature of r_o will be addressed in Chapter5 by numerical analysis.

5.4　A crack located in an elastic solid: problem B

Mode I, mixed mode and mode II slip line fields are developed for a crack located in a fully elastic solid while plasticity is restricted to the material ahead of the crack, $-\pi/2 \le \theta \le \pi/2$. The parameters which characterise these fields are identified.

5.4.1 Mode I slip line fields

The mode I slip line field features a constant stress region directly ahead of the crack complemented by centred fans as shown in Fig. 5.7. A statically admissible stress field can be determined in terms of the mean stress directly ahead of the crack tip, $\sigma_m(0)$ which is a free variable in the analysis. Starting with the constant stress sector ahead of the crack $(0 \leq \theta \leq \pi/4)$:

$$\sigma_{rr} = \sigma_m(0) + k\sin(2\theta - \frac{\pi}{2})$$

$$\sigma_{\theta\theta} = \sigma_m(0) - k\sin(2\theta - \frac{\pi}{2}) \tag{5.54}$$

$$\sigma_{r\theta} = k\cos(2\theta - \frac{\pi}{2})$$

The stresses in the adjoining centred fan $(\pi/4 \leq \theta \leq \pi/2)$ can be written as:

$$\sigma_{rr} = \sigma_{\theta\theta} = \sigma_m(0) - 2k(\theta - \frac{\pi}{4})$$

$$\sigma_{r\theta} = k \tag{5.55}$$

while at the interface $(\theta = \pi/2)$:

$$\sigma_{\theta\theta} = \sigma_m(0) - k\frac{\pi}{2} \tag{5.56}$$

$$\sigma_{r\theta} = k \tag{5.57}$$

The stresses in the elastic material ($\pi/2 \leq \theta \leq \pi$) can be determined from Eqs. (5.28)-(5.30) with:

$$E_1 = -\frac{k}{2} \tag{5.58}$$

$$E_2 = \frac{\sigma_m(0) - k\pi}{2} \tag{5.59}$$

$$E_3 = -2k \tag{5.60}$$

$$E_4 = \sigma_m(0) + k\pi \tag{5.61}$$

Although the solution is presented for the upper half ($0 \leq \theta \leq \pi$), it can be extended to the lower half such that hoop and radial stresses are symmetric and the shear stress is anti-symmetric about the $\theta = 0$ plane. Thus, the mean stress ahead of the crack tip parameterises a family of mode I crack tip fields which differ only through the mean stress. In the numerical work the dependence of the mean stress (constraint) on the elastic mismatch and T-stress is determined. The range of validity of the elastic solution can be established by checking a posteriori that the yield criterion is not violated in the elastic sectors. This leads to a restriction on the ratio of the yield stresses ($\sigma_o^{(1)}/\sigma_o^{(2)}$) which is addressed in the numerical solutions.

5.4.2   Mixed mode slip line fields

Depending on the ratio of shear to tension in the remote loading, there are three distinct forms of mixed mode fields: sub-critical, critical and super-critical fields. The critical field is unique and corresponds to the loading phase angle that is denoted by ϕ_{cr}. A range of loading phase angles give rise to the sub-critical field and super-critical fields. In this section

the form of these fields and the parameters that characterise them are described.

In the sub-critical field: $0 < \phi < \phi_{cr}$, the constant stress sector rotates and the symmetry of the mode I field is lost as shown in Fig. 5.8. The span of the centred fan sector in the upper half increases while the centred fan sector at the lower half decreases. The stress field is determined by both the mean stress and the mode mixity ahead of the crack tip defined by $\rho = \sigma_{r\theta}(0)/\sigma_{\theta\theta}(0)$. The stresses in the constant sector ahead of the crack tip in the angular range $\psi_{cs} - \pi/2 \le \theta \le \psi_{cs}$ are:

$$\sigma_{rr} = \sigma_m(0) + k\sin(2\theta - 2\psi_{cs})$$

$$\sigma_{\theta\theta} = \sigma_m(0) - k\sin(2\theta - 2\psi_{cs}) \tag{5.62}$$

$$\sigma_{r\theta} = k\cos(2\theta - 2\psi_{cs})$$

where ψ_{cs} can be determined from:

$$\rho\sigma_m(0) + \rho k\sin 2\psi_{cs} - k\cos 2\psi_{cs} = 0 \tag{5.63}$$

The stresses in the centred fan sector adjoining the constant sector in the range: $\psi_{cs} \le \theta \le \pi/2$, are given by:

$$\sigma_{rr} = \sigma_{\theta\theta} = \sigma_m(0) + 2k(\psi_{cs} - \theta) \tag{5.64}$$

$$\sigma_{r\theta} = k \tag{5.65}$$

The other centred fan sector in the angular span $-\pi/2 \le \theta \le \psi_{cs} - \pi/2$ has stresses of the form:

$$\sigma_{rr} = \sigma_{\theta\theta} = \sigma_m(0) + 2k\left[\theta - \left(\psi_{cs} - \frac{\pi}{2}\right)\right] \tag{5.66}$$

$$\sigma_{r\theta} = -k \tag{5.67}$$

In the elastic sector on the upper flank ($\pi/2 < \theta \leq \pi$) the stresses can be determined using Eqs. (5.28)-(5.30) with:

$$E_1 = -\frac{k}{2} \tag{5.68}$$

$$E_2 = \frac{1}{2}(\sigma_m(0) + 2k\psi_{cs} - k\pi) \tag{5.69}$$

$$E_3 = -2k \tag{5.70}$$

$$E_4 = \sigma_m(0) - 2k\psi_{cs} + \frac{k\pi}{2} \tag{5.71}$$

In the elastic region at the lower flank ($-\pi \leq \theta \leq -\pi/2$) stresses can be determined using Eqs. (5.28)-(5.30) with:

$$E_1 = \frac{k}{2} \tag{5.72}$$

$$E_2 = \frac{1}{2}\left(\sigma_m(0) - 2k\psi_{cs} - \frac{k\pi}{2}\right) \tag{5.73}$$

$$E_3 = 2k \tag{5.74}$$

$$E_4 = \sigma_m(0) - 2k\psi_{cs} + \frac{3k\pi}{2} \tag{5.75}$$

As the shear component of the loading is increased to $\dot{\phi}_{cr}$, the critical field is reached in which the constant stress sector stretches from the plane ahead of the crack tip to the interface in

the lower half such that the centred fan sector in the lower half disappears as shown in Fig. 5.9. The loading phase angle corresponding to this limiting field for elastically matched but plastically mismatched systems is approximately 26 degrees. The crack tip field can be fully described by the mean stress ahead of the crack tip, $\sigma_m(0)$. Starting from the centred fan sector that stretches from the plane ahead of the crack tip to the interface ($0 \le \theta \le \pi/2$), the stresses are:

$$\sigma_{rr} = \sigma_{\theta\theta} = \sigma_m(0) - 2k\theta \tag{5.76}$$

$$\sigma_{r\theta} = k \tag{5.77}$$

In the constant stress sector ($-\pi/2 \le \theta \le 0$):

$$\sigma_{rr} = \sigma_m(0) + k \sin 2\theta$$

$$\sigma_{\theta\theta} = \sigma_m(0) - k \sin 2\theta \tag{5.78}$$

$$\sigma_{r\theta} = k \cos 2\theta$$

In the elastic sector at the upper flank ($\pi/2 \le \theta \le \pi$):

$$E_1 = -\frac{k}{2} \tag{5.79}$$

$$E_2 = \frac{1}{2}\left[\sigma_m(0) - \frac{3k\pi}{2}\right] \tag{5.80}$$

$$E_3 = -2k \tag{5.81}$$

$$E_4 = \sigma_m(0) + \frac{k\pi}{2} \tag{5.82}$$

In the elastic sector at the lower flank $(-\pi \le \theta \le -\pi/2)$:

$$E_1 = \frac{k}{2} \tag{5.83}$$

$$E_2 = \frac{1}{2}\left[\sigma_m(0) - \frac{k\pi}{2}\right] \tag{5.84}$$

$$E_3 = 2k \tag{5.85}$$

$$E_4 = \sigma_m(0) + \frac{3k\pi}{2} \tag{5.86}$$

In the super-critical field $(\phi_{cr} < \phi < \pi/2)$, the limiting field rotates and a constant stress sector develops at the upper interface. A generic slip line field is shown in Fig. 5.10, the sector boundary of the centred fan being at $\theta = \theta^{cs+}$ and $\theta = \theta^{cs-}$. The stress field is established by the traction vector $(\sigma_{\theta\theta}^+, \sigma_{r\theta}^+)$ at the interface $(\theta = \pi/2)$ and the span of the centred fan, $2\theta^{cf} = \theta^{cs+} - \theta^{cs-}$. Starting from the upper flank which is elastic:

$$\sigma_{rr} = -\frac{\sigma_{r\theta}^+}{2}\sin 2\theta + \frac{1}{2}\left(\sigma_{\theta\theta}^+ - \frac{\pi}{2}\sigma_{r\theta}^+\right)\cos 2\theta + \frac{1}{2}\left[-2\sigma_{r\theta}^+\theta + \sigma_{\theta\theta}^+ + \frac{3\pi}{2}\sigma_{r\theta}^+\right]$$

$$\sigma_{\theta\theta} = \frac{\sigma_{r\theta}^+}{2}\sin 2\theta - \frac{1}{2}\left(\sigma_{\theta\theta}^+ - \frac{\pi}{2}\sigma_{r\theta}^+\right)\cos 2\theta + \frac{1}{2}\left[-2\sigma_{r\theta}^+\theta + \sigma_{\theta\theta}^+ + \frac{3\pi}{2}\sigma_{r\theta}^+\right] \tag{5.87}$$

$$\sigma_{r\theta} = -\frac{\sigma_{r\theta}^+}{2}\cos 2\theta - \frac{1}{2}\left(\sigma_{\theta\theta}^+ - \frac{\pi}{2}\sigma_{r\theta}^+\right)\sin 2\theta - \frac{1}{2}\sigma_{r\theta}^+$$

In the adjoining constant stress sector, $\theta^{cs+} \le \theta \le \pi/2$:

$$\sigma_{rr} = \sigma_{in}^{cs+} + k\sin(2\theta - 2\theta^{cs+})$$

$$\sigma_{\theta\theta} = \sigma_m^{cs+} - k\sin(2\theta - 2\theta^{cs+}) \tag{5.88}$$

$$\sigma_{r\theta} = k\cos(2\theta - 2\theta^{cs+}) $$

where,

$$\theta^{cs+} = \frac{\pi}{2} - \frac{1}{2}\cos^{-1}\left(\frac{\sigma_{r\theta}^+}{k}\right) \tag{5.89}$$

$$\sigma_m^{cs+} = \sigma_{\theta\theta}^+ + k\sin(2\pi - 2\theta^{cs+}) \tag{5.90}$$

In the centred fan ($\theta^{cs+} - 2\theta^{cf} \leq \theta \leq \theta^{cs-}$) the stresses are:

$$\sigma_{rr} = \sigma_m^{cs+} + 2k(\theta^{cs+} - \theta)$$

$$\sigma_{\theta\theta} = \sigma_m^{cs+} + 2k(\theta^{cs+} - \theta) \tag{5.91}$$

$$\sigma_{r\theta} = k$$

The centred fan is followed by a constant stress sector in the range $-\pi/2 \leq \theta \leq \theta^{cs+} - 2\theta^{cf}$, the stresses are given by:

$$\sigma_{rr} = \sigma_m^{cs-} + k\sin(2\theta + 2(\theta^{cs+} - 2\theta^{cf}))$$

$$\sigma_{\theta\theta} = \sigma_m^{cs-} - k\sin(2\theta + 2(\theta^{cs+} - 2\theta^{cf})) \tag{5.92}$$

$$\sigma_{r\theta} = k\cos(2\theta + 2(\theta^{cs-} - 2\theta^{cf}))$$

where $\sigma_m^{cs-} = \sigma_m^{cs+} + 4k\theta^{cf}$. In the elastic sector on the lower flank the stresses are of the form:

$$\sigma_{rr} = \frac{\sigma_{r\theta}^-}{2}\sin 2\theta + \frac{1}{2}\left(\sigma_{\theta\theta}^- + \frac{\pi}{2}\sigma_{r\theta}^-\right)\cos 2\theta + \frac{1}{2}\left[-2\sigma_{r\theta}^-\theta + \sigma_{\theta\theta}^- - \frac{3\pi}{2}\sigma_{r\theta}^-\right]$$

$$\sigma_{\theta\theta} = \frac{\sigma_{r\theta}^-}{2}\sin 2\theta - \frac{1}{2}\left(\sigma_{\theta\theta}^- + \frac{\pi}{2}\sigma_{r\theta}^-\right)\cos 2\theta + \frac{1}{2}\left[-2\sigma_{r\theta}^-\theta - \sigma_{\theta\theta}^- - \frac{3\pi}{2}\sigma_{r\theta}^-\right] \quad (5.93)$$

$$\sigma_{r\theta} = -\frac{\sigma_{r\theta}^-}{2}\cos 2\theta - \frac{1}{2}\left(\sigma_{\theta\theta}^- + \frac{\pi}{2}\sigma_{r\theta}^-\right)\sin 2\theta + \frac{\sigma_{r\theta}^-}{2}$$

where

$$\sigma_{\theta\theta}^- = \sigma_m^{cs-} + k(2(\theta^{cs+} - 2\theta^{cf})) \quad (5.94)$$

$$\sigma_{r\theta}^- = -k\cos(2(\theta^{cs+} - 2\theta^{cf})) \quad (5.95)$$

5.4.3 Mode II slip line fields

Mode II loading requires anti-symmetry of σ_{rr} and $\sigma_{\theta\theta}$ and symmetry of $\sigma_{r\theta}$ about the $\theta = 0$ plane. The sector composition of the mode II field is shown in Fig. 5.11. In the upper half ($0 \leq \theta \leq \pi$), the stresses in the centred fan of angular span, $2\theta^+$, are:

$$\sigma_{rr} = \sigma_{\theta\theta} = \sigma_m = 2k\theta \quad (5.96)$$

$$\sigma_{r\theta} = k \qquad\qquad (0 \leq \theta \leq \theta^+) \quad (5.97)$$

Stresses in the constant stress sector adjoining the centred fan are:

$$\sigma_{rr} = -2k\theta^+ + k\sin(2\theta - 2\theta^+) \quad (5.98)$$

$$\sigma_{\theta\theta} = -2k\theta^- - k\sin(2\theta - 2\theta^+) \tag{5.99}$$

$$\sigma_{r\theta} = k\cos(2\theta - 2\theta^+) \qquad (\theta^+ \leq \theta \leq \pi/2) \tag{5.100}$$

The stresses in the elastic region $(\pi/2 \leq \theta \leq \pi)$ are given by equations.(5.28-5.30) with:

$$E_1 = \frac{k}{2}\cos 2\theta^+ \tag{5.101}$$

$$E_2 = \frac{k}{2}\left[-2\theta^+ - \sin 2\theta^+ + \frac{\pi}{2}\cos 2\theta^+\right] \tag{5.102}$$

$$E_3 = 2k\cos 2\theta^+ \tag{5.103}$$

$$E_4 = -\frac{k}{2}\left[4\theta^+ + 2\sin 2\theta^+ + 3\pi\cos 2\theta^+\right] \tag{5.104}$$

The mode II stress field is expressed in terms of the span of the centred fan which the numerical work will show to be a function of elastic mismatch.

All the forms of fields described with their corresponding loading phase angle in degrees have been presented in Fig. 5.12 for elastically matched but plastically mismatched bi-material system.

5.5 Discussion

Slip line theory (Hill, 1950) was developed to deal with processes such as metal forming in which the plastic strains are very much larger than the elastic strains. This allows elastic strain increments to be neglected and the material response to be simplified as elastically rigid. When a plastically deforming region abuts an elastically rigid region, the slip lines must be orthogonal to the interface ensuring that the interface is a line of zero extension. This condition is met in mode I and sub-critical mixed mode fields when the centred fans adjoin the

elastic material on the crack flanks. Similarly in a critical mixed mode field, when a constant sector joins an elastic sector the condition holds if the sector boundary is along and perpendicular to the slip lines as shown in Fig. 5.9. In these fields, the material on the crack flanks can be approximated as elastically rigid. However, in the fields of higher mixity like super-critical mixed mode or mode II fields, the condition is not met as shown in Fig. 5.10-5.11 and the strains in the elastic material are comparable to the plastic strains of the adjoining constant stress sector. Although these fields cannot be formally expressed as slip line fields the elastic perfectly-plastic analysis remains valid. Significantly, unique statically admissible fields ($\phi_{cr} \leq \phi \leq 90^{\circ}$) cannot be determined from the local mixity ($\sigma_{r\theta}(0)/\sigma_{\theta\theta}(0)$) and mean stress ($\sigma_m(0)$) ahead of the crack but require additional information. These fields are not statically determinate but additionally require solutions to the compatibility equations.

5.6   Conclusion

Analytic solution of the plane strain asymptotic fields for a crack between elastically and plastically mismatched solids is developed. The discussion is based on two limiting cases: when the crack is located in perfectly-plastic material while the material ahead is fully elastic and a case when the crack is located in an elastic solid while the solid ahead deforms plastically.

When plasticity is limited to the material behind the crack, the elastic material ahead of the tip exhibits a logarithmic singularity. Only the Cartesian stress normal to the crack plane is singular. The fields can usefully be parameterised by the hoop stress on the interface. Behind the crack, the field comprises an elastic wedge and a centred fan, full plasticity behind the crack being a limiting case.

In the important case in which plasticity is restricted to the material ahead of the crack, for mode I loading, a family of plastic fields symmetric about the $\theta = 0$ plane arises which

are parameterised by constraint. As the shear component of the remote load is increased the symmetry is lost, the stress field is determined from the mean stress and the mode mixity $(\sigma_{r\theta}/\sigma_{\theta\theta})$ ahead of the crack tip. As the shear component of loading is increased further $(\phi > \phi_{cr})$ the stress field is established by the traction vector at the interface and the span of the centred fan, $2\theta^{-}$. The mode II field is antisymmetric about the $\theta = 0$ plane and the structure of the field is determined fully by the angular span of the centred fan ahead of crack.

PLASTIC   ELASTIC   ELASTIC   PLASTIC

Problem A   Problem B
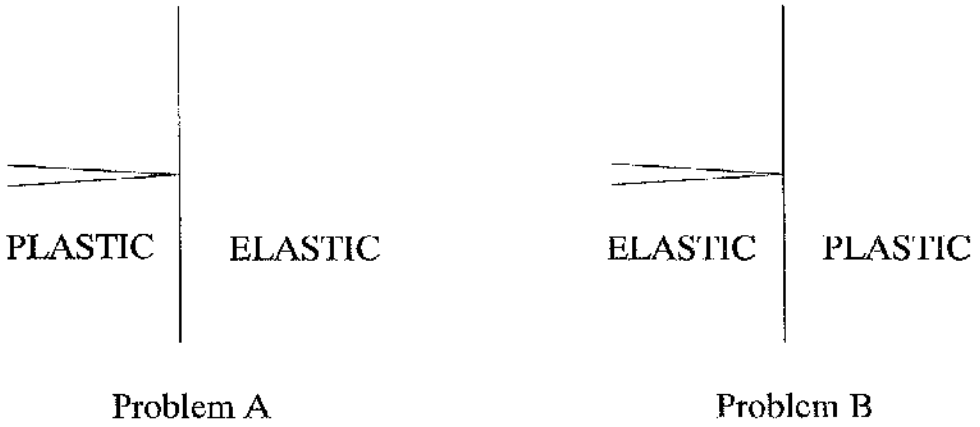
Fig 5.1: Schematic diagram of material configurations.

(a)   (b)
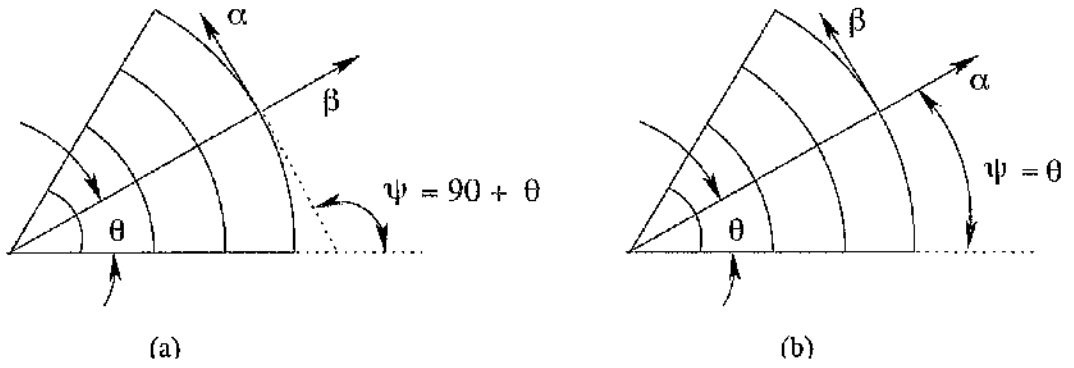
Fig 5.2: First shear (α) direction in centred fan sector.
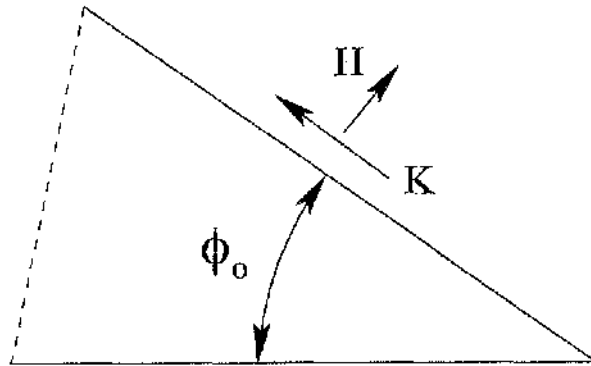
Fig 5.3: Elastic wedge at the crack surface.

(a)

(b)
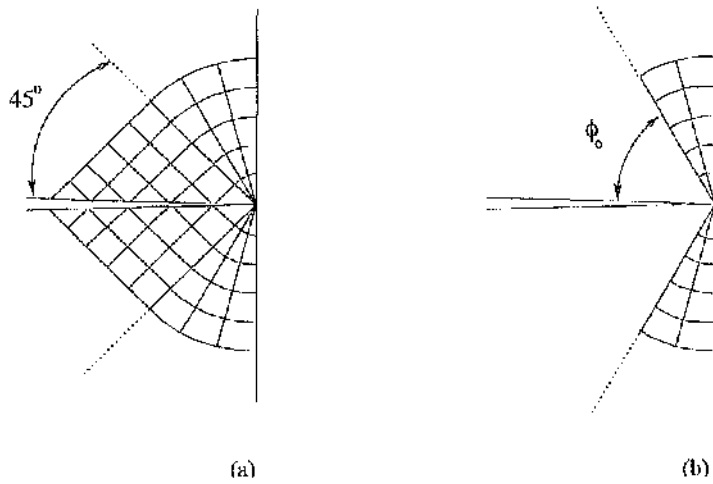
Fig 5.4: Mode I slip line field for a crack in an elastic perfectly plastic solid normal to the interface with an elastic solid (a) at tensile T-stress and (b) at compressive T-stresses.
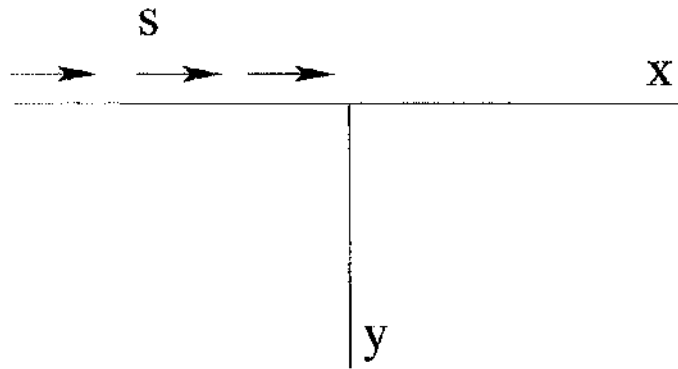
Fig 5.5: Semi-infinite plate subjected to shear loading in the half plane.
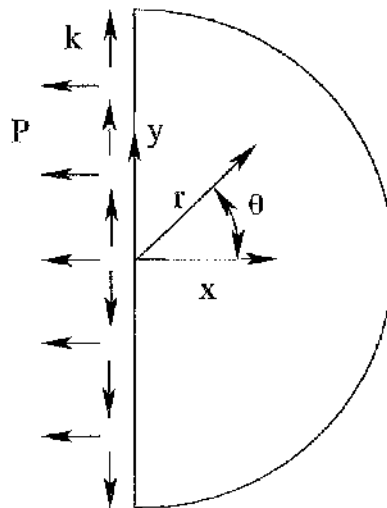
Fig 5.6: Loading configuration for the elastic region ahead of the crack.
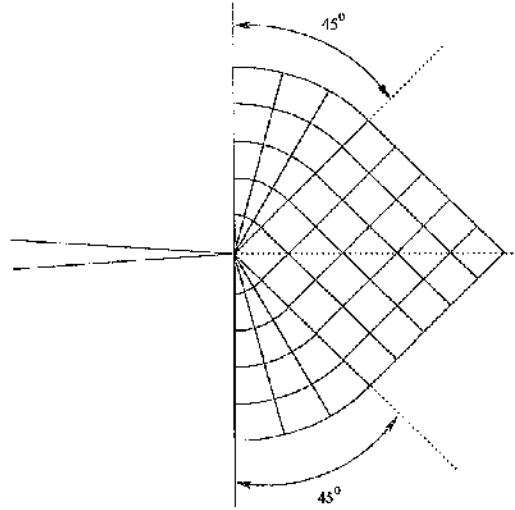
Fig 5.7: Slip line field for mode I loading.
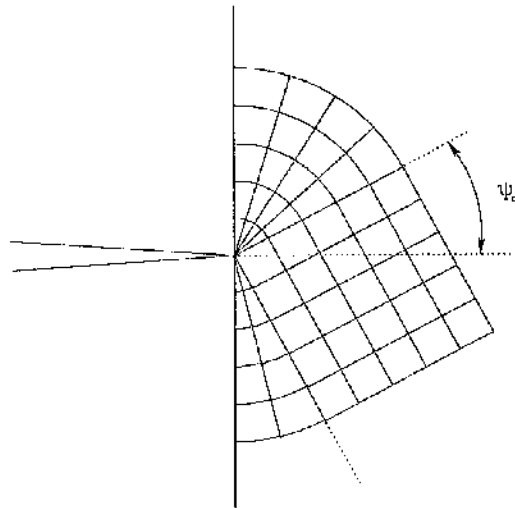
Fig 5.8: Mixed mode slip line field for near mode I loading.
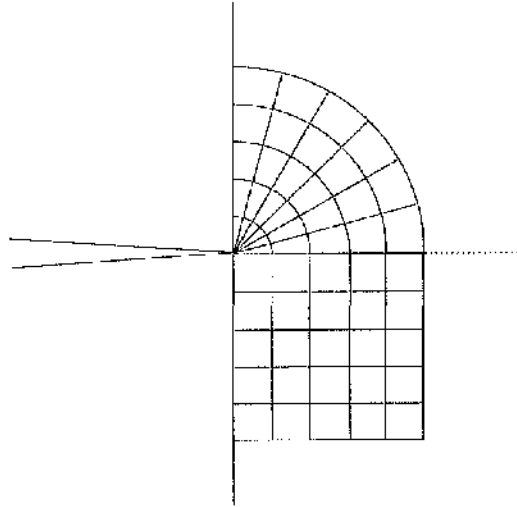
Fig 5.9: Limiting slip line field.
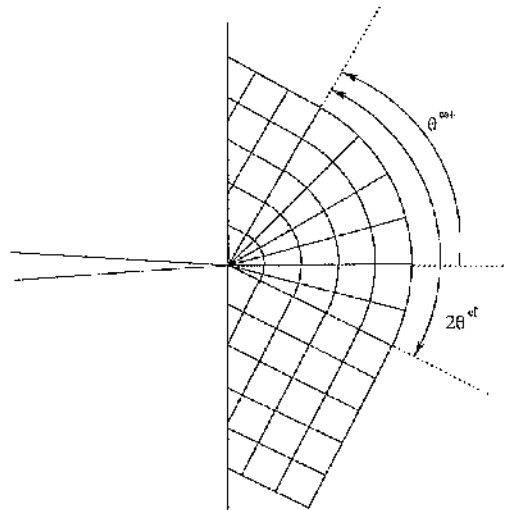
Fig 5.10: Mixed mode slip line field for loading phase angle, $\Phi > 26^o$.
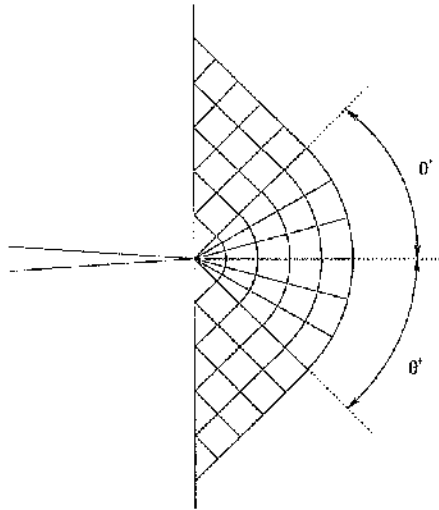
Fig 5.11: Slip line field for mode II loading.
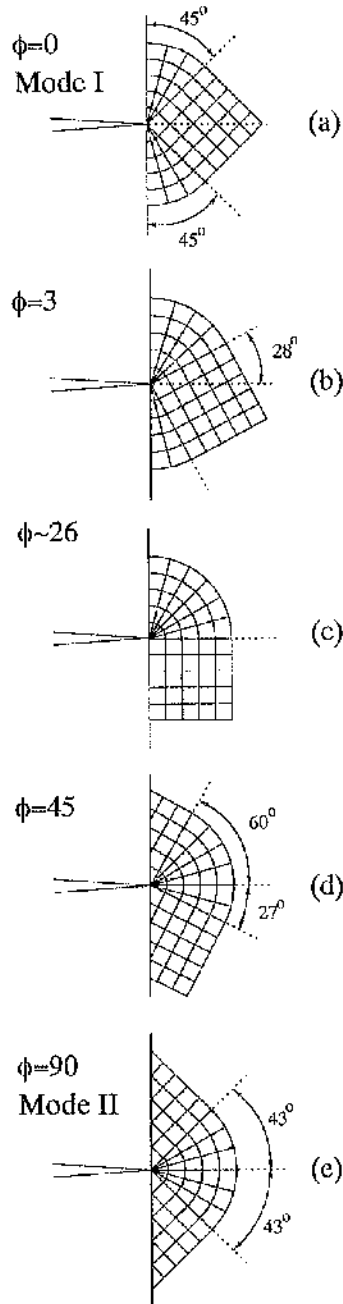
Fig 5.12: Slip line fields for different loading phase angles, for elastically matched but plastically mismatched systems.

A Crack Normal to an Interface: Elastic-Plastic Numerical Solution

Cracks normal to the interface between dissimilar solids are features of bi-material systems such as thermal barrier coatings, ceramic laminates and welds. An understanding of the factors that influence the crack tip field provides a basis for assessing the structural integrity and the reliability of these important technological systems. The analytic solution developed in Chapter 5 establishes the parameters that characterise the asymptotic fields. In this chapter, the dependence of these parameters on the elastic mismatch, non-singular term (T-stress) and the loading phase angle is determined computationally.

6.1 Modified boundary layer formulations

Rice and Tracey (1973) established an elegant technique to model crack tip plasticity using boundary layer formulations. Instead of modelling a crack in a full engineering structure, a domain centred at the crack tip is considered. At the outer boundary of the circular domain elastic displacements corresponding to the leading term in Williams expansion (Williams, 1957) are applied. Contained yielding is ensured by restricting the extent of crack tip plasticity to some small fraction of the radius of the domain. The concept is extended to incorporate the effect of the second order term of the elastic field in the form of modified boundary layer formulations, in which displacements corresponding to both the leading term and the second order term of Williams expansion are applied to the boundary.

In the present work, modified boundary layer formulations were based on a circular mesh comprising 576 reduced hybrid, second order isoparametric elements focused at the crack tip

which was represented by 49 coincident but independent nodes. This is shown schematically in Fig. 6.1. The ratio between the crack tip element and the outer boundary radius is $3/10^6$. A range of elastically mismatched systems are analysed in plane strain conditions. To describe the general mixed mode load, the ratio of tension to shear in the remote field is defined by a loading phase angle ϕ:

$$\phi = \tan^{-1}\left(\frac{K^{II}}{K^{I}}\right) \tag{6.1}$$

where K^{I} and K^{II} are the remotely applied stress intensity factors for mode I and mode II. Conditions close to elastic incompressibility are approximated by taking $\nu^{(1)} = \nu^{(2)} = 0.49$, the small elastic dilation inhibiting mesh-locking.

6.1.1 Displacement boundary conditions

Displacements of the outer elastic field corresponding to the first two terms in the asymptotic series can be expressed as the sum of contributions from the leading order terms of mode I and mode II plus a second order term:

$$u_x = u_x^{I} + u_x^{II} + u_x^{T} \tag{6.2}$$

$$u_y = u_y^{I} + u_y^{II} + u_y^{T} \tag{6.3}$$

The superscripts, I and II, distinguish the Cartesian displacements associated with the leading term of mode I and mode II loading while the superscript T identifies the displacements from the second order distance independent term. From Eqs. 4.6-4.7, the leading term of the polar displacements corresponding to mode I or mode II load can be expressed as:

$$u_r^{I/II} = \frac{(2\pi)^{\lambda-1} K^{I/II}}{2G^{(k)}} r^{\lambda}\left[\quad -A(\lambda+1)\sin(\lambda+1)\theta \cdot B(\lambda+1)\cos\theta \cdots \right.$$

$$\cdots \; + \; C\left(4(1-\nu^{(k)})-(\lambda+1)\right)\sin(\lambda-1)\theta \cdots \quad (6.4)$$

$$\cdots \; - \; D\left(4(1-\nu^{(k)})-(\lambda-1)\right)\cos(\lambda-1)\theta \bigg]$$

$$u_\theta^{I/II} = \frac{(2\pi)^{\lambda-1}K^{I/II}}{2G^{(k)}}r^\lambda\bigg[\quad -A(\lambda+1)\sin(\lambda+1)\theta + B(\lambda+1)\cos\theta\cdots$$

$$\cdots \; - \; C\left(4(1-\nu^{(k)})-(\lambda+1)\right)\sin(\lambda-1)\theta\cdots \quad (6.5)$$

$$\cdots \; + \; D\left(4(1-\nu^{(k)})-(\lambda+1)\right)\cos(\lambda-1)\theta\bigg]$$

where A, B, C and D are stress function coefficients determined in the linear elastic analysis in Chapter 4. The displacement field corresponding to the second order term under plane strain conditions can be derived from Eqs. (4.6) and (4.7) in the material ahead of the crack $(-\pi/2 \le \theta \le \pi/2)$ to be :

$$\begin{bmatrix} u_x^T \\ u_y^T \end{bmatrix} = \frac{Tr}{2G^{(2)}} \begin{bmatrix} \left[1-\nu^{(2)}(1+\eta)\right]\cos\theta \\ \left[\eta-\nu^{(2)}(1+\eta)\right]\sin\theta \end{bmatrix} \quad (6.6)$$

On the upper crack flank $(\pi/2 \le \theta \le \pi)$, the displacements are:

$$\begin{bmatrix} u_x^T \\ u_y^T \end{bmatrix} = \frac{Tr}{2G^{(1)}} \begin{bmatrix} (1-\nu^{(1)})\cos\theta \\ (-\nu^{(1)})\sin\theta \end{bmatrix} \quad (6.7)$$

The displacement field in the material in the angular range $(-\pi \le \theta \le -\pi/2)$ are obtained by symmetry about the $\theta = 0$ plane. A software program in language C was written to create the Cartesian displacement boundary condition for the 49 nodes at the outer boundary: the input of the program were the elastic mismatch and the corresponding λ and coefficients given in Tables 4.1-4.6, K^I, K^{II} and T. The program calculates the leading term polar displacements using Eqs. 6.5-6.6, converts them into Cartesian co-ordinates before adding the contribution from the second order term. Finite element analysis was performed using the commercial software package *ABAQUS* v 5.8 (2003). Insight into the elastic-plastic

behaviour is obtained by focusing on the elastic-plastic analysis of a crack normal to an interface such that one of the materials is non-hardening. The post-processor *Abaqus Post* was used to record the Cartesian stresses along radial lines at $7\frac{1}{2}$ degree intervals around the crack tip in a report file (*.rpt). A *Matlab* v 5.3 (1999) program was used to read the recorded data from the report file and fit a linear curve through the nodal values of the 2nd and 3rd element from the crack tip at $7\frac{1}{2}$ degree intervals around the crack tip. The asymptotic crack tip stresses for each angle were obtained by extrapolating the linear curve to the crack tip. For a crack located in an elastic perfectly-plastic solid the effect of the second order term is elucidated for elastically matched solids ($\Omega = 1$), however, the present work largely focuses on the problem of a crack in an elastic solid which has practical relevance for hard surface coatings.

6.2   Crack located in plastically deforming solid

Numerical solutions have been developed for elastically matched but plastically mismatched systems ($\Omega = 1$) for a crack located in a plastically deforming solid while the material ahead is fully elastic. The stress field in the material ahead of the crack is fully elastic and the stresses are singular at the tip, while in the plastically deforming material on the crack flank the crack tip stresses are finite and distance independent. Fig. 6.2 shows the hoop stress directly ahead of the crack as a function of the distance from crack tip normalised by the crack tip opening displacement, δ, determined by the construction proposed by Kumar et. al (1981). With this normalisation the stress profiles are self similar as evidenced by data at two load levels. The crack tip opening is proportional to $(K/\sigma_o)^{\frac{1}{1-\lambda}}$. The proportionality constant depends on the elastic mismatch and has insignificant dependence on the T-stress in contained yielding as discussed later in section 6.4.1. In the analytic expression for the singular elastic field given by Eq. 5.52, a constant r_o was left undefined by He et. al (1992).

To determine r_o, consider the hoop stress ahead of the crack tip ($\theta = 0$) using Eq. 5.52:

$$\sigma_{\theta\theta}(0) = -\frac{\sigma_o}{\pi\sqrt{3}}\left[4\ln\frac{r}{r_o} + 2\right] \tag{6.8}$$

r_o can be determined from the numerical results obtained for the hoop stress on the plane ahead of the crack tip using:

$$\frac{r_o}{\delta} = \lim_{r\to 0}\frac{r}{\delta}\,\exp\left(\frac{\pi\sqrt{3}\sigma_{\theta\theta}(0)}{4\sigma_o} + \frac{1}{2}\right) \tag{6.9}$$

Given self similarity, the right hand side of Eq. 6.9 is a constant for a given mismatch, and r_o is a loading parameter that depends on the crack tip opening displacement. For elastically matched ($\Omega = 1$) solids, $r_o = 8250\delta$, gives good agreement between the analytic and computational results.

6.2.1   Effect of T-stress

He et. al (1992) develop an asymptotic solution based on the leading term of the elastic field using a boundary layer formulation. The analytic solution was developed by proposing the slip line field assuming complete plasticity extending from the interface to the flanks as shown in Fig. 5.4(a). However, in the present work the mode I asymptotic cylindrical stresses for elastically matched solids shown for the angular region, $\pi/2 \leq \theta \leq \pi$ in Fig. 6.3, at $T = 0$ there is incomplete plasticity, with an elastic wedge angle, $\phi_o = 60.5^o$. However, for tensile T-stresses ($T = 0.5\sigma_o$), plasticity extends to the flanks. In both the cases the numerical and analytical solutions are found to be in close agreement. Thus, the assumption of complete plasticity at the flanks by He et. al (1992) is valid only for highly constrained ($T > 0$) fields.

6.3 Crack located in an elastic solid

In the context of cracks in hard surface coatings and laminates which have high yield strength, the crack tip field is obtained under the assumption that the solid containing the crack is fully elastic. Numerical solutions are developed for elastic mismatches, Ω, in the range 1 to 10 and a full range of load cases from Mode I to Mode II. Numerical results are presented to illustrate the effect of elastic mismatch, T-stress and mode mixity on the asymptotic plane strain stress field.

6.3.1 Effect of elastic mismatch

Numerical solutions for the mode I asymptotic stresses for elastic mismatches, $\Omega = 1$, 2 and 4 are compared with analytic solutions in Fig. 6.4. The mean stress and Mises stress are shown in Fig. 6.5. The stresses are normalised with the yield stress of material 2. The analytic and the numerical solution are found to be in close agreement. The plane of the maximum hoop stress is ahead of the crack tip ($\theta = 0$), while at the interface, the radial stresses exhibit a discontinuity which decreases with increasing elastic mismatch. The structure of the mode I field is independent of elastic mismatch and can be parameterised by the mean stress ahead of the crack tip, $\sigma_m(0)$. For perfect plasticity the variation of the mean stress ahead of the crack tip with increasing mismatch is shown in Fig. 6.6. Increases in elastic mismatch decrease the crack tip constraint and increase the resistance to crack extension by cleavage or ductile tearing.

6.3.2 Effect of T-stress

The effect of the non-singular term has been established as a function of T in mode I loading. A comparison of the effect of T on elastically matched but plastically mismatched bi-material systems and a fully homogeneous elastic perfectly plastic solid is given in Fig. 6.7. For

tensile T-stresses, the crack tip stresses in the homogeneous material saturate when the crack tip is fully surrounded by plasticity in the Prandtl field. However, in mismatched problems the material on the crack flanks is fully elastic and plasticity is confined to the material ahead of the crack. As a result, even for large tensile T-stresses the mean stress ahead of the crack does not saturate but continues to increase with T. For compressive T-stresses, the homogeneous crack features an elastic wedge on the crack flanks. The angular span of this wedge increases for large compressive T-stresses until the elastic wedge angle nears $\pi/2$ which is the elastic wedge angle in the bi-material system, and the loss of constraint becomes similar in both systems. Fig. 6.8 shows the normalised cylindrical stresses for $T = 0.5\sigma_o$, 0 and $-0.5\sigma_o$ while the normalised mean and mises stress are shown in Fig. 6.9. The structure of the mode I field is independent of the T-stress but T controls the mean stress ahead of the crack tip and thus the magnitude of the crack tip stress. A compressive T-stress results in a loss of crack tip constraint.

A similar loss of crack tip constraint is observed for higher elastic mismatches as shown in Fig. 6.10. Constraint effects can be expressed in terms of the constraint parameter,Q:

$$Q = \frac{\sigma_{\theta\theta}(0) - \sigma_{\theta\theta}(0)^{ref}}{\sigma_o} \tag{6.10}$$

where the reference state is taken to be the small scale yielding solution ($T = 0$) for the elastically matched but plastically mismatched system, such that $\sigma_{\theta\theta}(0)^{ref} = 3.45\sigma_o$. In a homogeneous solid, in small scale yielding $\sigma_{\theta\theta}(0)^{T=0} = 2.84\sigma_o$ and the HRR field has $\sigma_{\theta\theta}(0)^{HRR} = 2.97\sigma_o$. The constraint parameter can be expressed in terms of T as:

$$Q = 2.48\frac{T}{\sigma_o} \qquad\qquad \Omega = 1 \tag{6.11}$$

$$Q = 1.41\frac{T}{\sigma_o} - 0.64 \qquad\qquad \Omega = 2 \tag{6.12}$$

$$Q = 1.09\frac{T}{\sigma_o} - 0.98 \qquad\qquad \Omega = 4 \tag{6.13}$$

$$Q = 1.11\frac{T}{\sigma_o} - 1.31 \qquad \Omega = 10 \tag{6.14}$$

Constraint effects continue to be significant for compressive and tensile T-stresses even at higher elastic mismatches than those illustrated in Fig. 6.10.

6.3.3 Effect of loading phase angle

In mode I, the maximum hoop stress occurs directly ahead of the crack. However, as the remote shear component increases the plane of the maximum hoop stress rotates towards the interface as shown in Fig. 6.11. The maximum hoop stress increases with increasing loading phase angle to a phase angle $\sim 15^o$, beyond which it decreases as shown in Fig. 6.12.

The mode II asymptotic cylindrical stresses are shown in Fig. 6.13 and the corresponding mean and Mises stresses in Fig. 6.14. Since the field is antisymmetric with a centred fan sector ahead of the crack tip, $\sigma_{\theta\theta}(0) = \sigma_{rr}(0) = 0$ while $\sigma_{r\theta}(0) = k$, irrespective of elastic mismatch. Thus, elastic mismatch has little effect on the stress levels ahead of the crack but affects the angular span of the centred fan, $2\theta^+$, as shown in Fig. 6.15, and hence the hoop stress across the interface ($\theta = \mp\pi/2$):

$$\sigma_{\theta\theta} = \pm(2k\theta^+ + k\sin 2\theta^+) \tag{6.15}$$

The span of the centred fan increases with mismatch but can never be larger than π, when the hoop stresses at the interface are $\pm k\pi$, which are the maximum interfacial hoop stress for any material combination in mode II loading.

6.3.4 Range of validity of the solution

Analytic and numerical solutions were determined under the premise that the material behind the interface was fully elastic. However, the solutions are still valid for bi-material systems

which may have finite plastic mismatch, $\sigma_o^{(1)}/o_o^{(2)}$, provided the Mises stress of the present solution in the elastic region is below the yield point of the material. As a result, there is a critical plastic mismatch, $\sigma_o^{(1)}/\sigma_o^{(2)}$, for which the assumption of fully elastic crack flanks remains valid. The critical plastic mismatch for mode I solutions is a function of the mean stress ahead of crack as shown in Fig. 6.16. With increasing mean stress ahead of the crack tip the permissible plastic mismatch increases for maintaining fully elastic crack flanks and thus the validity of the solutions.

If the condition is not met and the plastic mismatch is slightly lower than the critical value, plasticity in the flank initially develops as a centred fan which does not extend to the interface as shown in Fig. 6.17(a). For even lower plastic mismatches the slip line field that develops has a constant stress sector at the interface adjoining the centred fan as shown in Fig. 6.17(b). In this configuration, the span of the constant stress sector at the interface, α, can be determined in terms of the plastic mismatch. If the shear at yield for the material at the flanks is $k^{(1)}$, the shear stress in the constant stress sector behind the interface is of the form:

$$\sigma_{r\theta} = k^{(1)} \cos(2\theta - (\pi - 2\alpha)) \tag{6.16}$$

and at the interface it satisfies the condition:

$$\sigma_{r\theta}(\pi/2) = k^{(2)} = \frac{\sigma_o^{(2)}}{\sqrt{3}} \tag{6.17}$$

where, $k^{(2)}$ is the yield stress in shear of material ahead of crack. The solution of the boundary conditions gives the span of the constant stress sector in terms of the plastic mismatch:

$$\alpha = \frac{1}{2}\cos^{-1}\left(\frac{\sigma_o^{(2)}}{\sigma_o^{(1)}}\right) \qquad 0 \le \frac{\sigma_o^{(2)}}{\sigma_o^{(1)}} \le 1 \tag{6.18}$$

Thus, the span of the constant stress sector, α, increases for high plastic mismatch and reduces to 0 for a plastically homogeneous material ($\sigma_o^{(1)} = \sigma_o^{(2)}$). The span of the centred

fan, β, depends upon the mean stress ahead of the crack, as discussed for homogeneous systems by Du and Hancock (1991).

6.4 Crack in an elastic solid approaching a strain hardening solid

Although non-hardening behaviour gives insight into the structure of the crack tip fields, practical material systems usually exhibit strain hardening. In this section, the effect of the non-singular term and elastic mismatch is analysed when the material ahead of the crack is allowed to strain harden with a uni-axial stress-strain relation of the form:

$$\sigma = \sigma_o \left[1 + \frac{\epsilon_p E}{\sigma_o} \right]^{\frac{1}{n}} \qquad \sigma > \sigma_o$$

$$= E\epsilon \qquad \sigma \leq \sigma_o$$

(6.19)

here ϵ_p is the plastic strain and n is the strain hardening exponent which is taken to be 10 giving the stress-strain curve illustrated in Fig. 6.18. The uni-axial stress-strain relation is generalised for multi-axial states of stress using a Mises yield criterion with an associated flow rule. Initially the technologically important geometries of a crack in a hard coating and a crack in a hard laminate detailed in Fig. 4.7 are analysed for an elastic mismatch, $\Omega = 10$. The non-singular T-stress can be compressive or tensile depending on geometry, loading and elastic mismatch as indicated in Fig. 4.9. The load is such that $T = +0.31\sigma_o$ for the coating and $T \sim 0$ for the lamina. The hoop stress ahead of the crack tip and at the interface as a function of the normalised distance from the crack tip are shown in the Fig. 6.19. At different levels of T, the stress curves remain parallel and the tensile T-stress raises the level of stress. For weakly strain hardening materials the deviatoric component of the stress is not affected by the T-stress as shown in Fig. 6.20, but the hydrostatic component increases with the T-stress.

Further insight into the effect of elastic mismatch and T-stress on the form of the strain hardening stress field is obtained for contained yielding conditions using the modified boundary layer formulation model described in Section 6.1. Small scale yielding solutions ($T = 0$) of the hoop stress at the plane ahead of crack tip ($\theta = 0$) are illustrated in Fig. 6.21 for elastic mismatches, $\Omega = 1$, 2, 4. With increasing elastic mismatch the hoop stress decreases, the effect is similar on the hydrostatic stress as indicated in Fig. 6.22. The deviatoric hoop stresses shown in Fig. 6.23 differ slightly for different elastic mismatches. Thus, increasing elastic mismatch decreases the crack tip mean stress, however, in strain hardening bi-material systems of different elastic mismatches, the deviatoric component shows a weak dependence on the mismatch.

6.4.1 Crack extension: penetration or delamination

There are two possible modes of extension for a crack normal to an interface: interface failure or penetration of the material ahead of the crack. He and Hutchinson (1989) address this issue in elastic solids by considering the ratio of the strain energy release rates of the two processes. Although strain energy release rate as a derivative of the potential energy with respect to crack length per unit area is imperfectly defined at the interface, following a dimensional argument the strain energy release rates have been expressed in terms of the stress intensity factor, K, and a finite increment of crack extension, Δa, which is either into the substrate or along the interface (He and Hutchinson, 1989). However, for both modes of failure, as $\Delta a \rightarrow 0$, the strain energy release rate becomes zero for $\lambda < \frac{1}{2}$, corresponding to a crack in the stiffer material. Alternatively, the strain energy release rate is unbounded for $\lambda > \frac{1}{2}$ when crack is located in the less stiff material. Nevertheless, as the ratio of strain energy release rates remains finite, it has been used to discuss the failure mode. It has subsequently become clear that the critical strain energy release rate is not a unique material property but depends on crack tip constraint. In homogeneous materials the strain

energy release rate (J_c) increases as crack tip constraint is lost (Betegón and Hancock, 1991; Sumpter and Hancock, 1994). Similar effects must also be expected for interface toughness. However, progress can be made by considering crack tip opening displacement, δ as defined by Kumar et. al (1981) as the parameter characterising the stress field. The crack tip opening displacement obtained numerically can be related to the stress intensity factor through a constant d which depends on elastic mismatch and is independent of T-stress as shown in Table 6.1-6.2:

$$\delta = d \left(\frac{K}{\sigma_o} \right)^{\frac{1}{1-\lambda}} \tag{6.20}$$

Ω	d
1	5616.7
4	4276.0
10	5238.4

Table 6.1: The effect of elastic mismatch on the constant, d, for $T = 0$.

T/σ_o	d
-0.5	5238.3
0	5238.4
0.5	5381.9

Table 6.2: The effect of T-stress on the constant, d, for elastic mismatch $\Omega = 10$.

In the present work the local failure criterion proposed by Ritchie et. al (1973) for cleavage is used. The crack is taken to penetrate the interface when the hoop stress ahead of the crack exceeds a critical stress taken to be, $\sigma_c = 3.5\sigma_o$, over a micro-structurally significant distance, r^*. The interface is subject to combinations of tension and shear, so that a distinction is made between interface failure dominated by a local opening mode and failure by local shearing. Tensile dominated failure is assumed to occur when the hoop stress at the interface over distance r^* exceeds a critical stress taken to be, $\sigma_c = 1.5\sigma_o$. Shear dominated failure is taken to occur when the shear stress at the interface exceeds a critical shear stress taken to be, $\tau = \sigma_o$, over the characteristic distance, r^*.

The hoop stress ahead of the crack is shown in Fig. 6.21 as a function of the distance from the crack tip normalised by the crack tip opening, δ. This defines a set of self similar curves at three levels of elastic mismatch. The critical hoop stress defines the ratio δ_p/r^*, for interface penetration as a function of elastic mismatch. Eliminating the critical distance r^*, allows the data to be presented as the ratio of the crack tip opening, $\delta_p(\Omega)/\delta_p(\Omega = 1)$, for an elastically mismatched system compared to that of an elastically matched system as shown in Fig. 6.24. The significant result is that the resistance to interface penetration increases with elastic mismatch due to constraint loss.

At the interface, the hoop stress decreases with increasing mismatch as shown in Fig. 6.25. Thus, elastic mismatch causes the hoop stress to fall both ahead of the crack tip and at the interface. However, the interfacial shear stress remains independent of the elastic mismatch as shown in Fig. 6.26. Interface failure criteria have yet to be fully established. Nevertheless it is useful to consider two limiting cases of tensile or shear dominated interface failure. Failure under general stress states must be expected to interpolate between these extremes. For tensile dominated interface failure, a similar argument to that developed for interface penetration leads to $\delta_d(\Omega)/\delta_d(\Omega = 1)$ where δ_d is the crack tip opening for delamination. The competition between penetration and delamination for tensile dominated interface failure is shown in Fig. 6.27 as the ratio of the crack tip openings for penetration and delamination. For tensile dominated interface failure, loss of constraint associated with increasing elastic mismatch promotes penetration compared to delamination, although the toughness of both processes is increased.

Significantly elastic mismatch has no effect on the interface shear stress. As a result, for shear dominated interface failure, the loss of constraint associated with elastic mismatch has no effect on δ_d while the toughness for penetration increases. The effect is that in this case, constraint loss promotes interface failure as illustrated in Fig. 6.27.

For a range of T-stresses, the hoop stress is shown as a function of the distance from the crack tip for elastic mismatch, $\Omega = 10$, in Figs. 6.28-6.29 while the shear stress at the interface is in Fig. 6.30. Loss of constraint due to compressive stress is observed both ahead of the crack and at the interface. Following an identical argument the loss of constraint due to negative T-stress is shown to increase the resistance to both interface penetration and interface delamination in the opening mode. However, constraint loss due to T-stress has no effect on the interface shear stress. Fig. 6.31 shows the ratio of crack tip opening for penetration and delamination as a function of the T-stress. The constraint loss associated with compressive T-stress promotes penetration for tensile dominated interface failure and delamination for shear dominated interfaces.

6.5 Conclusion

Numerical solutions of the plane strain elastic-plastic asymptotic fields of a crack normal to the interface between elastically and plastically mismatched solids have been obtained using modified boundary layer formulations.

When plasticity is limited to the material on the crack flanks, the elastic material ahead of the tip exhibits a logarithmic singularity. The logarithmic constant r_o is a loading parameter with the dimensions of distance that can conveniently be identified with $(K/\sigma_o)^{\frac{1}{1-\lambda}}$ or the crack tip opening displacement. The crack tip field in the material behind ($\pi/2 \leq \theta \leq \pi$ and $-\pi \leq \theta \leq -\pi/2$) is composed of elastic and plastic sectors that have finite crack tip stresses, full plasticity being achieved for tensile T-stresses when the characterising parameter of the field, hoop stress at the interface, reaches its peak value, $k(1 + \pi/2)$.

When the crack is located in an elastic solid, the structure of the mode I fields is similar and in the leading sectors only differ through a hydrostatic term. The mean stress or the constraint ahead of the crack tip, identified to be the characterising parameter of the

family of mode I fields, increases with increasing T-stress and decreasing elastic mismatch. Thus, for geometries with high elastic mismatch and negative T-stress the resistance for crack extension is expected to be be higher. As the mode mixity is increased , the plane of maximum stress rotates towards the interface. The mode II field parameter, θ^+, increases with increasing elastic mismatch, marginally increasing the stresses at the interface. The constraint effects associated with elastic mismatch and T-stress established in the limit of non-hardening are reproduced for moderately strain hardening material response.

The constraint loss associated with compressive T-stress and higher elastic mismatch increases the resistance to crack extension in the opening mode. A hard surface coating which has a high elastic stiffness compared to the substrate would have a high resistance to crack extension at small loads. However, since such a geometry would develop tensile T-stress, the loss of constraint as a result of elastic mismatch would get compensated by the tensile T-stress effects and the resistance to crack extension would fall with increasing load. However, in mismatched laminates compressive T-stresses develop, implying both elastic mismatch and T-stress would result in loss of constraint and higher toughness.

Loss of constraint increases the resistance to both interface penetration and delamination. However, if interface failure is dominated by normal stresses across the interface, loss of constraint favours interface penetration, whereas for interfaces which fail due to shear stress, constraint loss favours delamination.

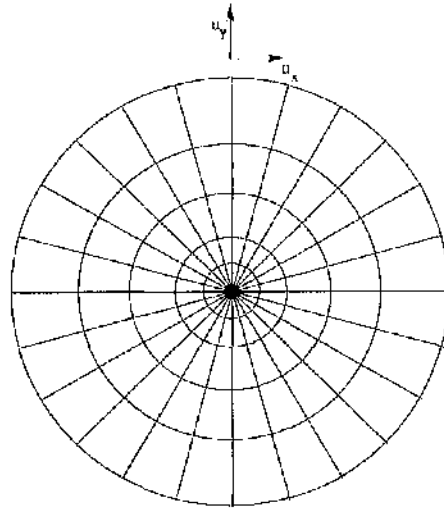Fig 6.1: Mesh of the modified boundary layer formulation
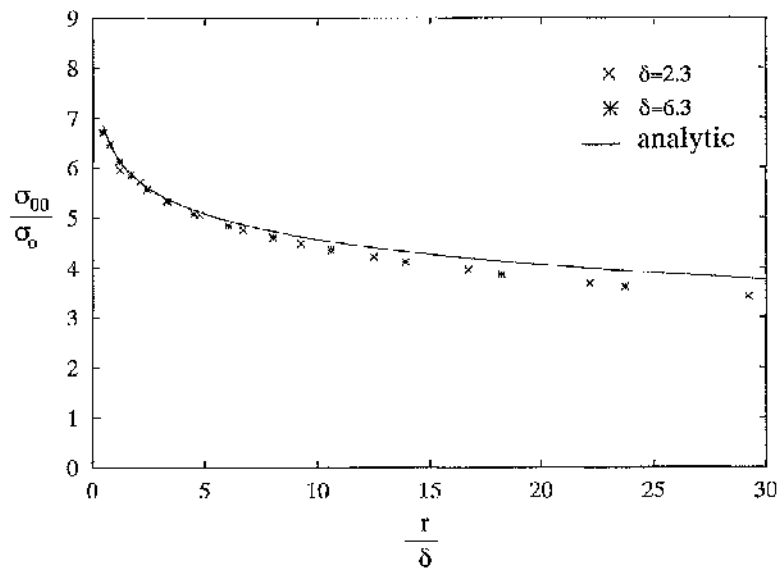
Fig 6.2: The hoop stress ahead of the crack tip as a function of the normalised distance from the crack tip for elastically matched solids ($\Omega = 1$) at $T = 0$.

Fig 6.3: The normalised asymptotic cylindrical stresses as function of the angle, θ (in degrees) for elastically matched solids ($\Omega = 1$) at different T-stresses.

Fig 6.4: Mode I normalised asymptotic cylindrical stresses as function of the angle, θ (in degrees) for different elastic mismatches at $T = 0$.

Fig 6.5: Mode I normalised mean and mises stresses as function of the angle, θ (in degrees) for different elastic mismatches at $T = 0$.

Fig 6.6: The effect of elastic mismatch on the mean stress ahead of the crack in mode I, $T = 0$.
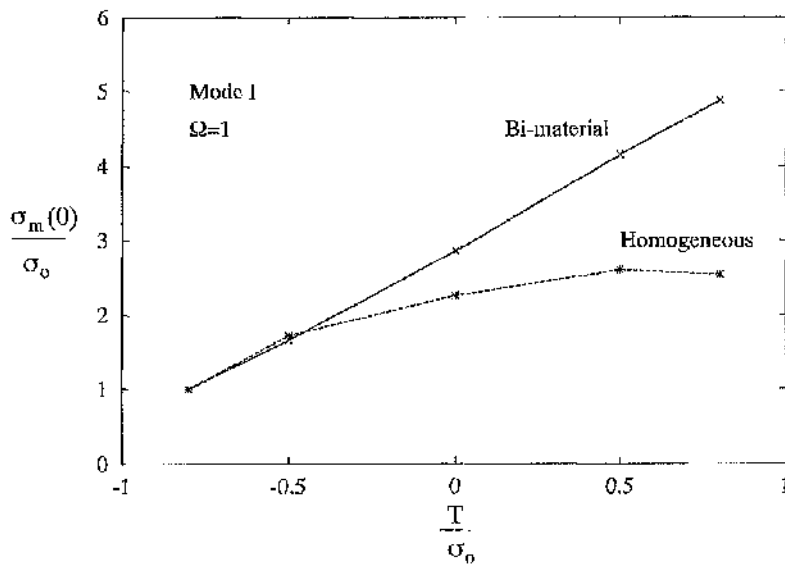
Fig 6.7: A comparison of the effect of the T-stress on an elastically matched but plastically mismatched bi-material, with an elastically and plastically homogeneous solid.
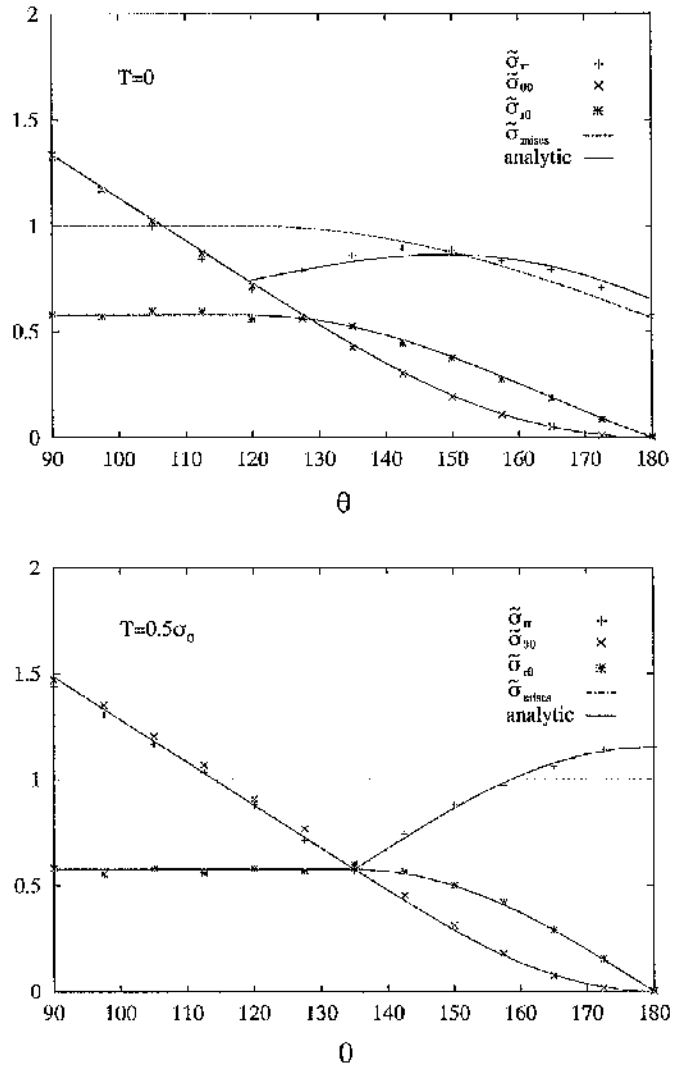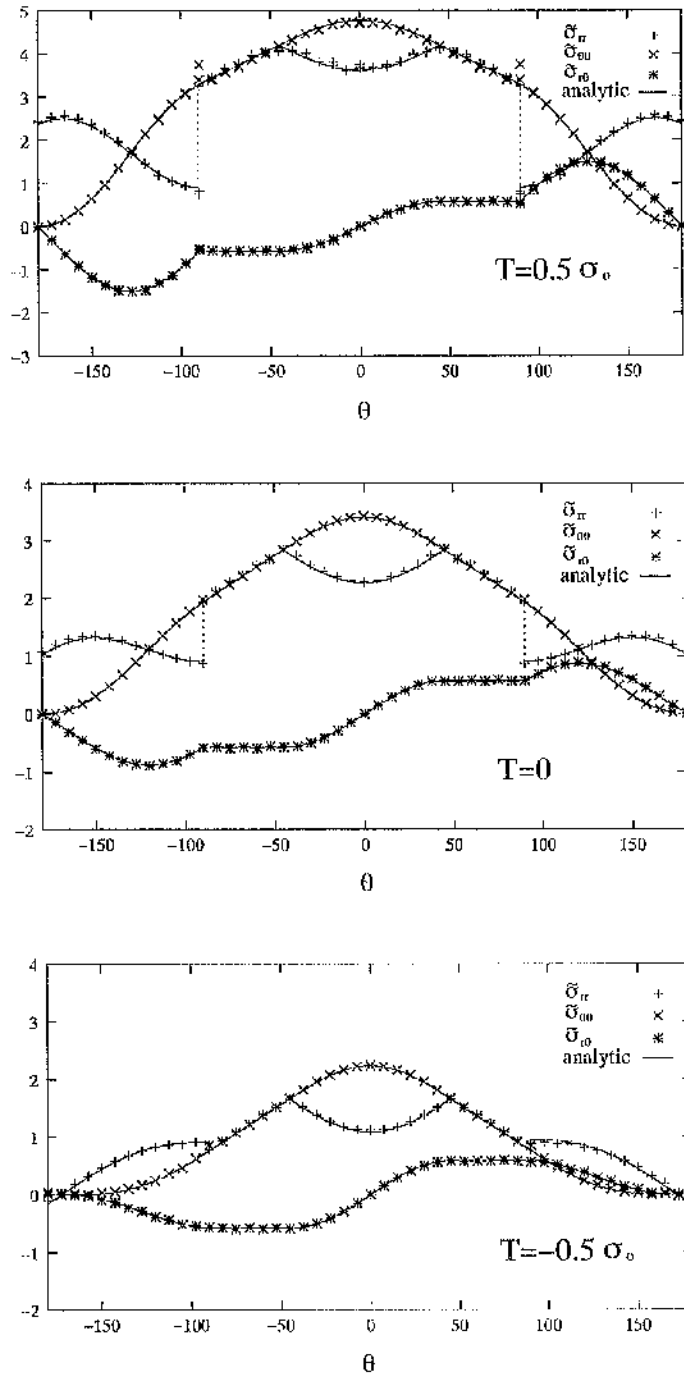
Fig 6.8: Mode I normalised asymptotic cylindrical stresses as function of the angle, θ (in degrees) for elastically matched solids ($\Omega = 1$) at $T/\sigma_o = 0.5$, 0, -0.5.
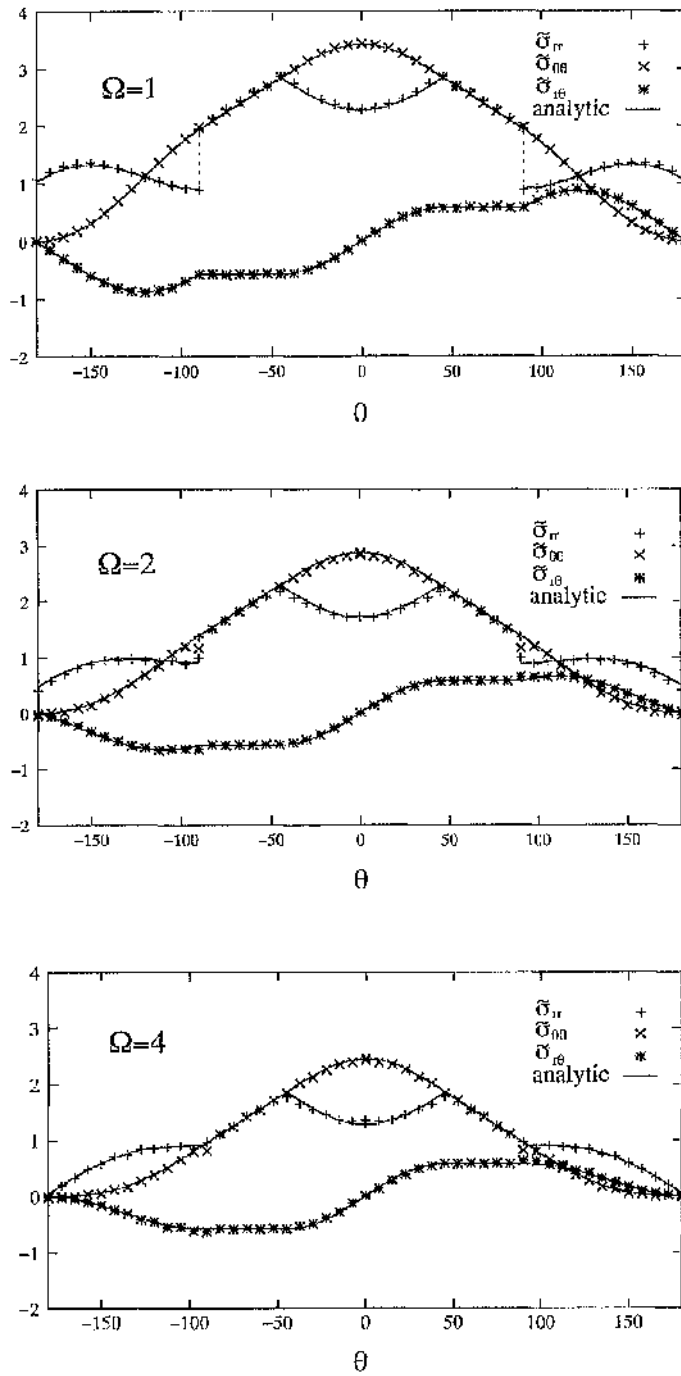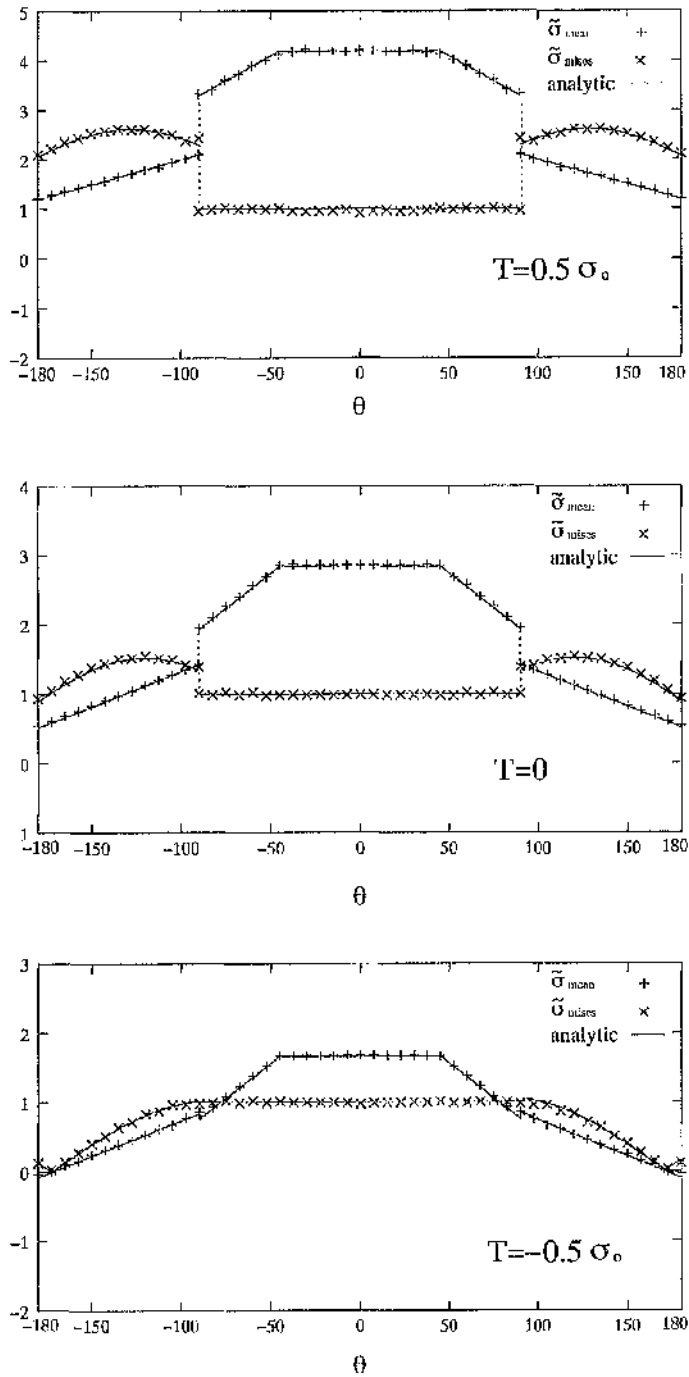
Fig 6.9: Mode I normalised mean and mises stresses as function of the angle, θ (in degrees) for elastically matched solids ($\Omega = 1$) at $T/\sigma_a = 0.5$, 0, -0.5.
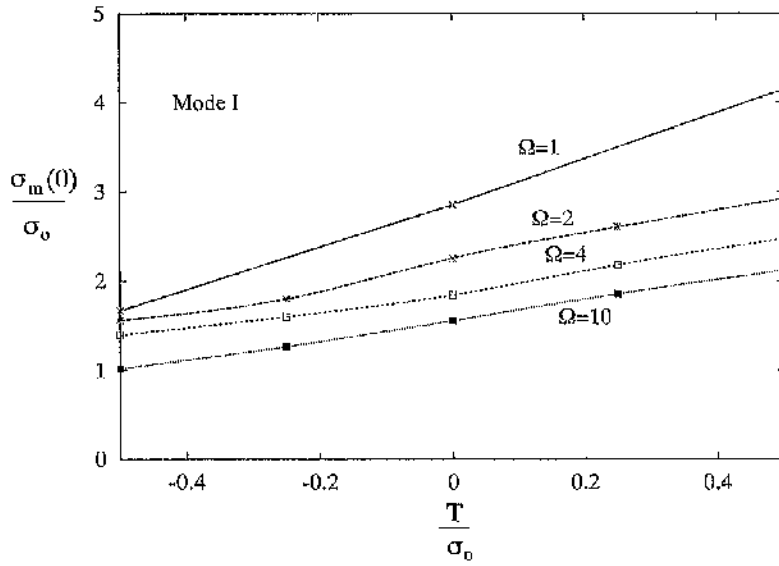
Fig 6.10: Effect of T-stress and elastic mismatch on crack tip constraint.
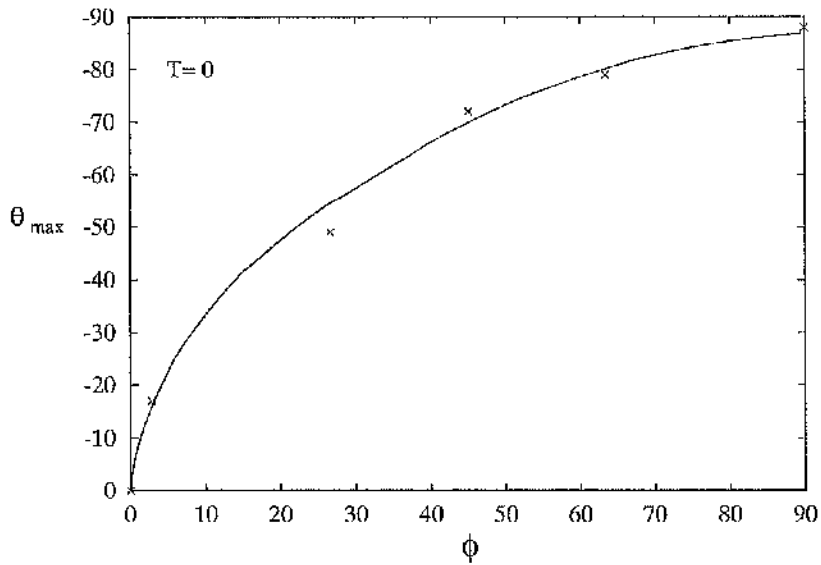
Fig 6.11: Direction of the plane of maximum hoop stress as a function of the loading phase angle for elastically matched but plastically mismatched solids ($\Omega = 1$).
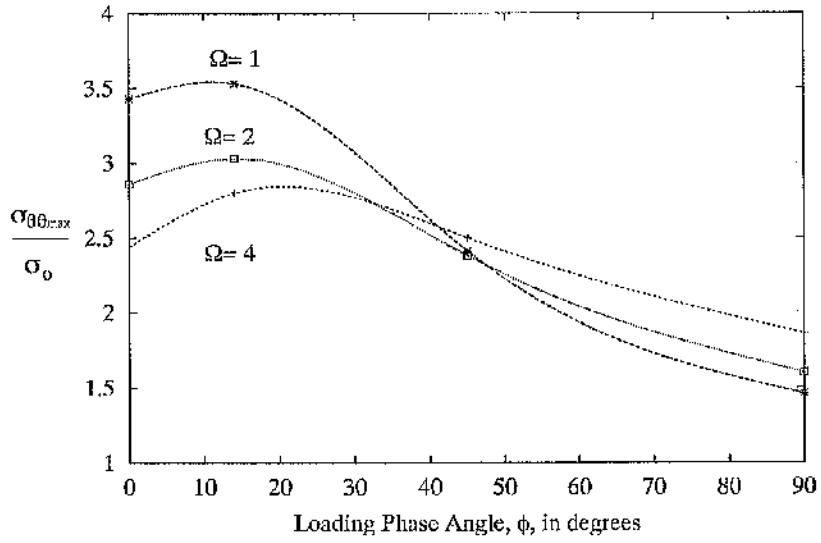
Fig 6.12: The effect of loading phase angle on the maximum hoop stress ahead of the crack, for three levels of mismatch, Ω, and $T = 0$.
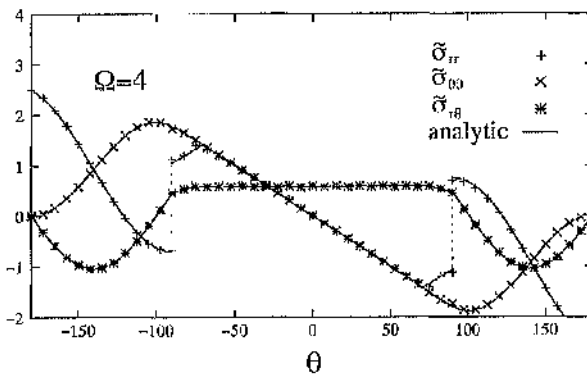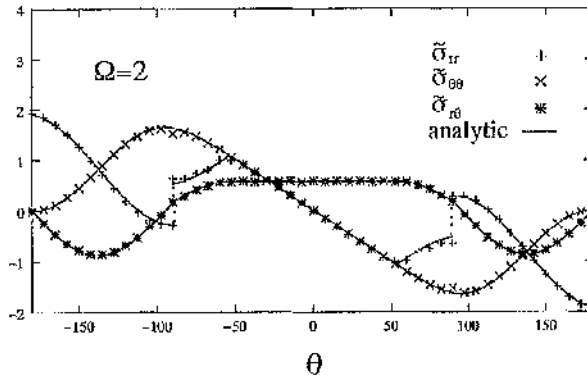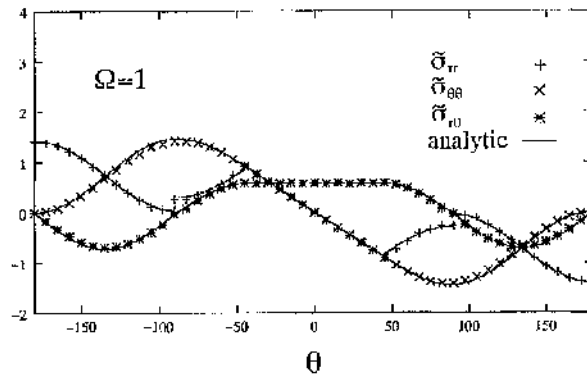
Fig 6.13: Mode II normalised asymptotic cylindrical stresses as function of the angle, θ (in degrees) for different elastic mismatches at $T = 0$.
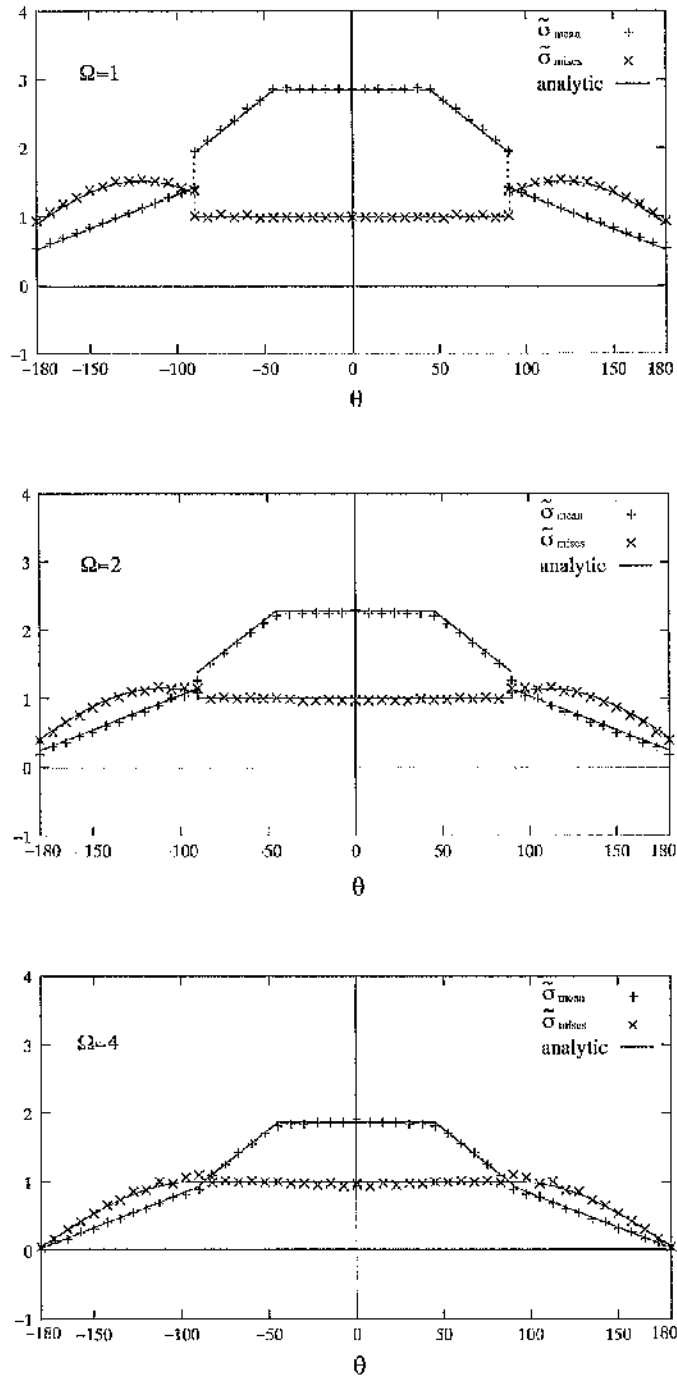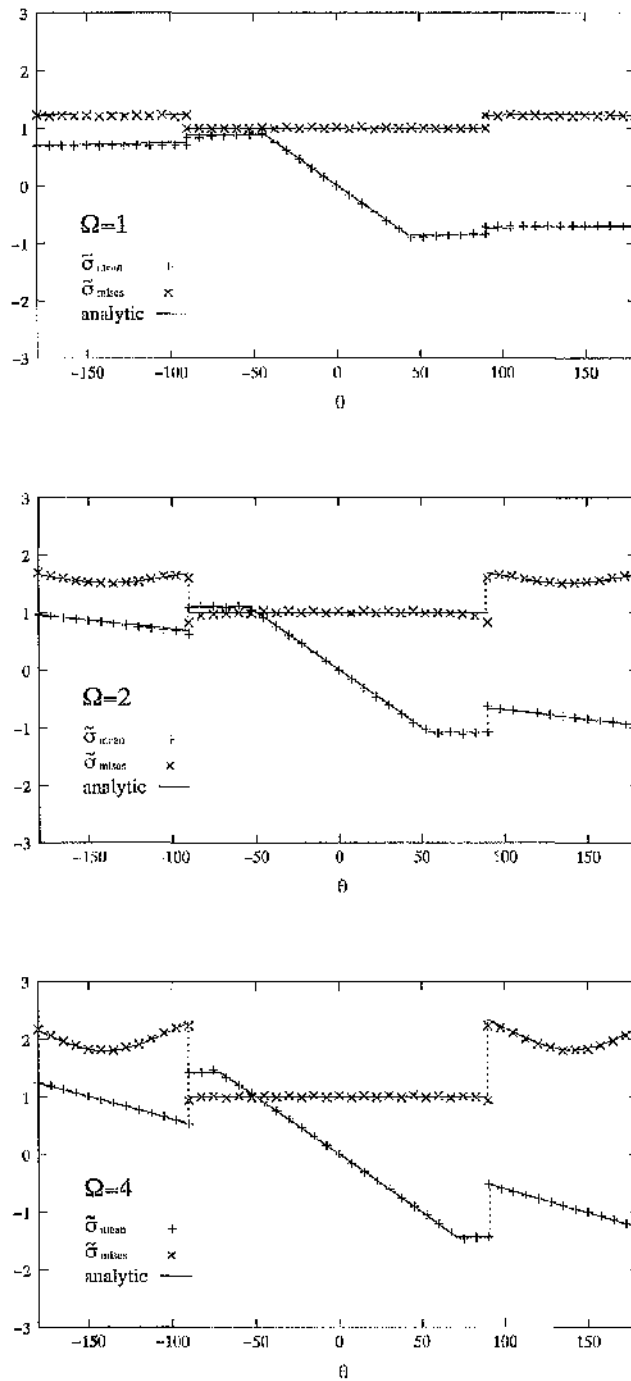
Fig 6.14: Mode II normalised asymptotic mean and mises stresses as function of the angle, θ (in degrees) for different elastic mismatches at $T = 0$.
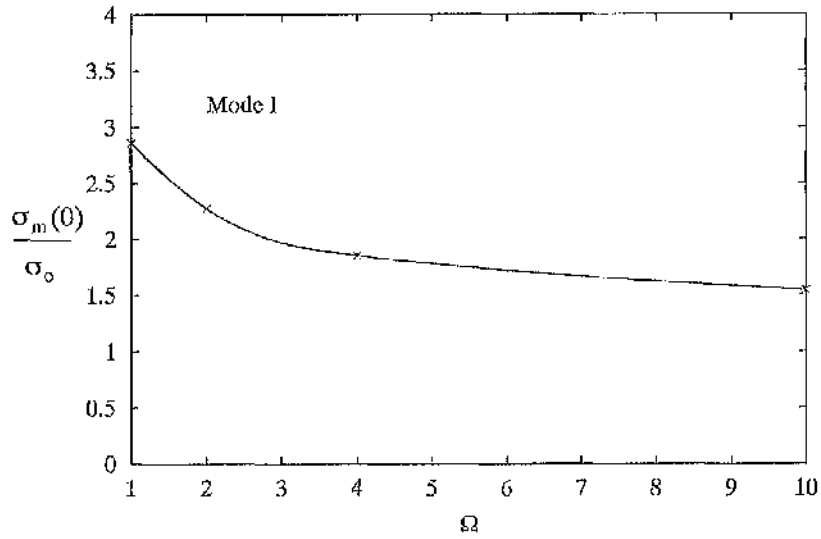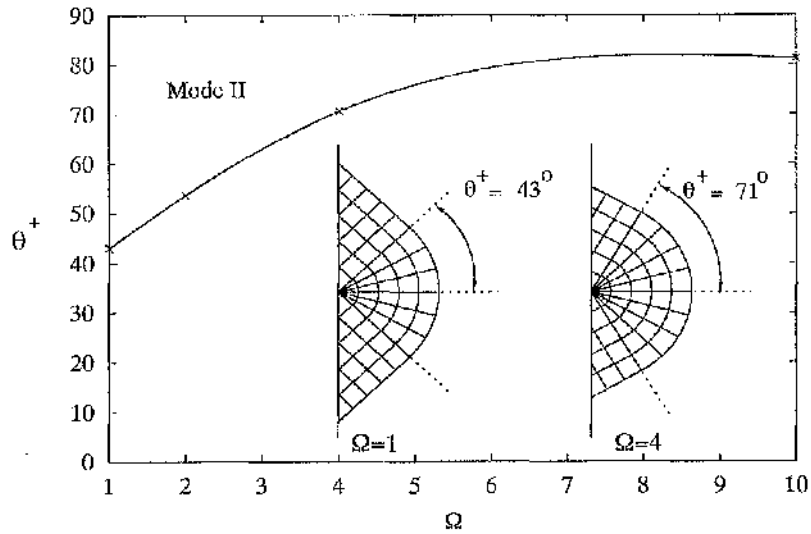
Fig 6.15: The effect of elastic mismatch on the span, θ^+, of the centred fan sector in mode II.
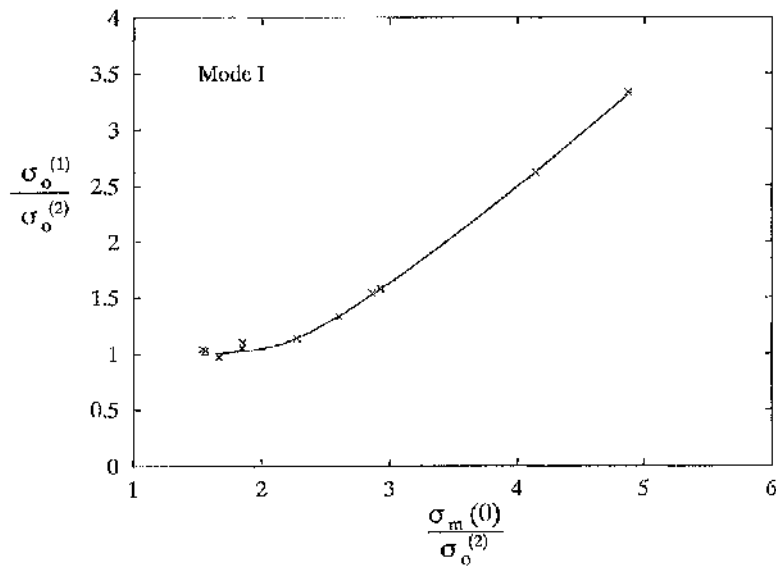
Fig 6.16: The critical ratio of yield stresses, $\sigma_o^{(1)}/\sigma_o^{(2)}$, for no plasticity behind interface.
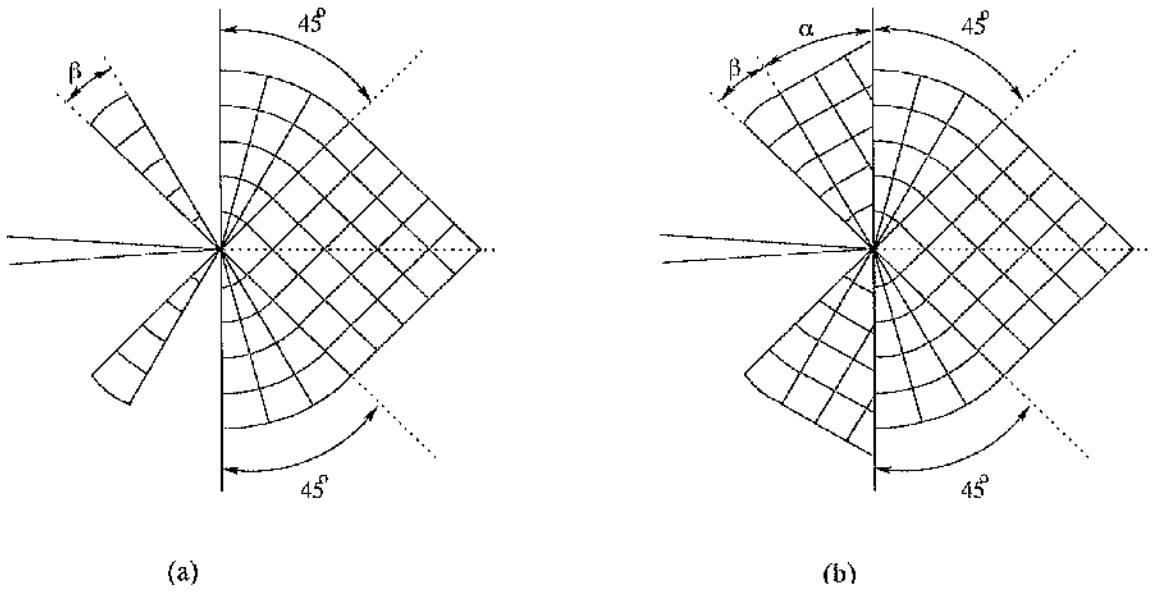
Fig 6.17: Mode I slip line fields when the yield stress ratio is less than critical.
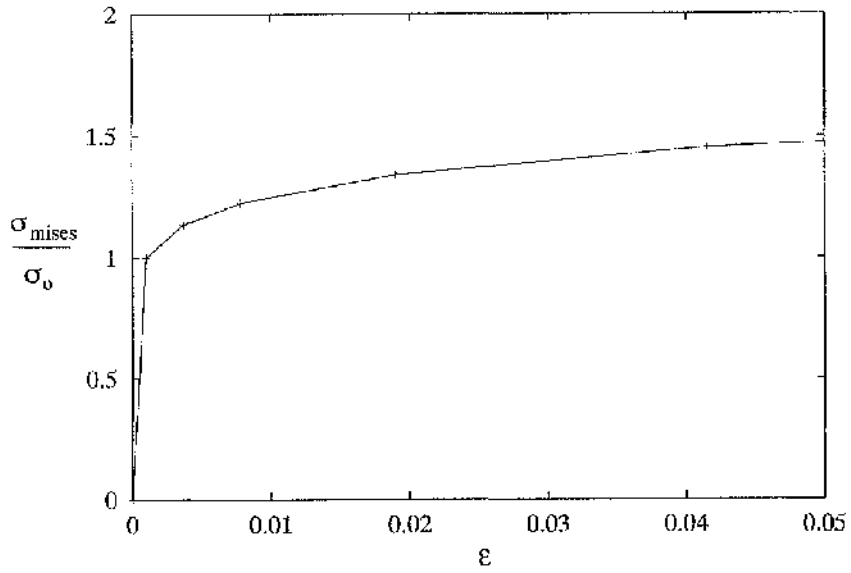
Fig 6.18: The stress-strain relationship for a strain hardening exponent, $n = 10$.
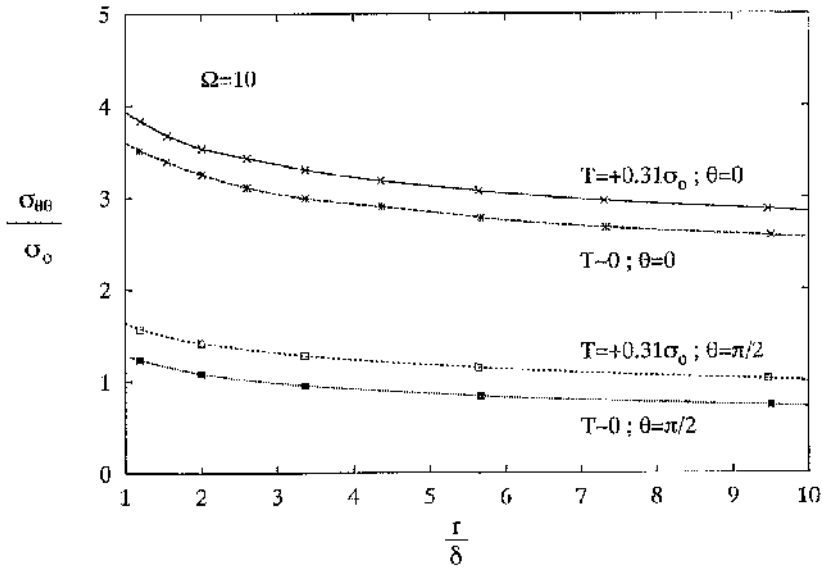
Fig 6.19: The effect of T-stress on hoop stress in the plane ahead of the crack tip in a strain hardening material.
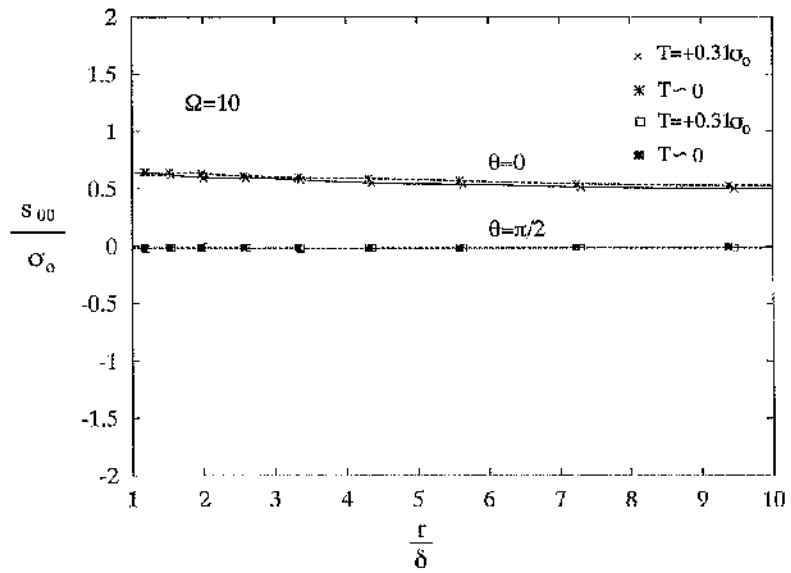
Fig 6.20: The effect of T-stress on deviatoric stress in the plane ahead of the crack tip in a strain hardening material.
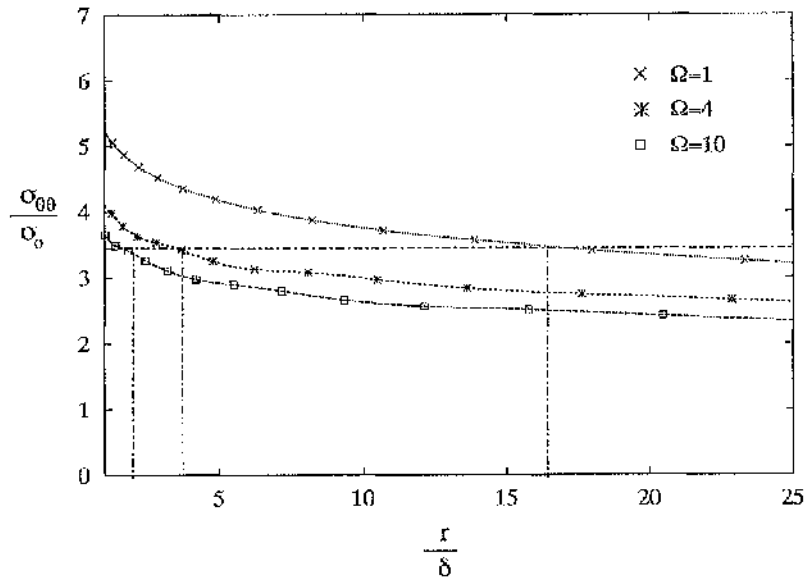
Fig 6.21: The effect of elastic mismatch on hoop stress ahead of the crack tip ($\theta = 0$) at $T = 0$.
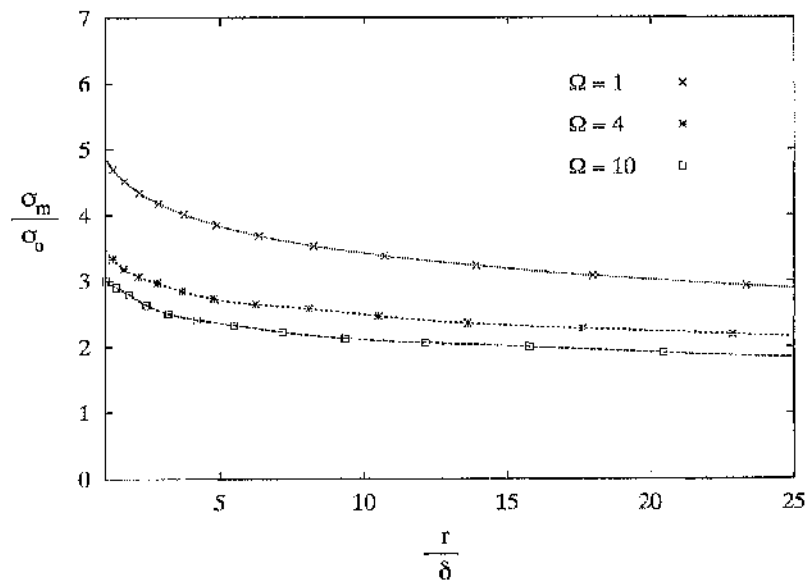
Fig 6.22: The effect of elastic mismatch on the hydrostatic component ahead of the crack tip ($\theta = 0$) at $T = 0$.
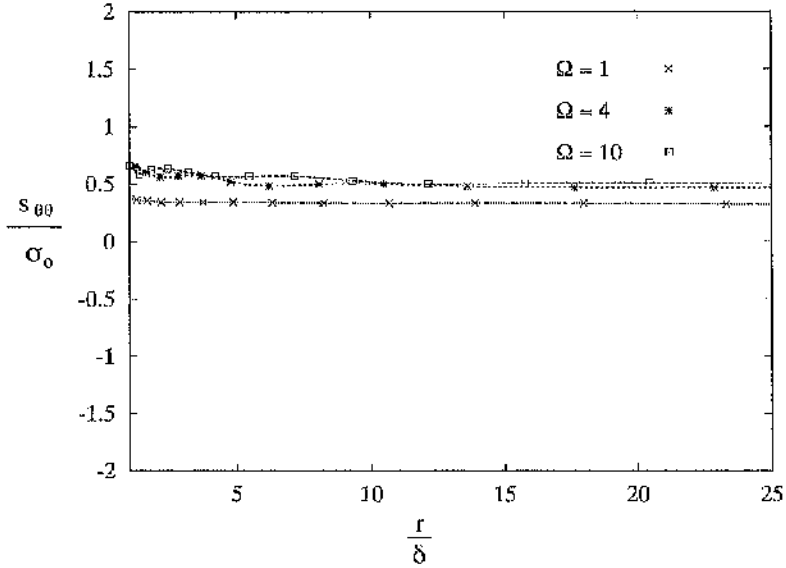
Fig 6.23: The effect of elastic mismatch on the deviatoric hoop stress ahead of the crack tip ($\theta = 0$) at $T = 0$.
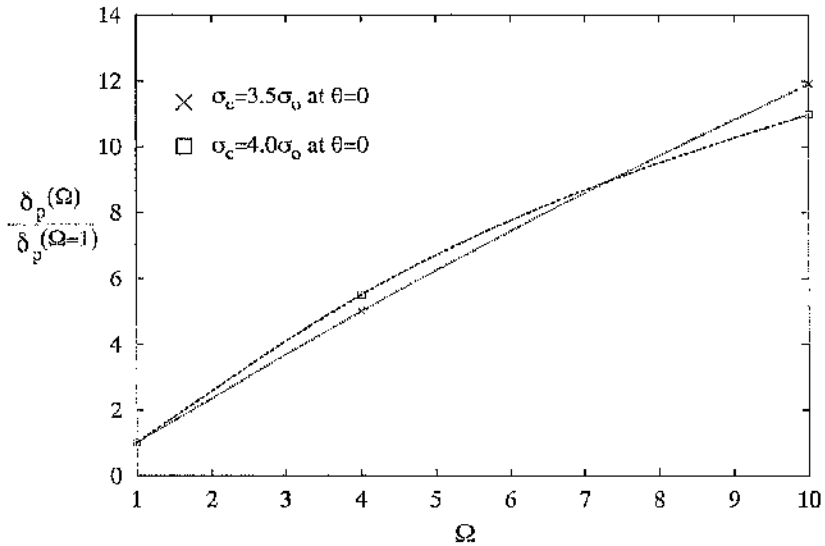
Fig 6.24: The effect of elastic mismatch on the crack opening displacement for $T = 0$.
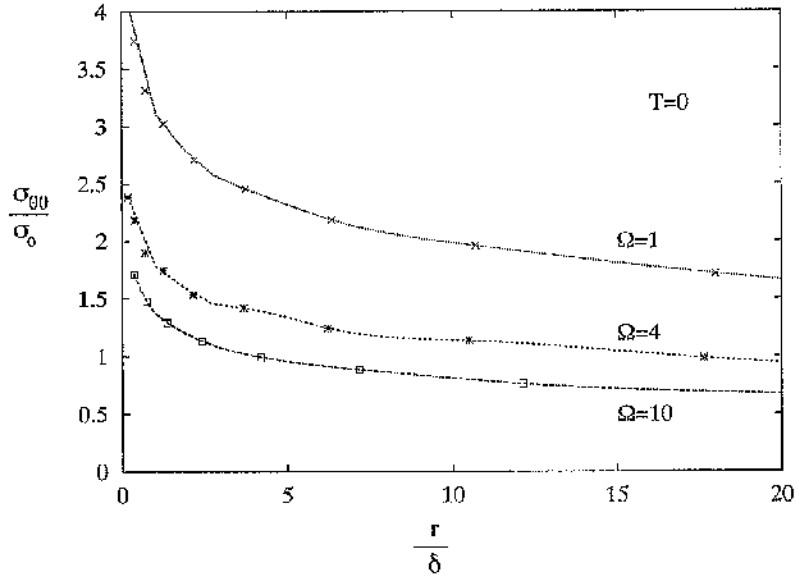
Fig 6.25: The effect of elastic mismatch on hoop stress at the interface ($\theta = \pi/2$) at T=0.
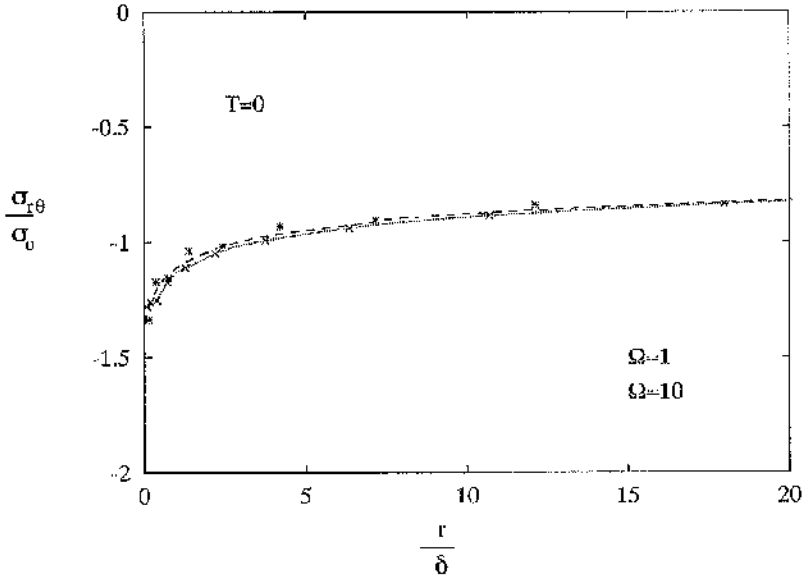
Fig 6.26: The effect of elastic mismatch on shear stress at the interface ($\theta = \pi/2$) at T=0.
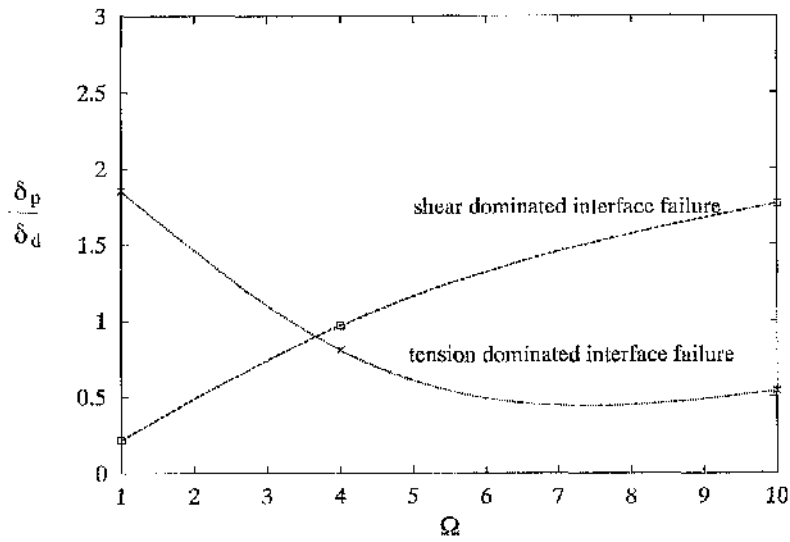
Fig 6.27: The effect of elastic mismatch on the ratio of the crack tip opening displacements, δ_p/δ_d for $T = 0$.
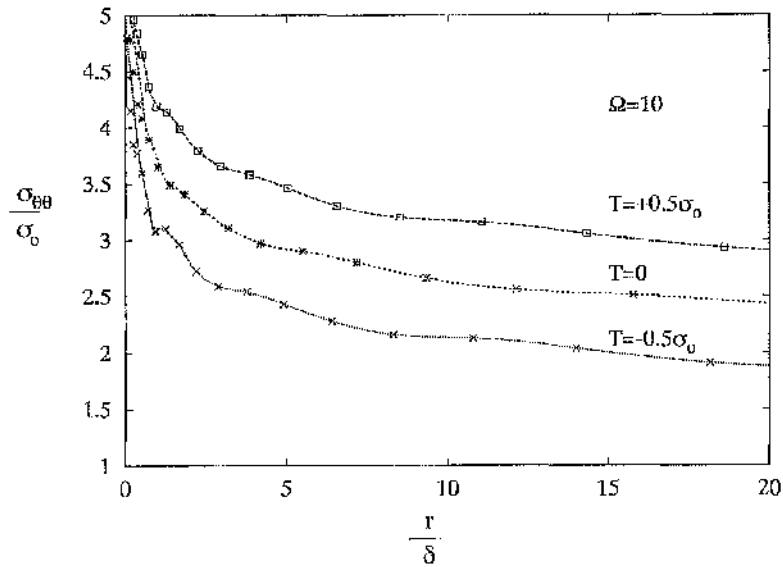
Fig 6.28: The effect of T-stress on hoop stress ahead of the crack tip ($\theta = 0$) for $\Omega = 10$.
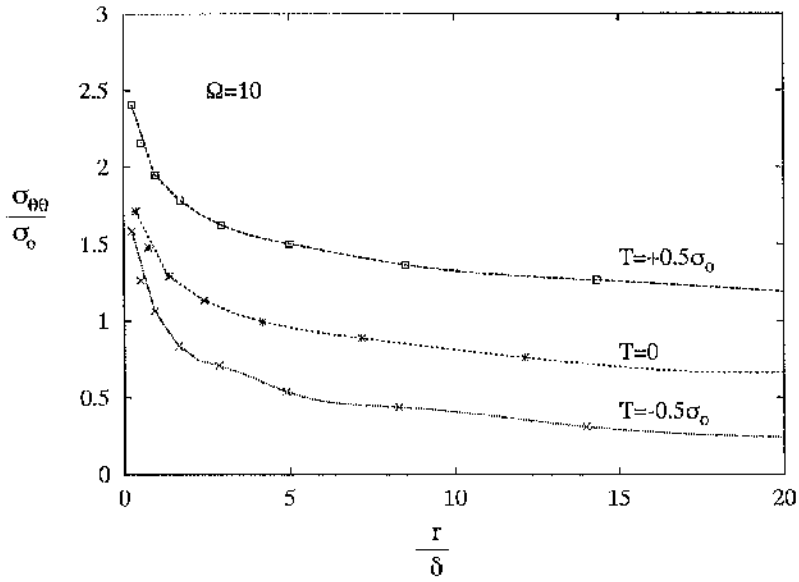
Fig 6.29: The effect of T-stress on hoop stress at the interface ($\theta = \pi/2$) for $\Omega = 10$.
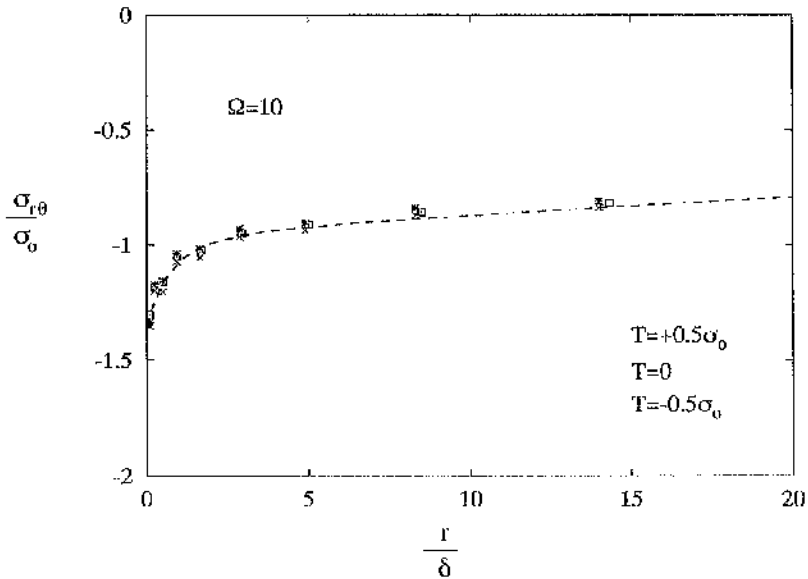
Fig 6.30: The effect of T-stress on shear stress at the interface ($\theta = \pi/2$) for $\Omega = 10$.
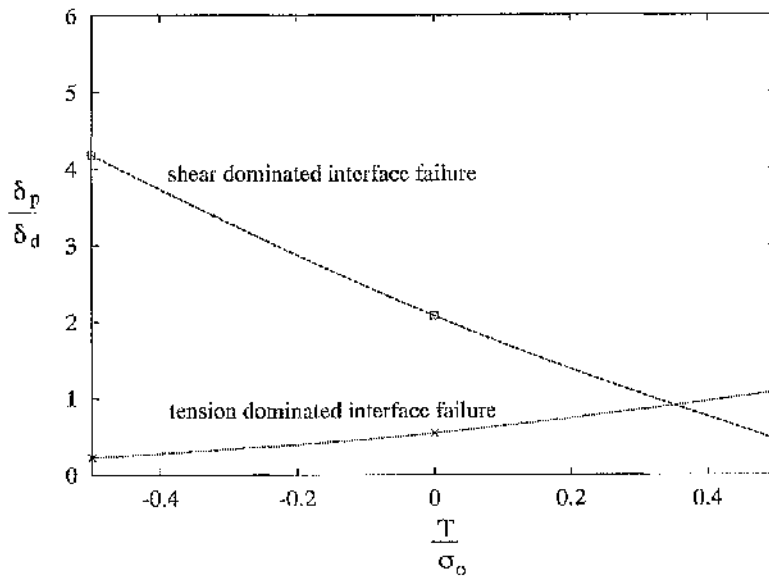
Fig 6.31: The effect of T-stress on the ratio of the crack tip opening displacements, δ_p/δ_d for $\Omega = 10$.

Cracks in Strength and Toughness Graded Materials

Functionally graded material systems are designed to avoid abrupt transitions in properties from one material to another by changing material properties in a continuous manner across an interfacial zone. A continuous spatial variation in properties may also result from manufacturing process such as welding. The present work is motivated towards the identifying effect of strength and toughness gradients, experienced by a crack in an interfacial zone of uniform elastic modulus. The problem may be considered as an idealisation of a crack in the heat affected zone between a weld and parent plate, or a crack subject to a non-uniform temperature field. Plane strain asymptotic stress fields under conditions of small scale yielding and non-hardening plasticity have been constructed. A statistical approach is used to discuss the effect of toughness and strength gradient on the failure probabilities and the crack trajectory.

7.1 Geometry

Consider two elastically matched homogeneous isotropic solids denoted by the superscript, $k = 1, 2$, which differ in yield strength, $\sigma_o^{(k)}$, and are joined by a graded zone of length $2l$. A crack is located at the centre of the zone with its flank parallel to the boundaries of the zone. Polar and Cartesian co-ordinate systems are centred at the crack tip as shown in Fig. 7.1. The yield strength within the zone is taken to be a linear interpolation between the yield strength of the two materials as shown in Fig. 7.2, such that:

$$\sigma_o(y) \;=\; \sigma_o^{(1)} \qquad\qquad\qquad (y > l)$$

$$= \left(\frac{\sigma_o^{(1)} - \sigma_o^{(2)}}{2l} \right) y + \left(\frac{\sigma_o^{(1)} + \sigma_o^{(2)}}{2} \right) \qquad (-l \le y \le l) \qquad (7.1)$$

$$= \sigma_o^{(2)} \qquad\qquad\qquad (y < -l)$$

and $\sigma_o^{(1)} \le \sigma_o^{(2)}$. The numerical solution is based on the boundary layer formulation technique developed by Rice and Tracey (1973) to model contained yielding. A circular focussed mesh centred at the crack tip was constructed for the elastic-plastic numerical analysis under conditions of plane strain contained yielding. The mesh was composed of 576 eight-noded isoparametric, reduced-hybrid elements, such that the ratio of the crack tip element to the outer radius of the mesh was $3/10^6$. The displacement field corresponding to the homogeneous elastic mode I solution was applied on the outer boundary of the mesh. The solids and the graded layer are taken to be almost plastically incompressible ($\nu = 0.49$) and non-hardening. In order to model plastically dissimilar solids joined by a graded interfacial zone, a C-program was written to assign a field variable to each node such that the field variable was a function of the nodal y-co-ordinate as indicated by Eq. 7.1, and the yield strength is assigned to be the field variable. Solutions were obtained for a range of plastic mismatches and constraint, as quantified by the second order term in the Williams expansion: the T-stress.

7.2 Plastic zone shape

In order to define the shape of plastic zone a numerical procedure prepared in *Matlab* v 5.3 (1999) was developed in which a Mises stress within 4 percent of the local yield strength was taken to be at yield. The plastic zone boundary was determined at radial intervals of 7.5 degrees around the crack tip. Due to the gradation in yield strength, even under a remote mode I load the plastic zone shapes are asymmetric about the crack plane. The co-ordinates of the plastic zone boundary points are normalised by the loading parameter $(K_I/\sigma_o^{tip})^2$

which has the dimensions of length: σ_o^{tip} being the yield stress at the crack tip. However, unlike plastic zones in homogeneous materials, this normalisation gives a plastic zone shape which depends on the load because the yield strength varies within the graded zone.

An important distinction is made between plastic zones comparable to or smaller than the graded zone width, and plastic zones with dimensions very much greater than the graded zone width. The maximum span of plastic zone normal to the crack plane, r_p, is taken as a measure of the plastic zone size as shown in Fig. 7.3. Plastic zone shapes for a system with mismatch, $M = 2$ and the ratio between the graded zone width and the outer boundary, $20/10^6$, are shown in Figs. 7.4-7.5.

When the plastic zone is small compared to the graded zone width ($r_p \ll 2l$), the difference in yield strength across r_p is insignificant. Thus, the shape of the plastic zone tends towards that of a crack in a homogeneous material under the same remote loading conditions, as shown in Fig. 7.4 for mode I. As the ratio $r_p/2l$ increases the plastic zone shape becomes asymmetric, the lobe within the softer material becoming larger than the lobe in the harder material. When the plastic zone is very much greater than the graded zone width ($r_p \gg 2l$), the effect of gradation on the plastic zone decreases as illustrated in Fig. 7.5, and the plastic zone shape tends towards that of an interface crack between plastically mismatched solids. An interface crack between dissimilar solids is the limiting configuration in which the graded zone width approaches zero ($2l \rightarrow 0$), corresponding to an abrupt change in properties across the interface. With increasing load the plastic zone shape evolves from a mode I shape till it saturates at a shape corresponding to a sharp interface crack as shown in Fig. 7.5.

For a general plastic mismatch, the crack tip stress field is asymmetric. The plastic mixity, $M_p = \lim_{r \to 0} \frac{2}{\pi} \tan^{-1} \left(\frac{\sigma_{\theta\theta}(0)}{\sigma_{r\theta}(0)} \right)$, is shown in Fig. 7.6 as a function of the non-dimensional loading parameter, $K/(\Delta\sigma_o\sqrt{l})$, where $\Delta\sigma_o = \sigma_o^{(2)} - \sigma_o^{(1)}$. Since in the geometry, $\sigma_o^{(2)}$ is taken to be greater than or equal to $\sigma_o^{(1)}$ and loading is mode I, stresses $\sigma_{\theta\theta}(0)$ and $\sigma_{r\theta}(0)$ are non-negative. Starting from the homogeneous mode I field which develops at a load level

asymptotically close to zero, the shear component at the crack tip increases, resulting in a decrease in plastic mixity with increasing load. The plastic mixity at the crack tip saturates at large loads when $r_p >> 2l$ as shown in Table 7.1. For a sharp interface problem, however, the plastic mixity is load independent, being 0.88 for $M = 2$ (Kim et. al, 1997).

In homogeneous solids mixity within the plastic zone only arises as a result of mixity in the remote loading. However, local mixity is an inherent feature of functionally graded problems. A crack in a homogeneous solid under a remote mixed mode loading ($K_I/K_{II} = 6$; $M_c = \tan^{-1}(K_I/K_{II}) = 0.89$) has the same crack tip plastic mixity, $M_p = 0.94$, as that of a crack in a graded zone between dissimilar solids at a plastic mismatch, $M = 2$, $r_p/2l = 207$ and under remote mode I loading. A comparison of the plastic zone shapes is shown in Fig. 7.7. Even though the plastic mixity at the crack tip is the same, the plastic zone shapes differ markedly. For a mixed mode field in a homogeneous material, asymmetry of the crack tip plasticity is associated with the rotation of the plastic lobes. However, in the case of dissimilar materials the plastic zone expands into the softer material resulting in a marked difference in the radius of the plastic lobes.

$\frac{r_p}{2l}$	$\frac{K}{(\Delta\sigma_o\sqrt{l})}$	M_p
$\to 0$	$\to 0$	$\to 1$
0.7	1.7	0.98
3	3.5.	0.958
25	10.5	0.94
207	31	0.94

Table 7.1: Mixity as a function of loading parameters.

7.3   Asymptotic analytic solution

For elastic perfectly-plastic homogeneous materials undergoing incompressible plane strain deformation, crack tip plasticity can be described by slip line theory. Following an argument developed by Rice (1982) and presented in section 5.1, but for graded material, the structure of the asymptotic field can be determined. In a graded material the yield stress is a function of r, θ. Differentiating the yield criterion with respect to θ gives:

$$\frac{3}{2}(\sigma_{\theta\theta} - \sigma_{rr})\frac{\partial}{\partial\theta}(\sigma_{\theta\theta} - \sigma_{rr}) + 6\sigma_{r\theta}\frac{\partial\sigma_{r\theta}}{\partial\theta} = 2\sigma_o\frac{\partial\sigma_o}{\partial\theta} \tag{7.2}$$

Substituting $(\sigma_{\theta\theta} - \sigma_{rr})$ and $\sigma_{r\theta}$ from Eq. 5.5-5.6 gives rise to the condition:

$$-\frac{3}{2}\frac{\partial\sigma_{r\theta}}{\partial\theta}\frac{\partial}{\partial\theta}(\sigma_{\theta\theta} + \sigma_{rr}) = 2\sigma_o\frac{\partial\sigma_o}{\partial\theta} \tag{7.3}$$

In the limit, as $r \to 0$, $\frac{\partial\sigma_o}{\partial\theta} \to 0$ as the material is locally homogeneous recovering Eq. 5.8. At the crack tip the stress field can be represented by a combination of constant stress sectors and centred fan sectors as described in Chapter 5. Numerical solutions of the asymptotic stress field show that the slip line field is composed of 6 sectors: an elastic sector at the upper flank, ES-6 ($\theta_5 \leq \theta \leq \pi$) followed by a constant stress sector, CS-5 ($\theta_4 \leq \theta \leq \theta_5$) that leads to a centred fan sector, CF-4 ($\theta_3 \leq \theta \leq \theta_4$) followed by a constant sector, CS-3 ($\theta_2 \leq \theta \leq \theta_3$), a centred fan sector, CF-2, ($\theta_1 \leq \theta \leq \theta_2$) and finally a constant stress sector at the lower flank, CS-1 ($-\pi \leq \theta \leq \theta_1$) as illustrated in Fig. 7.8. The configuration is the general 6-sector form identified by Zhu and Chao (2001) for homogeneous cracks under mixed mode loading. Ensuring continuity of tractions and traction free crack flanks, Zhu and Chao (2001) built up the analytical solution of the asymptotic field based on two parameters that are determined numerically, T_p and T_π defined as:

$$T_p = \sigma_{\theta\theta}(\theta = 0) - \sigma_{\theta\theta}(\theta = 0)^{prandtl} \qquad \text{for } \sigma_{r\theta}(\theta = 0) < k$$

$$= \sigma_{\theta\theta}(\theta = 0) - (1 + \frac{3\pi}{2})k \qquad \text{for} \quad \sigma_{r\theta}(\theta = 0) = k \qquad (7.4)$$

$$T_{\pi} = \frac{\sigma_{rr}(\theta = \pi) - \sigma_{rr}(\theta = \pi)^{prandtl}}{2} \qquad (7.5)$$

where, $\sigma_{\theta\theta}(\theta = 0)^{prandtl} = k(2 + \pi)$ and $\sigma_{rr}(\theta = \pi)^{prandtl} = 2k$ while the sector defining angles, $\theta_1 = -3\pi/4$, $\theta_2 = \theta_3 - \pi/2$, θ_3, θ_4 and θ_5 can be determined from:

$$\frac{T_{\pi}}{k} = -\frac{\cos(\theta_5 - 2\theta_4)}{\sin\theta_5} - 1 \qquad (7.6)$$

$$4\left(\theta_3 - \frac{\pi}{4}\right) = \left(2\theta_4 - \frac{3\pi}{2} - 1\right) - (\pi - \theta_5)\frac{\cos 2\theta_4}{\sin^2\theta_5} - \frac{\cos(\theta_5 - 2\theta_4)}{\sin\theta_5} \qquad (7.7)$$

$$\frac{T_p}{k} \quad - \quad \left(2\theta_3 - 1 - \frac{\pi}{2}\right) + \sin 2\theta_3 \qquad \text{for} \quad \sigma_{r\theta}(\theta = 0) < k$$

$$= \quad 4\theta_3 - \pi \qquad \text{for} \quad \sigma_{r\theta}(\theta = 0) = k \qquad (7.8)$$

Thus, in a 6-sector configuration the sector defining angle θ_1 is a constant, angles θ_2 and θ_3 depend only on T_p while θ_4 and θ_5 depend on both T_p and T_{π}. The asymptotic field then can be expressed in terms of the sector defining angles. The asymptotic stress field in the constant stress sector at the lower flank, CS-1, $(-\pi \leq \theta \leq \theta_1)$ is:

$$\sigma_{rr} = k(1 + \cos 2\theta)$$

$$\sigma_{\theta\theta} = k(1 - \cos 2\theta) \qquad (7.9)$$

$$\sigma_{r\theta} = -k \sin 2\theta$$

In the centred fan sector, CF-2, $(\theta_1 \leq \theta \leq \theta_2)$ the stresses are:

$$\sigma_{rr} = \sigma_{\theta\theta} = k\left(1 + \frac{3\pi}{2} + 2\theta\right) \tag{7.10}$$

$$\sigma_{r\theta} = -k$$

The stresses in the following constant stress sector, CS-3, $(\theta_2 \leq \theta \leq \theta_3)$ are:

$$\sigma_{rr} = k\left(1 + \frac{\pi}{2} + 2\theta_3\right) + k\sin 2(\theta - \theta_3)$$

$$\sigma_{\theta\theta} = k\left(1 + \frac{\pi}{2} + 2\theta_3\right) - k\sin 2(\theta - \theta_3) \tag{7.11}$$

$$\sigma_{r\theta} = k\cos 2(\theta - \theta_3)$$

The stress field in centred fan sector, CF-4, $(\theta_3 \leq \theta \leq \theta_4)$ is:

$$\sigma_{rr} = \sigma_{\theta\theta} = k\left(1 + \frac{\pi}{2} + 4\theta_3 - 2\theta\right) \tag{7.12}$$

$$\sigma_{r\theta} = k$$

The stresses in constant stress sector, CS-5, $(\theta_3 \leq \theta \leq \theta_4)$ are:

$$\sigma_{rr} = k\left(1 + \frac{\pi}{2} + 4\theta_3 - 2\theta_4\right) + k\sin 2(\theta - \theta_4)$$

$$\sigma_{\theta\theta} = k\left(1 + \frac{\pi}{2} + 4\theta_3 - 2\theta_4\right) - k\sin 2(\theta - \theta_4) \tag{7.13}$$

$$\sigma_{r\theta} = k\cos 2(\theta - \theta_4)$$

At the upper flank, the stresses in the elastic sector, ES-6, are:

$$\sigma_{rr} = C(1 + \cos 2\theta) + D(2\pi - 2\theta - \sin 2\theta)$$

$$\sigma_{\theta\theta} = C(1 - \cos 2\theta) + D(2\pi - 2\theta + \sin 2\theta) \tag{7.14}$$

$$\sigma_{r\theta} = -C\sin 2\theta + D(1 - \cos 2\theta)$$

where $C = -k\cos(\theta_5 - 2\theta_4)/\sin\theta_5$ and $D = -k\cos 2\theta_4/(1 - \cos 2\theta_5)$. To summarise, for a crack in a graded zone the crack tip field in general there is a 6-sector configuration. In the limiting case of a homogeneous crack it is a 5-sector configuration identified by Du and Hancock (1991). In the 6-sector configuration, the stress field in the sectors at the lower flank, CS-1 and CF-2, is independent of plastic mismatch. In the following constant stress sector, CS-3, the stress field can be expressed in terms of θ_3 which depends only on T_p. The plane of maximum hoop stress lies within CS-3, its orientation being at angle $\theta_3 - \pi/4$.

7.4 Numerical results

A boundary layer formulation analysis was performed using the commercial software *ABAQUS* v 5.8 (2003). The output stress data was processed using the routine described in Section 6.1.1. The asymptotic stresses at the interval of 7.5 degrees around the crack tip are compared with the analytic solutions for a plastic mismatch, $M = 2$ in Fig. 7.9. The analytic solution is based on the parameters identified by Zhu and Chao (2001): $T_p/k = -0.60$ and $T_\pi/k = -1.97$, the angles defining sectors are determined from the solution of transcendental Eqs. 7.6-7.8 using *Mathematica* to be: $\theta_1 = -135°, \theta_2 = -59°, \theta_3 = 31°, \theta_4 = 111°$, $\theta_5 = 155°$. The numerical solution of the stress field is in close agreement with the analytic solution. The crack tip mixity is $M_p = 0.94$. In a similar manner the asymptotic stress field

is obtained for a range of plastic mismatch to evaluate the effect of plastic mismatch. The effect of the second order term of the outer elastic field has also been examined at tensile and compressive T-stresses.

7.4.1   Effect of plastic mismatch on the asymptotic field

Analytic and numerical solutions for the asymptotic field have been determined for a range of plastic mismatches, $M = 1.2, 1.5, 2.0, 3.0$ and 4.0. The parameters characterising the 6-sector configuration of the crack tip field, T_p/k, T_π/k, and the sector boundaries are tabulated in Table. 7.2, the locations of the sector boundaries are tabulated in Table. 7.3.

For a mode I crack in a homogeneous solid, symmetry of the field requires the shear stress on the plane ahead of crack tip to be zero and the plastic mixity to be unity, $M_P = 1$. When a plastic mismatch is introduced, crack tip plasticity becomes asymmetric and the shear stress at the crack tip becomes non-zero, resulting in a decrease in plastic mixity. The plastic mixity is shown as a function of the plastic mismatch in Fig. 7.10. Increasing plastic mismatch results in lower hoop stresses at the crack tip ($\sigma_{\theta\theta}(0)/\sigma_o^{tip}$). The radial stress at the flank, $\sigma_{rr}(\pi)/\sigma_o^{tip}$, becomes more negative until it reaches the limit for yield: $-\sqrt{4/3}\sigma_o^{tip}$. The span of the centred fan sector in the lower half (CF-2) decreases with increase in plastic mismatch. Thus, the constant stress sector ahead of the crack tip CS-3, rotates towards the lower flank resulting in the plane of maximum hoop stress to rotate towards the higher yield strength material. The orientation of the plane of maximum hoop stress, θ_{max}, as a function of the yield strength mismatch is indicated in Fig. 7.11. Starting from a crack in a homogeneous solid in which the maximum hoop stress acts in the crack plane ($\theta = 0$), the orientation of the plane of maximum hoop stress saturates at an angle close to 20 degrees for plastic mismatches, $M > 3$. The span of the sector: CF-4, initially increases with plastic mismatch but for higher mismatches it decreases. The angular span of the trailing constant stress sector, CS-5, increases with plastic mismatch and saturates to 45 degrees.

Finally, the elastic wedge at the upper flank, ES-6, its span first decreases with increasing plastic mismatch but starts increasing for higher mismatches. Fig. 7.12 shows that increase in plastic mismatch results in a decrease in the mean stress in the plane ahead of the crack tip.

M	$\frac{\sigma_{\theta\theta}(0)}{\sigma_o^{tip}}$	$\frac{\sigma_{rr}(\pi)}{\sigma_o^{tip}}$	$\frac{T_p}{k}$	$\frac{T_\pi}{k}$	θ_1 (deg)	θ_2 (deg)	θ_3 (deg)	θ_4 (deg)	θ_5 (deg)
1.2	2.83	0.36	-0.24	-0.69	-135	-51	39	117	132
1.5	2.77	-0.58	-0.34	-1.50	-135	-54	36	118	158
2.0	2.62	-1.14	-0.60	-1.97	-135	-59	31	111	155
3.0	2.45	-1.14	-0.89	-1.97	-135	-64	26	102	147
4.0	2.38	-1.14	-1.00	-1.97	-135	-66	24	100	144

Table 7.2: The slip line field characterising parameters and sector boundaries for a range of yield strength mismatches.

M	CF-2 (deg)	CF-4 (deg)	CS-5 (deg)	ES-6 (deg)
1.2	84	78	15	48
1.5	81	82	40	22
2.0	76	80	44	25
3.0	71	76	45	33
4.0	69	76	44	36

Table 7.3: The angular span of sectors for a range of yield strength mismatches.

7.4.2 Effect of T-stress on the asymptotic field

The effect of the second order term in Williams expansion, T-stress, has been determined for a yield strength mismatch, $M = 2$, at $T/\sigma_o^{tip} = -0.33$, 0 and 0.33. The characterising parameters of the 6-sector configuration, T_p/k and T_π/k and sector boundaries are tabulated in Table. 7.4. In the crack tip fields shown in Fig. 7.13, the angular spans of the constant sectors: CS-1 and CS-3 remain constant while there is negligible effect of T on the trailing constant stress sector: CS-5. However, compressive T-stress results in an increase in the elastic wedge angle at the upper flank as observed for a crack in a homogeneous material (Du and Hancock, 1991). For compressive T the angular spans of centred fans: CF-2 and CF-4, decrease. Decrease in the span of centred fan, CF-2, causes the constant stress sector ahead of the crack tip to rotate towards the lower flank, thereby rotating the plane of maximum hoop stress towards the plastically stronger material and decreasing the plastic mixity as shown in Table. 7.4. The decrease in plastic mixity and increase in the angle of orientation of the maximum hoop stress associated with compressive T-stress is illustrated in Figs. 7.14-7.15.

$\frac{T}{\sigma_o^{tip}}$	$\frac{\sigma_{\theta\theta}(0)}{\sigma_o^{tip}}$	$\frac{\sigma_{rr}(\pi)}{\sigma_o^{tip}}$	$\frac{T_p}{k}$	$\frac{T_\pi}{k}$	θ_1 (deg)	θ_2 (deg)	θ_3 (deg)	θ_4 (deg)	θ_5 (deg)	M_p
-0.33	2.22	-1.02	-1.29	-1.88	-135	-71	19	92	134	0.87
0	2.62	-1.14	-0.60	-1.97	-135	-59	31	111	155	0.94
0.33	2.79	-1.14	-0.31	-1.97	-135	-53	37	120	165	0.96

Table 7.4: The effect of T-stress on the slip line characterising parameters and the sector boundaries for yield strength mismatch, $M = 2$.

7.4.3 Crack path based on the asymptotic stress field

In mixed-mode tests of homogeneous brittle solids, a range of steels were tested by Maccagno and Knott (1991) and polycrystalline alumina by Suresh and Shih (1991). In all cases, the crack tip mixity caused the crack to deviate from its original plane. Predictions of the crack extension direction based on the direction of asymptotic maximum hoop stress (Erdogan and Sih, 1963) and the direction of maximum strain energy release rate (Palaniswamy and Knauss, 1978) were in close agreement with the experimental results. In functionally graded elastic materials Gu and Asaro (1997) assuming local homogeneity use the crack tip mixity to predict failure towards the material of lower elastic stiffness in agreement with the experiments of Rousseau and Tippur (2000).

On the basis of local homogeneity at the crack tip a discussion can be developed to predict failure based on the asymptotic stress field. In the asymptotic stress field of a crack in a plastically graded zone, the structure of the 6-sector field is such that there is complete plasticity from the lower flank to the plane of maximum hoop stress. Thus, the mean stress in the plane of maximum hoop stress can be expressed in terms of the angle of the orientation of the plane, θ_{max}:

$$\sigma_m(\theta_{max}) = k(1 + \pi) - 2k\theta_{max} \tag{7.15}$$

In the asymptotic field if local homogeneity is assumed, an increase in θ_{max}, as a consequence of high plastic mismatch and compressive T-stress, implies loss of constraint and higher toughness favouring crack extension towards the harder solid.

7.4.4 Near tip field

The hoop stress normalised with the yield strength at the crack tip is shown as a function of distance normalised with l in Fig. 7.16 for $\frac{1}{2l}\left(\frac{K}{\sigma_o}\right)^2 = 88, 362$ when the graded zone

width was held constant. Fig. 7.17 shows the stress for $\frac{1}{2l}\left(\frac{K}{\sigma_o}\right)^2 = 145, 362$ when K was held constant while the width of the graded zone was changed. From these figures it is evident that for a non-hardening response, normalising the distance with the graded zone width results in self similar curves. The cylindrical stresses, σ_{rr}, $\sigma_{\theta\theta}$ and $\sigma_{r\theta}$, are shown in Figs. 7.18-7.20 as a function of distance from the crack tip at $\theta = 0^o$, 45° and 75° for a mismatch, $M = 2$. The stresses are normalised with the yield strength at the crack tip while the radial distance is normalised with l. Comparing the stress field with the stress field of an interface with the same mismatch, it was noted that the stresses at the boundary of the graded zone which is at a distance $l/\sin\theta$ from the crack tip shown in Fig. 7.21 have a form which is similar to the asymptotic stresses in a problem of a sharp interface as shown by the solid lines in Fig. 7.21. The stresses cannot be determined at $\theta - 0^o$ and $\pm 180^o$ as the boundary is an infinite distance from the tip. The asymptotic stresses for the problem of a sharp interface were obtained numerically by taking the limiting case when the graded zone width, $2l = 0$. This observation implies that if the boundary of the graded interfacial zone is within the critical distance at which cleavage failure initiates, the gradation in properties would have minimal difference on failure.

7.5 Statistical aspects

An important feature of cleavage failure is the scatter in the experimental data, which makes cleavage toughness data inherently irreproducible. The scatter maybe explained by the fact that the micro-structure of real materials is not homogeneous and that microcracks or defects are statistically distributed throughout the material. The material properties are thus distributed functions. A weakest link concept has been widely used to describe the scatter in strength and fracture toughness (Freudenthal, 1968; Beremin, 1983; Wang and Parks, 1992; O'Dowd et. al, 2000). In the weakest link approach, the failure of the whole system is determined by the weakest element. Failure is the result of the unstable propagation of the most

critical micro-crack within the weakest volume element. In this section, the key concepts in the development of a statistical approach to describe failure in homogeneous materials are reviewed and a framework is established which is extended for a crack in a graded material.

In the weakest link approach, the failure of the whole system is determined by the weakest element, possibly caused by propagation of the most critical micro-crack within the weakest volume element. For a volume V_o subjected to a uniform stress, σ, the cumulative probability, P_o, that V_o will fail at or before the stress σ, can be expressed as a two parameter Weibull distribution (Freudenthal, 1968):

$$P_o(\sigma) = 1 - \exp\left[-\left(\frac{\sigma}{\sigma_u}\right)^m\right] \tag{7.16}$$

where σ_u and m are the Weibull parameters. The corresponding probability density function, $p_o(\sigma)$ is of the form:

$$p_o(\sigma) = \frac{dP_o(\sigma)}{d\sigma} = \frac{m}{\sigma_u}\left(\frac{\sigma}{\sigma_u}\right)^{m-1}\exp\left[-\left(\frac{\sigma}{\sigma_u}\right)^m\right] \tag{7.17}$$

The average strength of the volume V_o is:

$$\bar{\sigma} = \int \sigma p_o(\sigma)d\sigma - \sigma_u\Gamma\left(1 + \frac{1}{m}\right) \tag{7.18}$$

The physical significance of the Weibull parameter, σ_u, can be inferred to be a measure of average strength:

$$\sigma_u = \frac{\bar{\sigma}}{\Gamma\left(1 + \frac{1}{m}\right)} \tag{7.19}$$

where $\Gamma\,()$ is the gamma function tabulated in standard mathematics textbooks. The failure of a larger volume V which is composed of V/V_o number of element volume, V_o, subject

to a uniform stress σ is the result of the failure of the weakest V_o within V. Survival of V requires survival of each V_o element, thus the probability that V survives, $P^{survival}$, is:

$$P^{survival} = (1 - P_o)^{\frac{V}{V_o}} = \left(\exp\left[-\left(\frac{\sigma}{\sigma_u}\right)^m\right]\right)^{\frac{V}{V_o}} \tag{7.20}$$

Therefore, the probability of failure of the volume V at or before the stress σ is attained is of the form:

$$P(\sigma) = 1 - \left(\exp\left[-\left(\frac{\sigma}{\sigma_u}\right)^m\right]\right)^{\frac{V}{V_o}} = 1 - \exp\left[-\frac{V}{V_o}\left(\frac{\sigma}{\sigma_u}\right)^m\right] \tag{7.21}$$

The corresponding probability density function can be written as:

$$p(\sigma) = \frac{\mathrm{d}P(\sigma)}{\mathrm{d}\sigma} = \frac{m}{\sigma_u}\frac{V}{V_o}\left(\frac{\sigma}{\sigma_u}\right)^{m-1}\exp\left[-\frac{V}{V_o}\left(\frac{\sigma}{\sigma_u}\right)^m\right] \tag{7.22}$$

The average strength of volume V is:

$$\bar{\sigma} = \int \sigma p(\sigma)\mathrm{d}\sigma = \sigma_u\left(\frac{V_o}{V}\right)^{\frac{1}{m}}\Gamma\left(1 + \frac{1}{m}\right) \tag{7.23}$$

Comparison of Eqs. 7.18 and 7.23 shows a *volume effect* such that with increasing volume of the material under stress, the average strength decreases. In other words, increasing the stressed volume increases the number of flaws that may cause failure. For instance, for a material with a Weibull modulus, $m = 20$, an increase in volume by a factor of 5 decreases the average strength by 8 percent.

The concept can be extended to a system with a non-uniform stress distribution, by dividing the stressed zone into n smaller volumes V_i which have approximately uniform stress σ_i (Freudenthal, 1968). The probability of survival, $P^{survival}$, of such a system would be:

$$P^{survival} = \prod_n (1 - P_i)$$

$$= \exp\left[-\frac{V_{(1)}}{V_o}\left(\frac{\sigma_{(1)}}{\sigma_u}\right)^m\right] \cdot \exp\left[-\frac{V_{(2)}}{V_o}\left(\frac{\sigma_{(2)}}{\sigma_u}\right)^m\right] \cdots \exp\left[-\frac{V_{(n)}}{V_o}\left(\frac{\sigma_{(n)}}{\sigma_u}\right)^m\right]$$

$$= \exp\left[\sum_n -\frac{V_i}{V_o}\left(\frac{\sigma_i}{\sigma_u}\right)^m\right] \tag{7.24}$$

The total probability of failure, P, of the system then can be expressed as:

$$P = 1 - P^{survival} = 1 - \exp\left[-\sum_n \frac{V_i}{V_o}\left(\frac{\sigma_i}{\sigma_u}\right)^m\right] \tag{7.25}$$

The Weibull stress, σ_w, is defined as (Freudenthal, 1968):

$$\sigma_w = \left[\sum_{i=1}^n \frac{\sigma_i^m V_i}{V_o}\right]^{\frac{1}{m}} \tag{7.26}$$

where, σ_i is the stress associated with volume, V_i, and V_o is a reference volume. The cumulative probability of failure in terms of Weibull stress becomes:

$$P = 1 - \exp\left[-\left(\frac{\sigma_w}{\sigma_u}\right)^m\right] \tag{7.27}$$

The argument can be developed to determine the failure probability in presence of a macroscopic defect such as a crack (Beremin, 1983). Lei et. al (1998) consider a crack in a homogeneous strain hardening solid, using cylindrical co-ordinates (r, θ) located at the tip of a crack in a plate of uniform thickness, an incremental volume $dV = rdrd\theta$ can be considered. Summation over the entire plastic zone can be replaced by an integral such that:

$$\sigma_w^m = \int \frac{\sigma_i^m}{V_o}dV = \frac{1}{V_o}\int_\pi^\pi \int_0^{r_c} \sigma_i^m Brdrd\theta \tag{7.28}$$

where $r_c(\theta)$ is the radius of the plastic zone and B is the thickness of the plate containing the defect. Dimensionally $r \sim J/\sigma_o\epsilon_o$, where J is the J-integral. For a strain hardening solid using the HRR field and ignoring all the non-dimensional terms:

$$\sigma_w^m \sim \frac{B}{V_o}\int_{-\pi}^\pi \int_0^{r_c} \left\{\frac{J}{\sigma_o\epsilon_o r}\right\}^{\frac{m}{n+1}} rdrd\theta \tag{7.29}$$

Integrating with respect to r and ignoring the integration with respect to θ which has no effect on the dimensions:

$$\sigma_w^m \sim \frac{B}{V_o} \left\{ \frac{J}{\sigma_o \epsilon_o} \right\}^{\frac{m}{n+1}} \frac{r^{\frac{2(n+1)-m}{n+1}}}{\frac{2(n+1)-m}{n+1}} \Big|_0^{r_c} \tag{7.30}$$

For the integral in Eq. 7.28 to be defined for a strain hardening solid of hardening exponent, n, the Weibull modulus, m, must be less than $2(n+1)$. For a linear elastic solid the condition reduces to $m > 4$. When $m \geq 2(n+1)$, the suggested method is to consider a notch at the crack tip which has a finite root radius. Introducing the limits of integration where the plastic zone radius, $r_c \sim J/\sigma_o \epsilon_o = JE/\sigma_o^2$:

$$\sigma_w^m \sim \frac{B}{V_o} \left\{ \frac{J}{\sigma_o \epsilon_o} \right\}^{\frac{m}{n+1}} \left\{ \frac{EJ}{\sigma_o^2} \right\}^{\frac{2(n+1)-m}{n+1}} \tag{7.31}$$

On simplification, the dependence of Weibull stress on dimensional terms is of the form:

$$\sigma_w \sim \left(\frac{B}{V_o} J^2 E^2 \sigma_o^{m-4} \right)^{\frac{1}{m}} \tag{7.32}$$

Lei et. al (1998) usefully introduce a non-dimensional Weibull stress $\tilde{\sigma}_w$, that is independent of crack tip deformation under J-dominant conditions:

$$\tilde{\sigma}_w^m = \frac{\sigma_w^m V_o}{J^2 E^2 \sigma_o^{m-4} B} \tag{7.33}$$

In the present work, the discussion is further developed by relating the Weibull parameter, σ_u, which is a material property to the average Weibull stress at failure by:

$$\sigma_u = \frac{\overline{\sigma}_w}{\Gamma \left(1 + \frac{1}{m} \right)} \tag{7.34}$$

substituting $\overline{\sigma}_w$ from Eq. 7.33, σ_u becomes:

$$\sigma_u = \tilde{\sigma}_w \left[\frac{\sigma_o^{m-4} E^2 B}{V_o} \right]^{\frac{1}{m}} \frac{J_c^{\frac{2}{m}}}{\Gamma \left(1 + \frac{1}{m} \right)} \tag{7.35}$$

On substitution the cumulative probability of failure becomes:

$$P = 1 - \exp\left[-\frac{J^{\frac{2}{m}}\Gamma\left(1+\frac{1}{m}\right)}{J_c^{\frac{2}{m}}}\right]^m = 1 - \exp\left[-\frac{J^2\Gamma\left(1+\frac{1}{m}\right)^m}{\overline{J_c^{\frac{2}{m}}}^m}\right] \qquad (7.36)$$

Using a dimensional argument $\overline{J_c^{\frac{2}{m}}}^m$ can be related to the mean toughness, $\overline{J_c}$, by:

$$\frac{\overline{J_c^{\frac{2}{m}}}^m}{\Gamma\left(1+\frac{1}{m}\right)^m} = \alpha^2 \overline{J_c}^2 \qquad (7.37)$$

where, α is a non-dimensional constant which depends on the toughness distribution. The probability of failure then can be written in the simple form:

$$P = 1 - \exp\left[-\frac{J^2}{\alpha^2 \overline{J_c}^2}\right] \qquad (7.38)$$

in which $J/\alpha\overline{J_c}$ is a loading parameter which controls the probability of failure. A crack in a homogeneous isotropic strain hardening material with strain hardening exponent $n = 10$ has been considered at three different load levels. The loading parameter and the cumulative failure probability of the system are given in Table. 7.5. As expected, increasing load results in a higher probability of failure,

$\frac{J}{\alpha \overline{J_c}}$	P
0.096	0.008
0.37	0.145
1.79	0.978

Table 7.5: The loading parameter and the failure probability.

In order to develop a framework to calculate the direction of crack propagation, the angular region around the crack tip is divided into sectors following a development given by Becker et. al (2002). Each sector is defined by the central angle, θ, and an angular span, $\Delta\theta$ as shown

in Fig. 7.22. The Weibull stress was calculated numerically for each sector, $\sigma_w^{sect}(\theta, \Delta\theta)$ using the boundary layer formulation in which the angular span, $\Delta\theta$ was 7.5 degrees. From the finite element analysis results, the principal stresses, Mises stresses, the co-ordinates and the volumes associated with each integration station of the 576 elements were recorded in a text file. The data was post-processed using a routine created in *Matlab* v 5.3 (1999) which evaluated the Weibull stress of each sector by summing over all the elements within a sector which were within the plastic zone. The weakest link approach requires that failure of the entire system occurs if a single sector fails or if more than one sector fails. The probability that the sector is involved in the failure process, including single or multiple sector failures, is given by:

$$P_{sect}(\theta, \Delta\theta) = 1 - \exp\left[-\left(\frac{\sigma_w^{sect}(\theta, \Delta\theta)}{\sigma_u}\right)^m\right] \tag{7.39}$$

Following the argument which led to the non-dimensionalisation of the Weibull stress, the Weibull stress for the sector, $\sigma_w^{sect}(\theta, \Delta\theta)$, has the dimensional dependence of $\sim J^{\frac{2}{m}}$. The probability of a sector being involved in the failure process can be written in the form:

$$P_{sect}(\theta, \Delta\theta) = 1 - \exp\left[-\frac{f(\theta, \Delta\theta)J^2}{\alpha^2 \overline{J_c}^2}\right] \tag{7.40}$$

where, $f(\theta, \Delta\theta) = (\sigma_w^{sect}(\theta, \Delta\theta)/\sigma_w)^m$. The probability that a sector of angular span 7.5^o is involved in the failure process has been determined as a function of θ in Fig. 7.23 for three load levels. A probability density function, $p(\theta)$, can be obtained by dividing P_{sect} by the angular span and normalising with the area under the curve such that $\int_{-\pi}^{\pi} p(\theta)\mathrm{d}\theta = 1$. The probability density function for the three load levels is shown in Fig. 7.24. A measure of the centralness of the crack extension direction is given by:

$$\overline{\theta} = \int_{-\pi}^{\pi} \theta p(\theta)\mathrm{d}\theta \tag{7.41}$$

For a mode I crack in a homogeneous material $\overline{\theta} = 0$. The probability that a sector is involved

in failure is bi-modal, the modal values occurring at $\theta \sim \pm 33^{\circ}$. The most likely directions of cleavage initiation are thus at $\pm 33^{\circ}$ to the crack plane.

The present work focuses on the effect of gradation in yield strength and toughness on the failure probabilities and the crack propagation directions. In functionally graded material systems, the Weibull stress continues to be a loading parameter. However, in contrast to homogeneous material in which σ_u is a constant material property σ_u in a graded material is a material property averaged over the process zone and is thus also dependent on loading. The probability of failure of a graded system can be written as:

$$P \;=\; 1 - \exp\left(\int \frac{\sigma^m}{V_o \sigma_u^m} \mathrm{d}V\right) \tag{7.42}$$

$$=\; 1 - \exp\left(-\int_V \left(\frac{\sigma^m}{\sigma_o^{m-4} J_c^{\frac{2}{m}} V_o}\right) \left[\frac{V_o \Gamma^m \left(1 + \frac{1}{m}\right)}{\tilde{\sigma}_w^m E^2 B}\right] \mathrm{d}V\right) \tag{7.43}$$

The formulation allows E and m to vary spatially. However for simplicity and relevance to experiments done on homogeneous material subject to non-uniform temperature field, interest is restricted to cases in which E, m are spatially independent. However, the strength and toughness, σ_o and J_c, are spatially dependent and are within the integral. Comparison with the probability of failure of a homogeneous material at the same applied J can be made by:

$$\frac{\ln(1 - P^{graded})}{\ln(1 - P^{hom})} = \left(\frac{\sigma_w^m}{\sigma_u^m}\right)^{graded} \cdot \left(\frac{\sigma_u^m}{\sigma_w^m}\right)^{hom} \tag{7.44}$$

For small probability of failures $\ln(1 - P) \sim -P$ such that:

$$\frac{P^{graded}}{P^{hom}} \;=\; \left(\frac{\sigma_w^m}{\sigma_u^m}\right)^{graded} \cdot \left(\frac{\sigma_u^m}{\sigma_w^m}\right)^{hom} \tag{7.45}$$

$$= \frac{\left(\int_V \left(\frac{\sigma^m}{\sigma_o^{m-4} J_c^{\frac{2}{m}} V_o} \right) \left[\frac{V_o \Gamma^m \left(1 + \frac{1}{m} \right)}{\bar{\sigma}_w^m E^2 B} \right] dV \right)}{\left(\frac{J^2}{J_c^{\frac{2}{m}}} \right) \Gamma^m \left(1 + \frac{1}{m} \right)}$$

An interfacial zone was considered across which toughness was uniform but there was plastic mismatch, $M = 2$. Toughness and yield strength were assumed to interpolate linearly across the interfacial zone. The Weibull modulus, m, was assumed to be 20 for both materials. For the same applied load, $J/\alpha J_c = 0.6$, at the outer boundary, different interface zone widths were considered such that the normalised plastic zone size $r_p/2l = 1.6, 4, 7, 15, 35$, the associated probability density functions are shown compared to the probability density function of an interface crack ($r_p/2l \rightarrow \infty$) in Fig. 7.25. At low values of $r_p/2l$, the density function is bi-modal and similar to the homogeneous mode I distribution. When the plastic zone becomes larger than the graded zone width, the peak in the harder material falls and the peak in the softer material grows such that the modal value, θ_{modal}, shifts towards the plane ahead of crack as illustrated in Fig. 7.26. Correspondingly, the direction of crack propagation increases and subsequently decreases with increasing $r_p/2l$, tending towards the prediction for a sharp interface as shown in Table. 7.6. The probability density function interpolates between the bi-modal distribution representation of a mode I crack in a homogeneous solid to a single peak distribution of an interface crack under remote mode I.

The relative probability of failure for a crack in a graded zone compared to a crack in a homogeneous solid with the properties at the tip of the graded material as evaluated using Eq. 7.45 is presented in Table 7.6. The relative probability of failure at low deformation levels is close to unity. As $r_p/2l$ increases, the relative probability of failure decreases which means the graded interface is more reliable. However, as the width of the graded zone is further decreased, the relative probability of failure starts increasing towards the sharp interface failure probability. Thus, whether the functionally graded material is more reliable

$\frac{r_p}{2l}$	$\frac{1}{2l}\left(\frac{K}{\sigma_o^{tip}}\right)^2$	$\frac{J}{\alpha J_c}$	$\left(\frac{\sigma_{1o}^m}{\sigma_u^m}\right)^y \cdot \left(\frac{\sigma_{1L}^m}{\sigma_{lo}^m}\right)^h$	$\bar{\theta}$(degrees)	θ_{modal}(degrees)
1.5	3.5	0.6	0.975	0.5	33
4	8.8	0.6	0.72	3	33
7	17.5	0.6	0.72	13	33
15	35.1	0.6	1.78	25	27
35	87.8	0.6	3.78	26	19
$\to \infty$	$\to \infty$	0.6	28.5	19	12

Table 7.6: Effect of deformation level as measured by $r_p/2l$ or $(1/2l)(K/\sigma_o^{tip})^2$ on the relative probability of failures for solids which have uniform toughness but are plastically mismatched, $M = 2$.

than a homogeneous solid of the crack tip properties depends on the size of the plastic zone compared with the width of the interface. For low values of $r_p/2l$ the interfacial zone is tougher whereas for large plastic zones, a crack in an interfacial zone is more likely to cause failure than a crack in a homogeneous solid of crack tip properties.

The crack propagation direction depends on both the toughness and the yield strength mismatch. To elucidate the effect of toughness and yield strength mismatch separately the case of a sharp interface crack is first considered at a plastic mismatch, $M = 1$ and the effect of toughness mismatch was determined at three different toughness mismatches, $\overline{J}_c^{(1)}/\overline{J}_c^{(2)} = 1, 2, 5$. Fig. 7.27 shows the effect of toughness mismatch on the crack extension direction for an interface crack when the two solids have identical yield strengths ($M = 1$). When the solids are toughness matched, the angular probability density function is that of a homogeneous solid and the average crack path angle is zero. As the toughness mismatch is increased, the modal peak in the tougher material decreases while the peak in the less tough material increases. As a consequence of increasing toughness mismatch, the average direction of crack initiation, tabulated in Table. 7.7, becomes more negative and bends towards

the less tough material.

In order to demonstrate the effect of plastic mismatch, the toughness is taken to be uniform $(\bar{J}_c^{(1)}/\bar{J}_c^{(2)} = 1)$ at different plastic mismatches, $M = 1, 1.2, 2$. When the solids are plastically matched ($M = 1$) the bi-modal angular probability density function is symmetric about the crack plane. However, as the plastic mismatch is increased, the peak in the harder material decreases while the peak in the softer material increases as shown in Fig. 7.28. The average crack extension direction is oriented towards the plastically weaker material as shown in Table. 7.8. Clearly mismatch in yield strength and toughness have opposing effects, the plastic mismatch favours crack extension into the softer material while toughness mismatch favours crack initiation in less tough material.

$\frac{\bar{J}_c^{(1)}}{\bar{J}_c^{(2)}}$	1	2	5
$\bar{\theta}$	0	-18	-29

Table 7.7: The effect of toughness mismatch, $\frac{J^{(1)}}{J^{(2)}}$, on the average angle of crack extension, $\bar{\theta}$.

M	1	1.2	2
$\bar{\theta}$	0	22	16

Table 7.8: The effect of plastic mismatch, M, on the average angle of crack extension, $\bar{\theta}$.

The location of a crack may also play a role in the crack initiation direction. The effect of crack location on the average crack extension direction graded zone with either solids as

shown in Fig. 7.29. For a mismatch of $M = 2$ and uniform toughness, $\bar{J}_c^{(1)}/\bar{J}_c^{(2)} = 1$, in the limit of $r_p >> 2l$, the probability density function is shown in Fig. 7.30 for three different locations of crack in the graded zone. When the crack is located at the boundary between the softer solid and the graded zone the average angle of crack extension is $17°$ towards the softer solid, the angle increases to $21°$ for the central crack and $30°$ for the lower boundary crack when the plasticity towards the harder material is comparatively restricted. The closer the location of the crack to the boundary with the harder material, the higher is the inclination of the angle of extension towards the softer side. The effect of location is most pronounced at high plastic mismatch and vanishes for plastically matched solids ($M = 1$).

7.6 Experiments

The effect of strength and toughness gradient on the crack extension direction was investigated experimentally for gradients normal to the crack plane. A non-uniform temperature field was created across a crack in a carbon steel of grade En32 whose chemical composition is shown in Table. 7.9. As the yield strength of ferritic steels is strongly dependent on temperature (Ritchie et. al, 1973; Bowen et. al, 1987), the temperature gradient causes a gradient in yield strength. The yield strength-temperature relation for En32 was measured in tensile tests performed at different temperatures by Bezensek (2003) and fitted with a curve as illustrated in Fig. 7.31. Nine fracture mechanics specimens were machined to the dimensions described in Fig. 7.32 with a 2.5 mm deep notch. The notched specimens were subject to fatigue in three point bending following ASTM E399-88 (1988) to introduce a sharp crack of length equal to half the width of the specimen ($a/w = 0.5$).

To develop the temperature gradient two chambers were installed on either side of the crack as shown in the schematic diagram in Fig. 7.33. One chamber had water circulated from a reservoir maintained at a temperature ($\sim 30°C$) while the other had liquid nitrogen to provide

C	Si	Mn	P	S	Cr	Mo	V
0.18	0.26	0.70	0.014	0.027	0.10	0.02	<0.003

Table 7.9: Chemical composition by percentage weight (wt%) of En32 steel.

cooling. The specimen passed through the two chambers such that 50 mm of the length was submerged in each chamber. A thermal calibration test was performed in which a series of thermocouples were used to record the temperature as a function of the location. Two thermocouples were spot welded on the surface and 5 were inserted into holes drilled to half the thickness. The temperatures are shown as a function of location in Fig. 7.34. In steady state conditions the temperature varied linearly between the two chambers, and there was only a small difference ($\sim$1-2°C) between the temperatures on the surface and within the specimen.

Pre-cracked fracture specimens were deformed in three point and four point bending using a 250 kN servo controlled electro-hydraulic INSTRON machine operating under displacement control at the rate of 0.5 mm/min. The results from the three point bend tests are ignored as the indentor influences the near crack tip temperature. In the four point bending experiments the span between the supports was 230 mm while the indentors were separated by 160 mm. To record the test-temperatures two thermocouples were spot welded on the surface on either side of the crack as shown in Fig. 7.33 such that crack tip temperature was taken as the average of the two recordings. The crack tip temperature for all tests was maintained between -70°C and -80°C causing cleavage failure. After fracture the specimen was cut across the centre and crack initiation angle was measured, a typical specimen cross section is shown in Fig. 7.35. The experimental data including the crack tip temperature (T_{tip}),

the temperature gradient, the load at failure (P_f) and the corresponding fracture toughness (J_c^g) calculated following ASTM 813 E are presented in Table 7.10. Cleavage failure initiation in En32 grade steel which was subjected to a graded temperature field shows a tendency to occur towards the hotter side which is the side of lower yield strength. With increasing temperature gradients the orientation of the crack initiation plane inclined more towards the softer side and the apparent fracture toughness increased. The trend of the crack growing towards the softer material matches with the prediction from the statistical approach in contained yielding. The crack path is thus not determined by the asymptotic field, using either a local maximum hoop stress or greatest potential energy release rate.

Weibull calculations were performed by Bezensek (2003) on a full-field model based on the present set of experiments. Elastic modulus, $E = 217$GPa, a strain hardening exponent $n = 10$, and a Weibull moduli, $m = 20$ were used. Initially the effect of gradient in yield strength was examined by taking the material to have a uniform toughness of 180 N/mm (corresponding to the crack tip temperature $T^{tip} = -80^{\circ}$C) but a spatially varying yield strength approximated by a curve fit to the experimental data from brittle fracture of En32 steel shown in Fig. 7.31. The probability density function is shown in Fig. 7.36 for a temperature gradient of 10 °C/mm and the average initiation angle was predicted to be 3.8° towards the warmer side.

When the yield strength was taken to be uniform at a temperature of -80°C, and the toughness to be dependent on temperature as in Fig. 7.37, extension is predicted to be 9° towards the colder side. The probability density function is shown in Fig. 7.38. The effect of toughness and yield strength mismatch observed in contained yielding solution are also observed in the full field analysis. When the combined effect of gradient in yield strength and toughness was taken into account the probability density function is shown in Fig. 7.39. Although the average extension direction is 2° towards the colder side, the most likely direction of crack propagation is ~30° towards the warmer side. The experimental results

show the crack extends towards the warmer side. Since the yield strength gradient due to a non-uniform temperature field is mild the sensitivity to the toughness gradient becomes very high and the curve used in the model may over-estimate the toughness of the warmer side. In the model the temperature is assumed to be have a uniform gradient which was based on a thermal test. Thus, better predictions using a statistical model may require a more accurate representation of the temperature field and the relation between the temperature and the toughness.

T_{tip} (°C)	Gradient (°C/mm)	$\bar{\theta}_{initiation}$	P_f (kN)	J_c^g (N/mm)
-71.0	3.0	6	17.85	147
-78.0	5.7	10	15.3	161
-78.5	6.3	17	16.2	177

Table 7.10: Experimental data from cleavage failure of En32 steel subjected to a temperature gradient.

7.7 Conclusions

A crack within a graded interfacial zone between two elastically similar but plastically dissimilar elastic-perfectly plastic solids has been studied. Asymptotic stress fields under contained yielding were constructed for remote mode I loading. At the crack tip, due to the non-uniform yield stress there is asymmetry in the plastic zone shape which depends upon the loading parameter $r_p/2l$. At very small levels of plasticity the field is near mode I, with increasing load the asymmetry in plasticity increases and eventually saturates. Due to the asymmetry, the shear component at the crack tip is non-zero such that the plane of maximum hoop stress is inclined towards the material of higher yield strength. The general structure of

the asymptotic slip line field is composed of 6-sectors as proposed by Zhu and Chao (2001) for homogeneous mixed-mode field. Increasing mismatch and compressive T-stress result in higher crack tip mixity and the constraint parameter, the mean stress, in the plane of maximum hoop stress decreases with increasing angle of inclination of the plane of maximum hoop stress. Thus, for increasing plastic mismatch and compressive T-stresses the direction of crack propagation inclines more towards the material of higher yield strength and the toughness increases.

Contact between the asymptotic field for a crack along an interface across which the plastic properties change abruptly (Kim et. al, 1997) and the stress field of a crack in a graded zone has been established. The stresses along the boundary of the graded zone correspond to the asymptotic stress field of the sharp interface crack such that for a graded zone width reaching the limit zero the asymptotic field of the sharp interface crack is recovered. Thus, the effect of gradation becomes negligible when the boundary of the graded zone is within a critical distance in which cleavage failure might initiate.

Using a statistical approach based on a weakest link model the effect of a gradient in yield strength and toughness on failure probability and crack extension direction was examined. In the statistical model the deformation level as measured by $r_p/2l$ plays an important role. At low $r_p/2l$ a crack in a graded zone is tougher than a crack in a homogeneous material of crack tip properties. However, for larger $r_p/2l$ the graded interface is less tough. The model establishes that the asymmetry of the plastic zone lobes on either side of the crack plane (resulting from the yield strength mismatch) drives the crack towards the softer side while the toughness mismatch causes the opposite effect, driving the crack towards the low toughness material. The effect of plastic mismatch is seen to dominate over the toughness variation except for cases of low plastic mismatches. Thus, unlike homogeneous solids the prediction of the maximum hoop stress direction in the asymptotic stress field and the average angle based on probabilistic arguments may give very different crack initiation directions.

Cleavage failure in En32 grade steel when subjected to a non-uniform temperature field confirms the predominant volume effect as the crack consistently initiates towards the hotter side (the side of lower yield strength).

Material 1

Graded Zone
Width $= 2l$
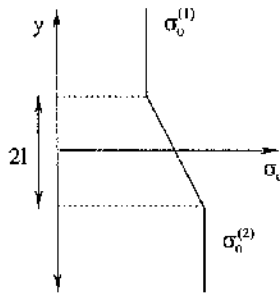
Material 2
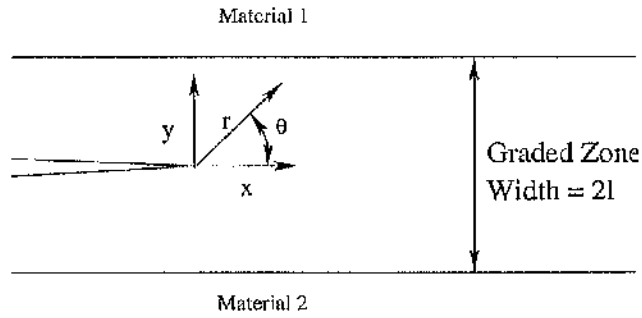
Fig 7.1: Crack located at the centre of a zone of graded yield strength.

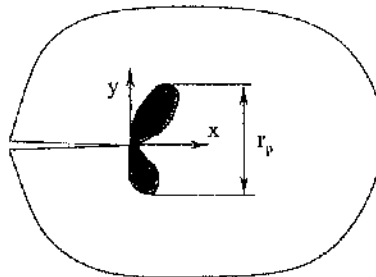Fig 7.2: Variation of the yield strength in normal to the crack plane.
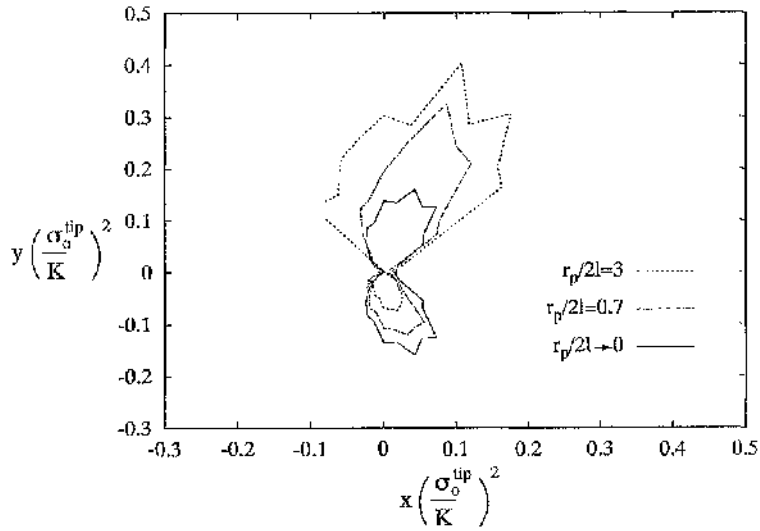

Fig 7.3: Measure of plastic zone size, r_p.

Fig 7.4: Plastic zone shapes for plastic zone sizes comparable to the graded zone width.
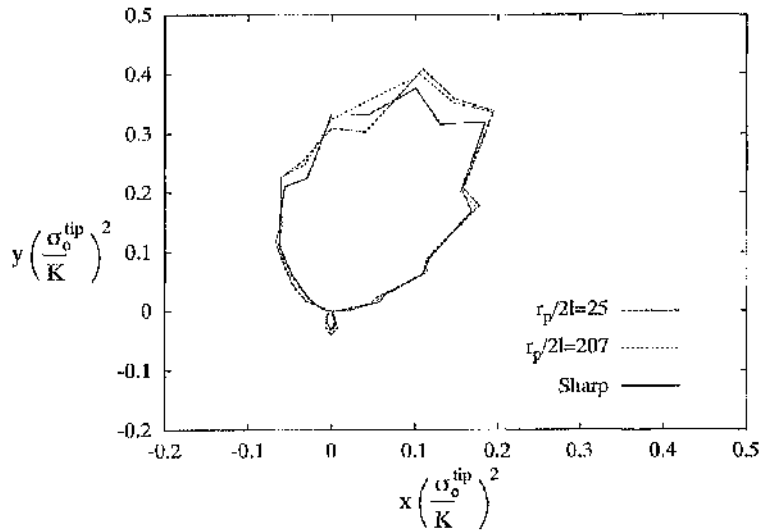
Fig 7.5: Plastic zone shapes for plastic zone sizes much greater than the graded zone width.
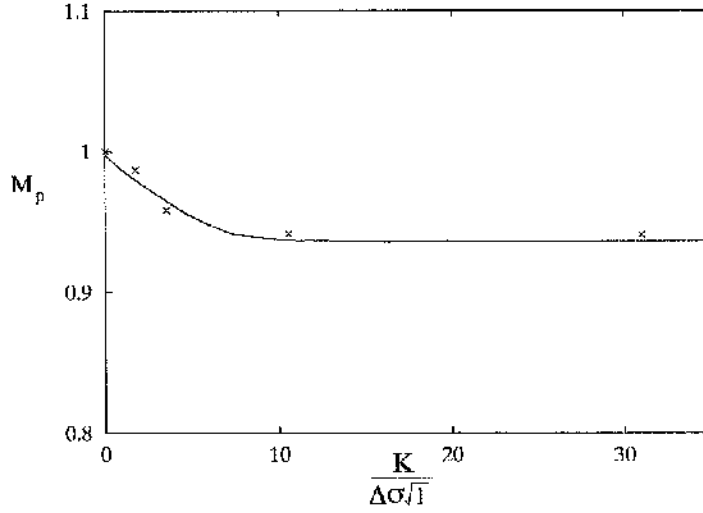
Fig 7.6: Plastic mixity, M_p, as a function of the remote load for mismatch, $M = 2$ and graded zone width, $2l$.
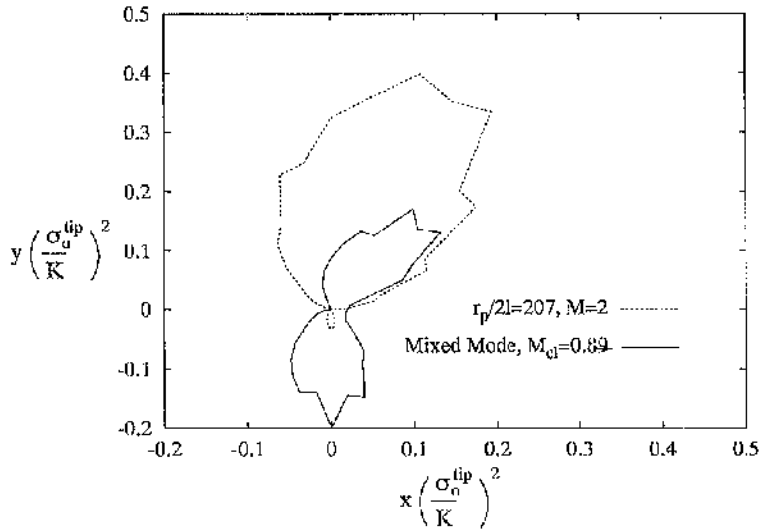
Fig 7.7: Plastic zones for a crack in a homogeneous material under mixed mode load ($K_I/K_{II} = 6$) and a crack in a graded zone between plastically mismatched solids ($M = 2$; $r_p/2l \rightarrow \infty$).
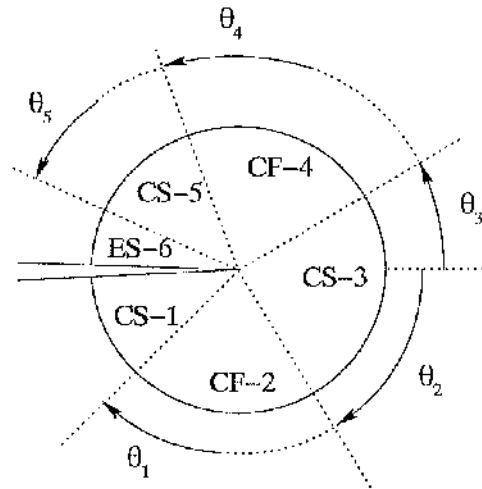
Fig 7.8: Structure of the crack tip slip line field.
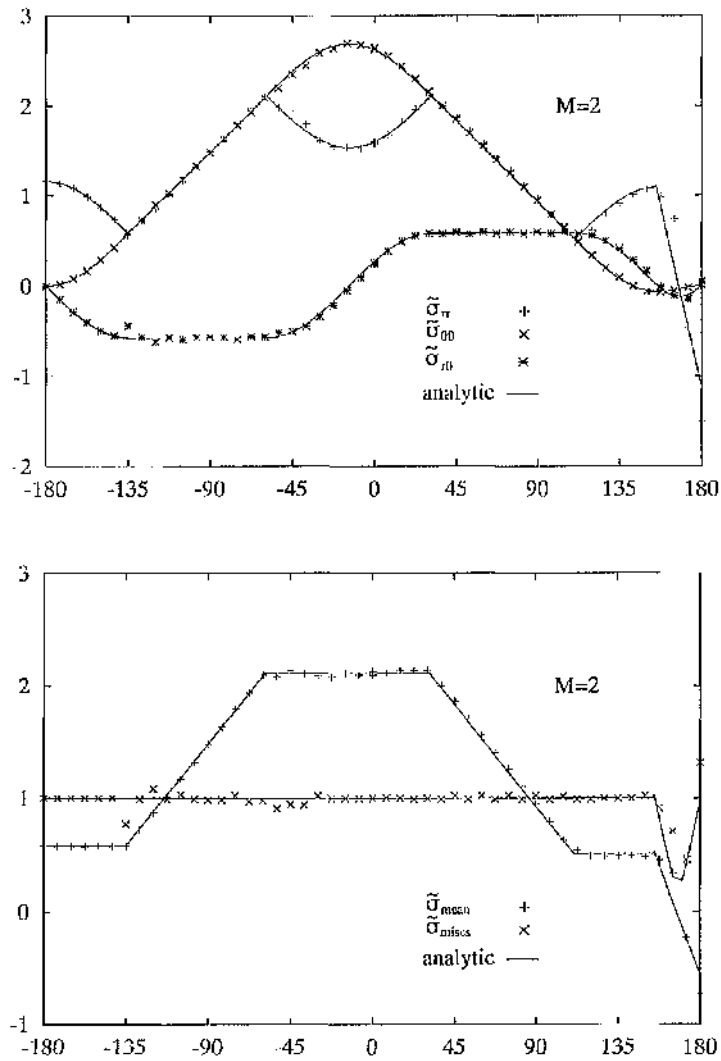
Fig 7.9: Asymptotic stresses for yield strength ratio, $M = 2$.
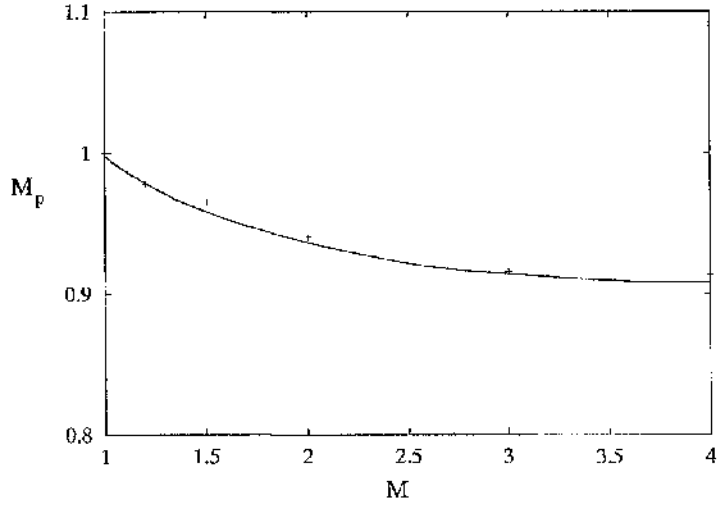
Fig 7.10: Plastic mixity, M_p, as a function of the mismatch, M.
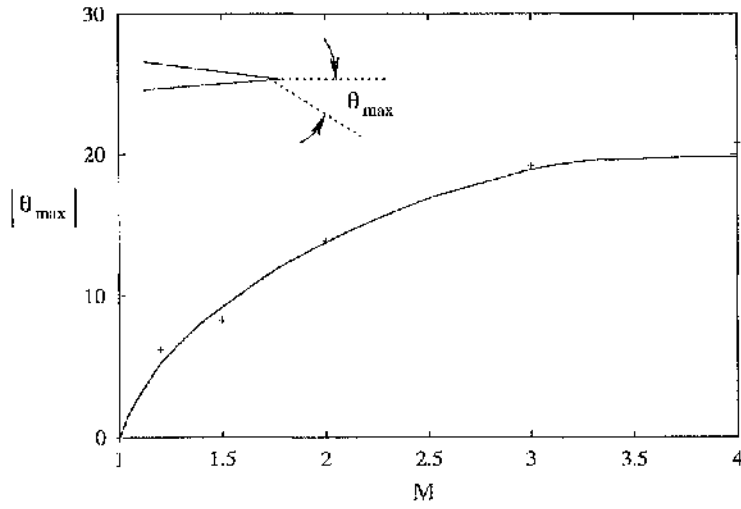
Fig 7.11: Direction of plane of maximum hoop stress as a function of the yield strength mismatch.
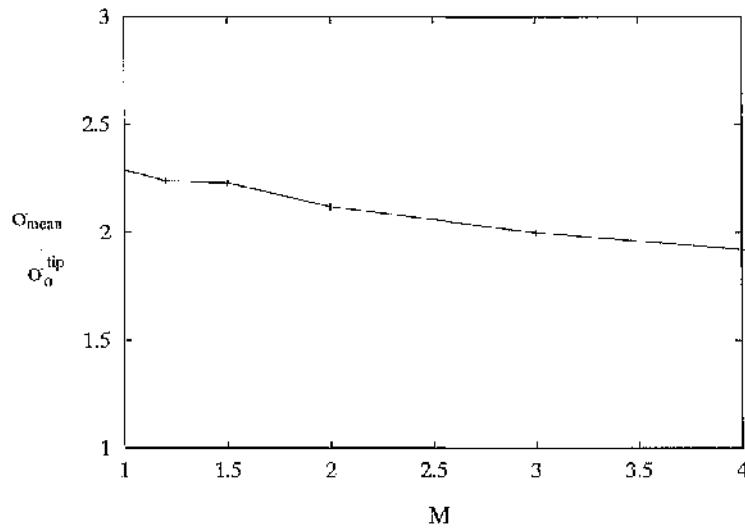
Fig 7.12: The mean stress in the plane ahead of crack tip as a function of the yield strength mismatch.
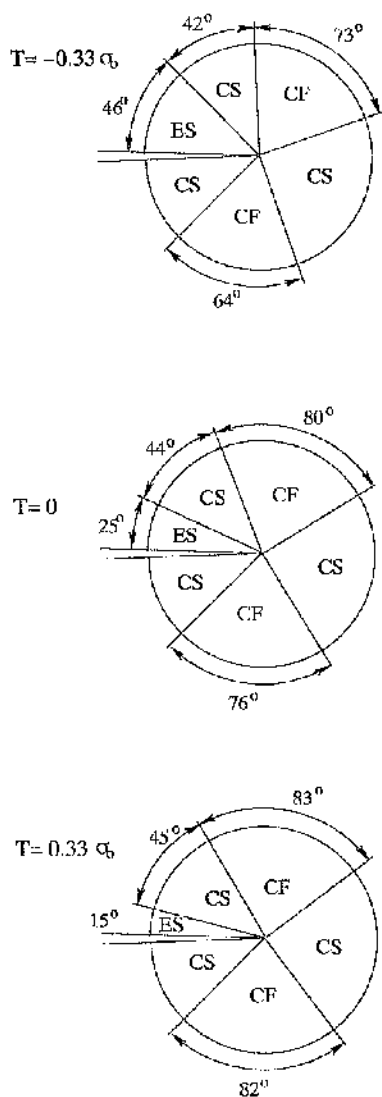
Fig 7.13: Effect of T-stress on slip line field, for yield strength ratio, $M = 2$.
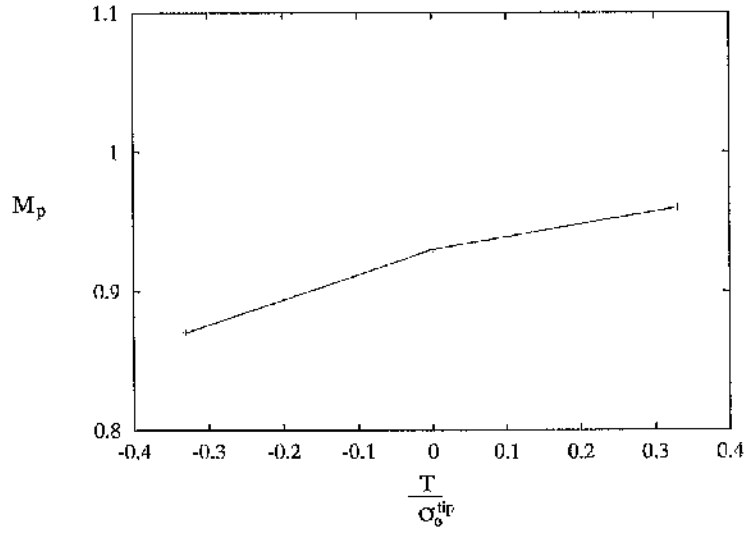
Fig 7.14: Plastic mixity as a function of the second order term, T-stress.
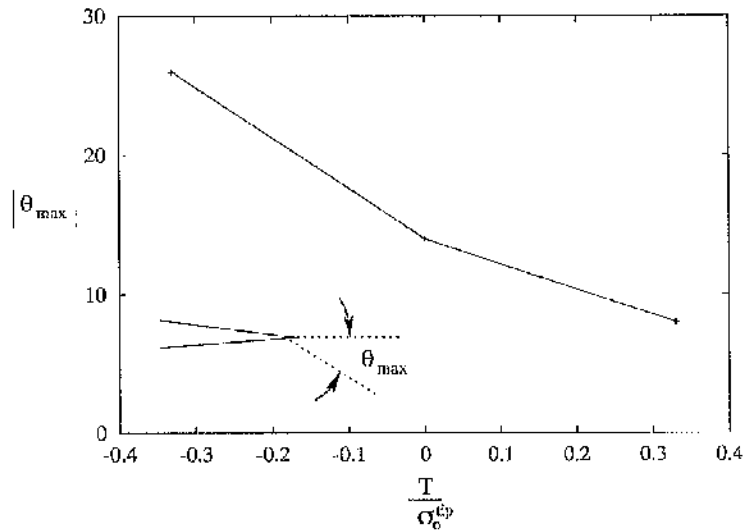
Fig 7.15: Direction of plane of maximum hoop stress as a function of the second order term for mismatch, $M - 2$.
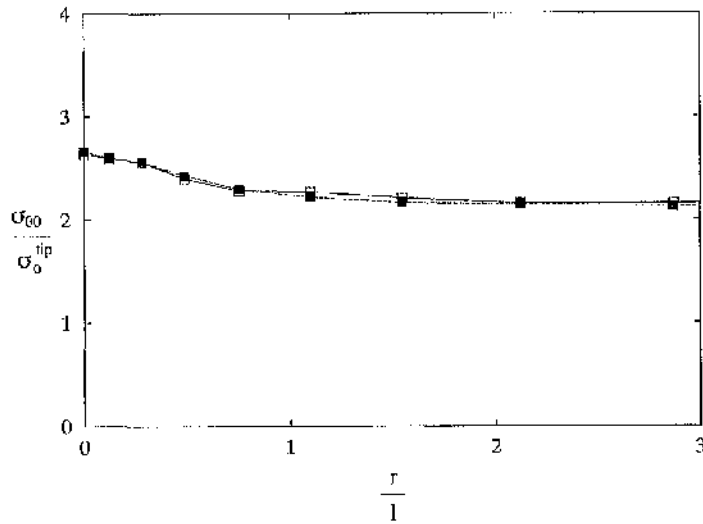
Fig 7.16: Hoop stress in the plane ahead of crack tip, solid symbols represent the stresses for $\frac{1}{2l}\left(\frac{K}{\sigma_o}\right)^2 = 88$ while the open symbols represent stresses for $\frac{1}{2l}\left(\frac{K}{\sigma_o}\right)^2 = 362$. The graded zone width was held constant.
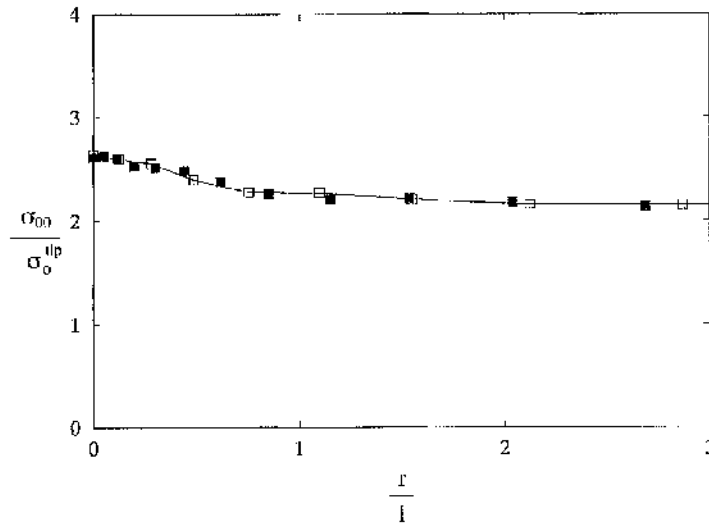

Fig 7.17: Hoop stress in the plane ahead of crack tip, solid symbols represent the stresses for $\frac{1}{2l}\left(\frac{K}{\sigma_o}\right)^2 = 145$ while the open symbols represent stresses for $\frac{1}{2l}\left(\frac{K}{\sigma_o}\right)^2 = 362$. The applied K was held constant.
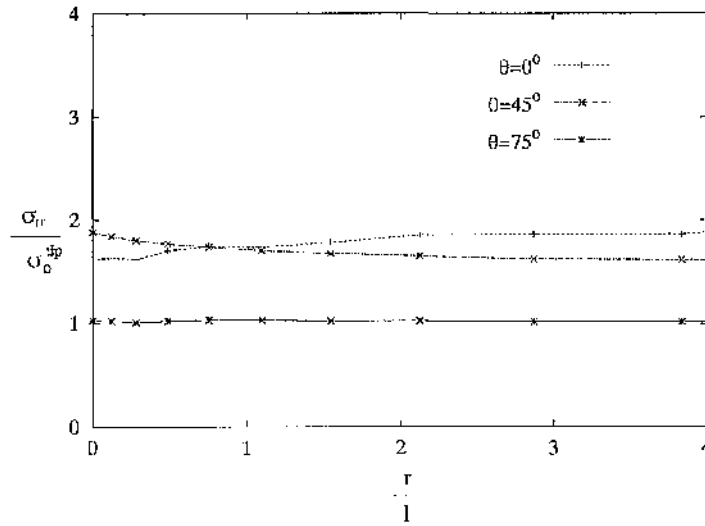
Fig 7.18: Radial stress at different angles as a function of the radial distance for plastic strength mismatch, $M = 2$, for $\frac{1}{2l} \left(\frac{K}{\sigma_o} \right)^2 - 362$.
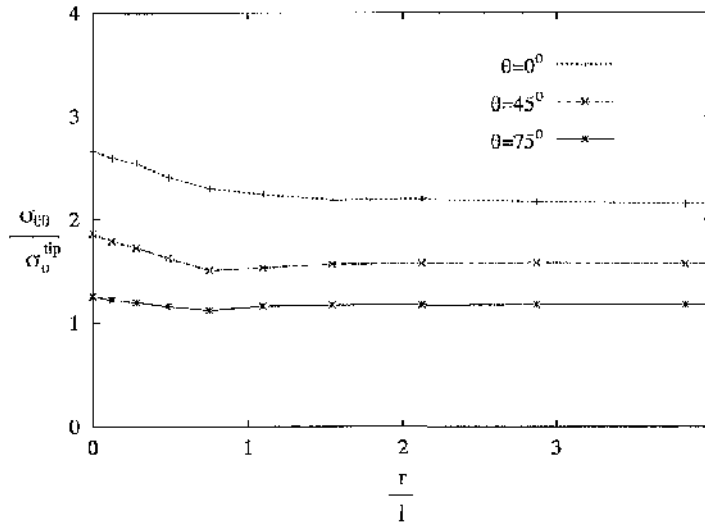

Fig 7.19: Hoop stress at different angles as a function of the radial distance for plastic strength mismatch, $M = 2$, for $\frac{1}{2l} \left(\frac{K}{\sigma_o} \right)^2 = 362$.
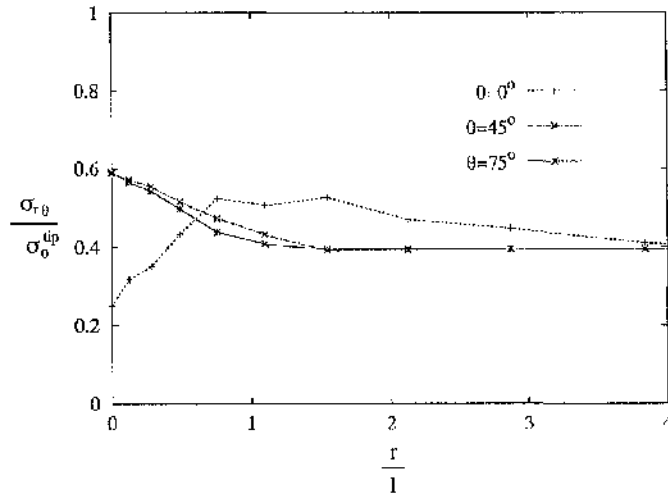
Fig 7.20: Shear stress at different angles as a function of the radial distance for plastic strength mismatch, $M = 2$, for $\frac{1}{2l}\left(\frac{K}{\sigma_o}\right)^2 = 362$.
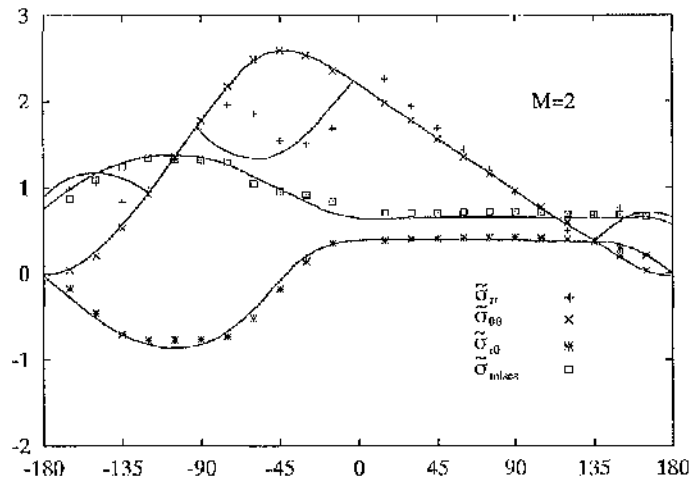

Fig 7.21: Stresses normalised with the yield stress at the crack tip, σ_o^{tip}, at the boundary of the graded zone, $M = 2$, compared to the asymptotic crack tip stresses for a corresponding interface crack shown as solid lines.
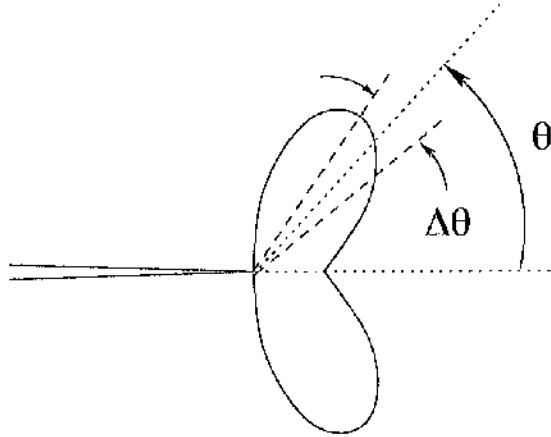
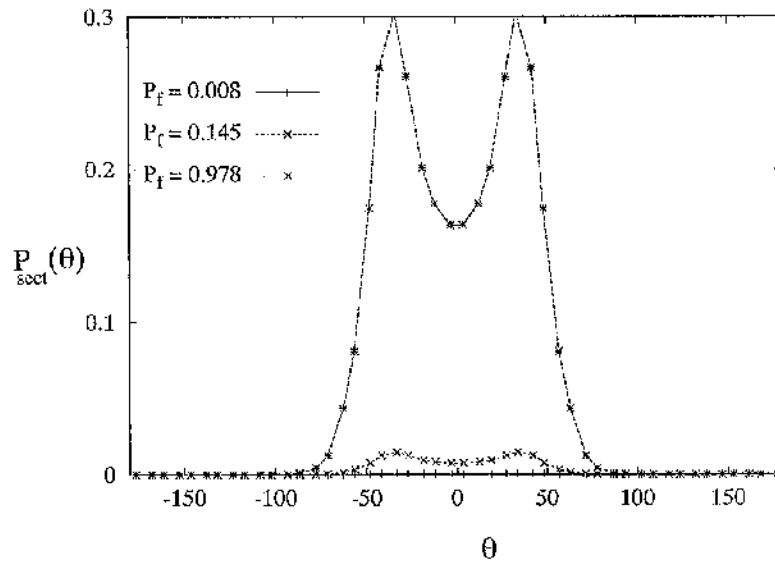Fig 7.22: Sector centred at an angle θ and with an angular span of $\Delta\theta$.

Fig 7.23: Probability of failure of a sector of angular span 7.5 degrees and is in the direction θ for three different load levels corresponding to the total probability of failure, P_f.
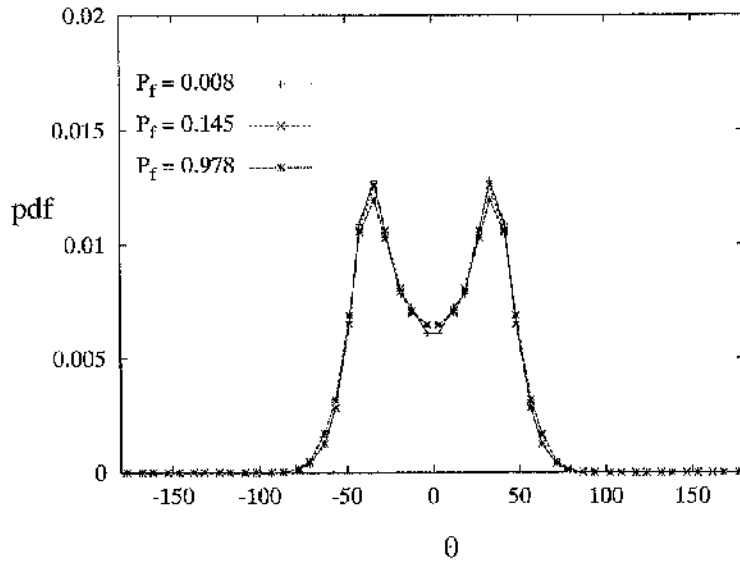
Fig 7.24: Probability density function as a function of the angle, θ, for three different load levels corresponding to the total probability of failure, P_f.

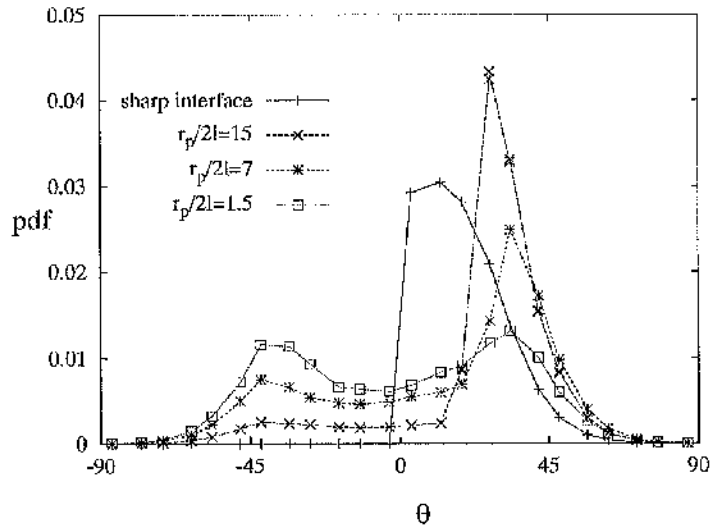Fig 7.25: The probability density function for a crack in zone of graded yield strength, $M = 2$, but uniform toughness.
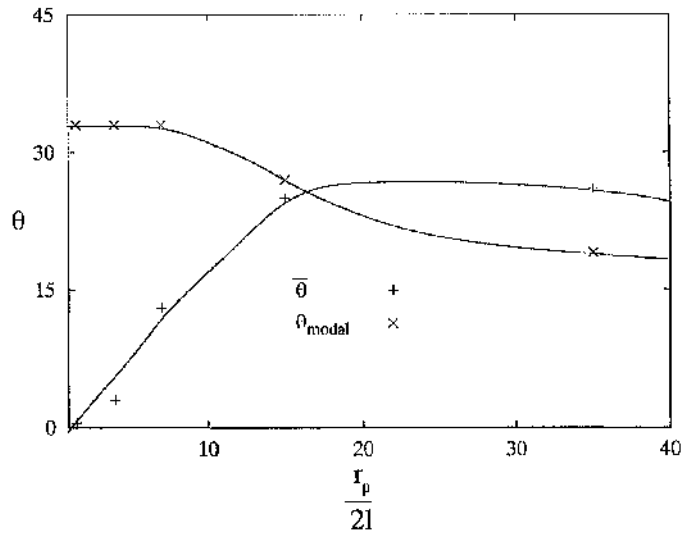
Fig 7.26: The average angle of extension, $\overline{\theta}$, and the modal value, θ_{modal}, as a function of the loading parameter, $\frac{r_p}{2l}$.
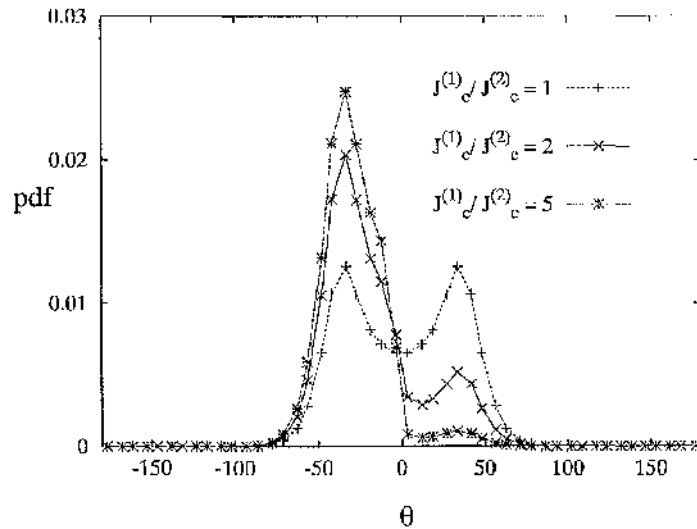
Fig 7.27: The probability density function for an interfacial crack between solids of similar yield strength but mismatched toughness.
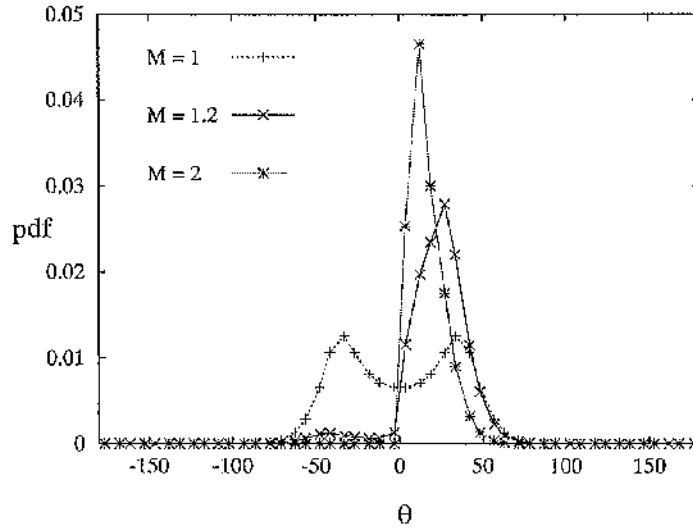
Fig 7.28: The probability density function for an interfacial crack between plastically mismatched solids which have similar toughness.
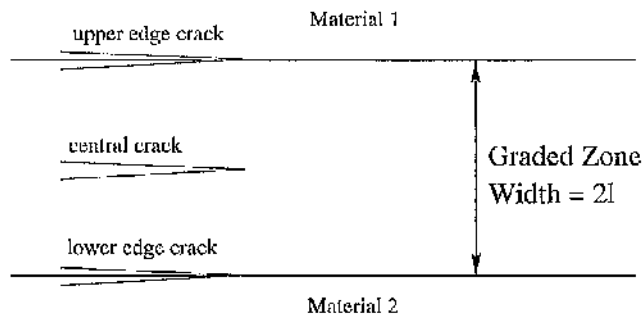
Fig 7.29: Different locations of cracks in a zone of graded yield strength.
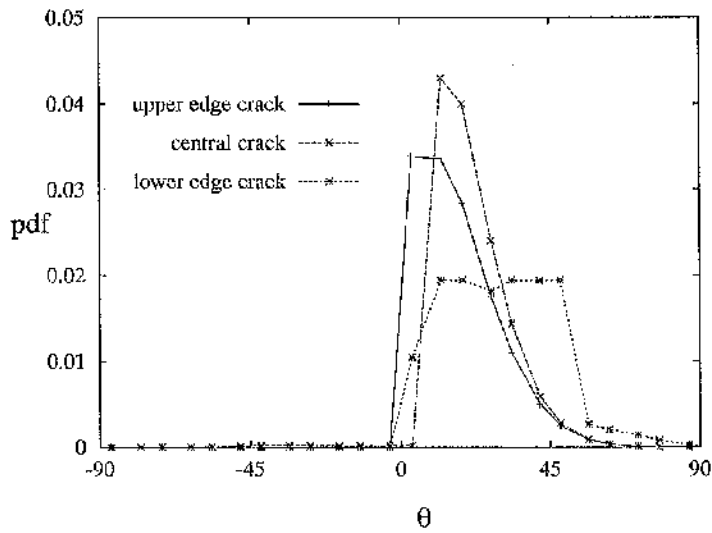
Fig 7.30: The probability density function from cracks at different locations in a zone of graded yield strength, $M = 2$, but uniform toughness.
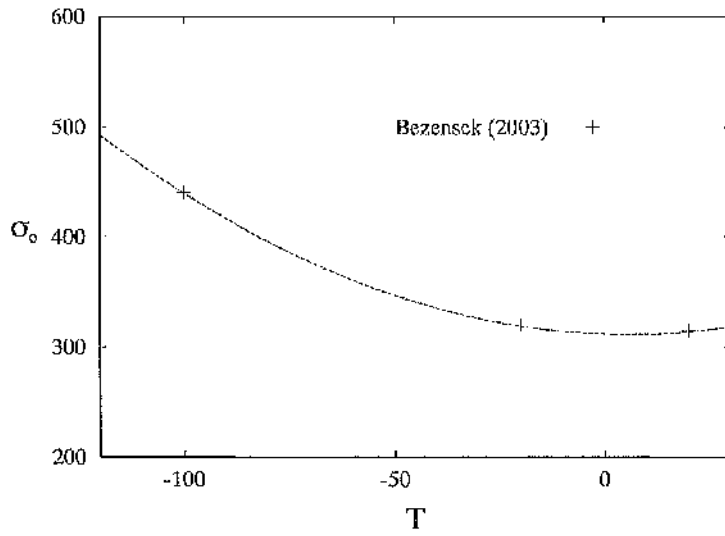
Fig 7.31: Yield-strength (MPa)-temperature($^\circ$C) relation for En32 grade steel.
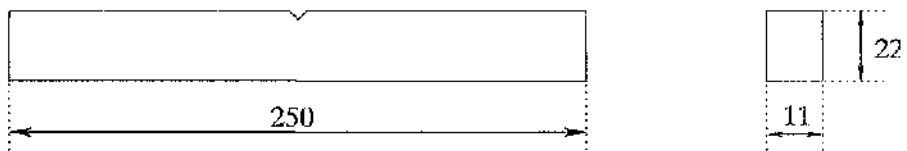
Fig 7.32: Dimensions (in mm) of the fracture test specimen.
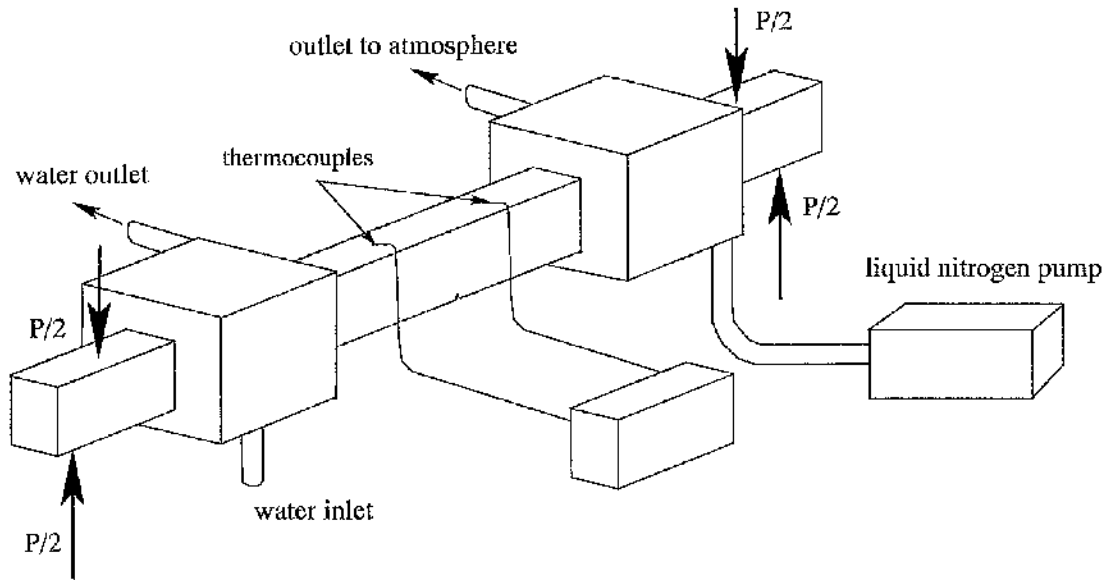
Fig 7.33: Schematic diagram of the experimental setup.
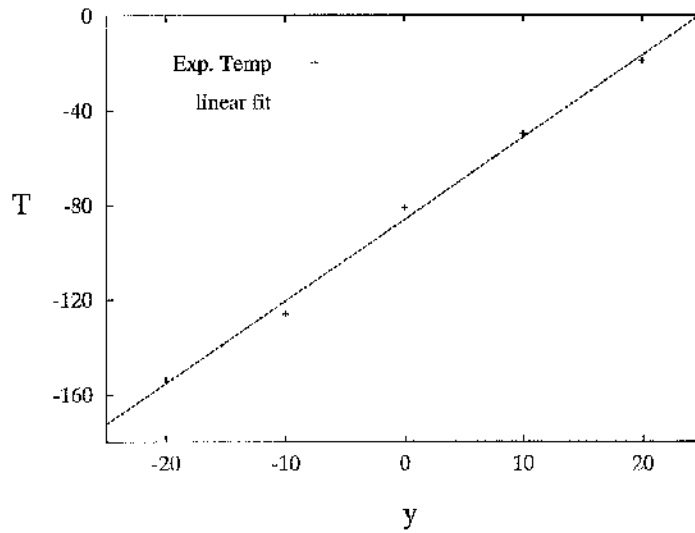
Fig 7.34: Temperature (in $^\circ$C) as a function of the distance (mm) in y direction.
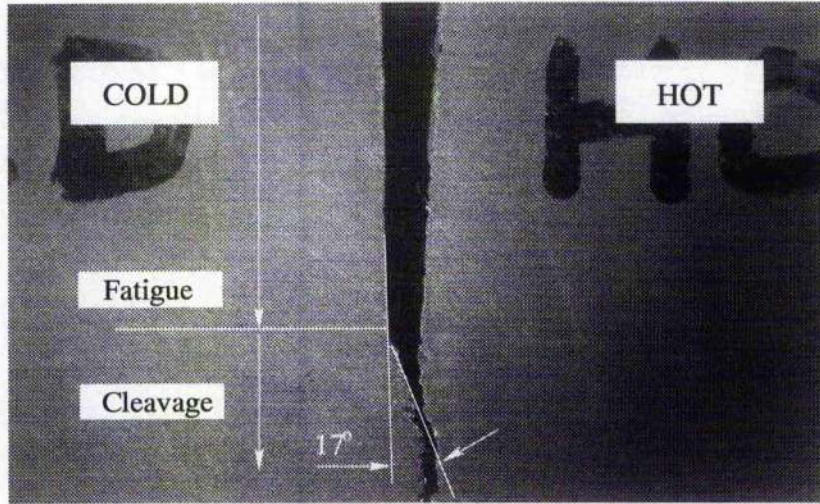
Fig 7.35: Post-fracture digital photograph of cleavage initiation angle.
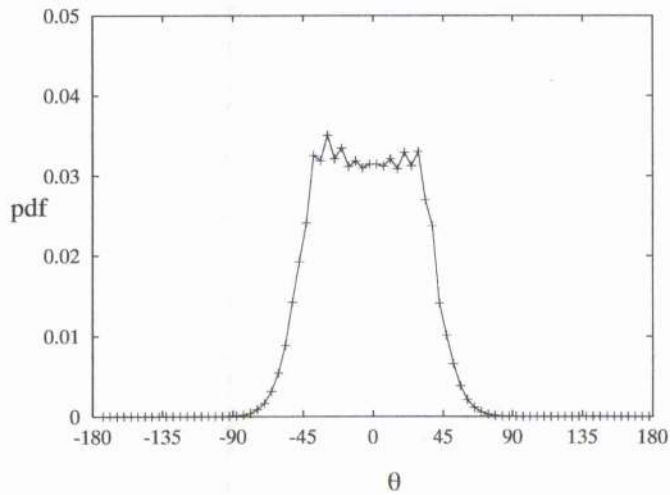
Fig 7.36: The probability density function when toughness (180 N/mm) was uniform but the yield strength varied spatially.
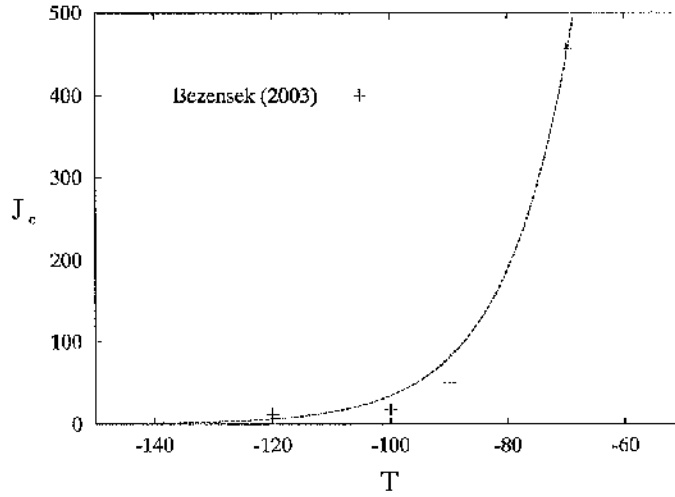
Fig 7.37: Toughness(N/mm) - temperature($^\circ$C) relation for En32 grade steel.
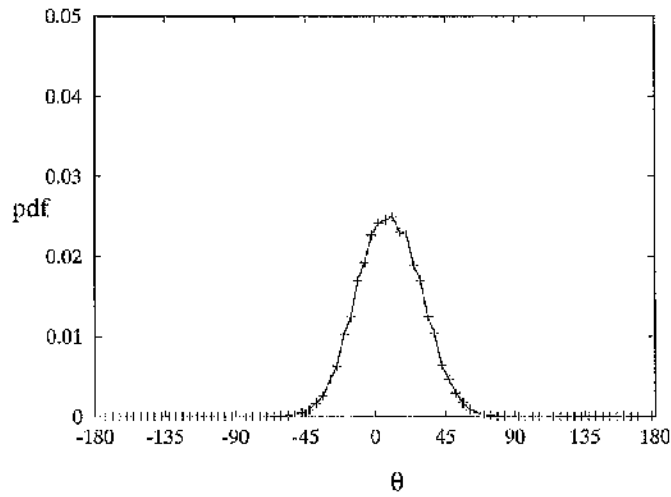
Fig 7.38: The probability density function when yield strength was uniform while toughness was graded.
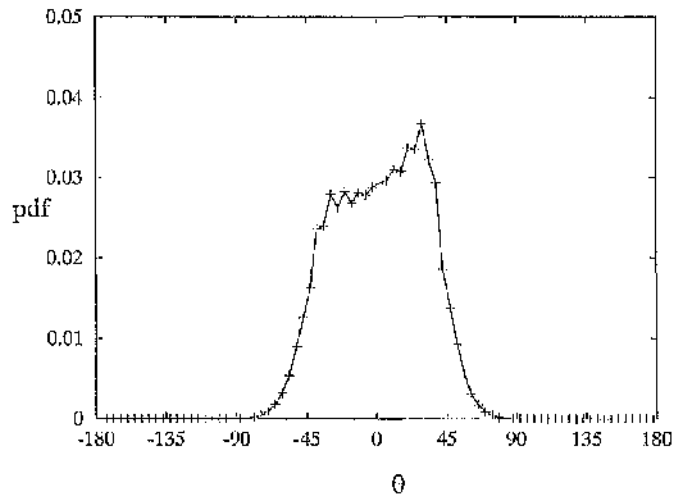
Fig 7.39: The probability density function when both yield strength and toughness were graded.

Conclusions

In the study of the constraint effects of a crack normal to the interface between mismatched solids, the first two terms in the asymptotic elastic crack tip fields of technologically significant bi-material systems have been determined. For the leading term, the strength of the singularity and the angular functions depend on mismatch. The second order term is distance independent for all elastic mismatches although the angular functions depend on mismatch. The amplitudes of both the terms depend on loading and geometry. In general the second order term in the stress field in material ahead of crack is biaxial. The biaxiality depends on elastic mismatch and vanishes for elastically matched solids.

The analytic and numerical solutions of the plane strain asymptotic fields for a crack between elastically and plastically mismatched solids have then been developed. The discussion was based on two limiting cases: when the crack was located in perfectly-plastic material while the material ahead was fully elastic and a case when the crack was located in an elastic solid while the solid ahead deformed plastically.

When plasticity was limited to the material behind the crack, the elastic material ahead of the tip exhibited a logarithmic singularity. The logarithmic constant r_o is a loading parameter with the dimensions of distance that can conveniently be identified with $(K/\sigma_o)^{\frac{1}{1-\lambda}}$ or the crack tip opening displacement. The crack tip field in the material behind ($\pi/2 \leq \theta \leq \pi$ and $-\pi \leq \theta \leq -\pi/2$) is composed of elastic and plastic sectors that have finite crack tip stresses, full plasticity being achieved for tensile T-stresses when the characterising parameter of the field, hoop stress at the interface, reaches its peak value, $k(1 + \pi/2)$.

When the crack was located in an elastic solid, the structure of the mode I fields was similar and in the leading sectors only differed through a hydrostatic term. Mean stress or the

constraint ahead of the crack tip, identified to be the characterising parameter of the family of mode I fields, increases with increasing T-stress and decreasing elastic mismatch. Thus, for geometries with high elastic mismatch and negative T-stress the resistance for crack extension is expected to be higher. As the mode mixity is increased the plane of maximum stress rotates towards the interface. The mode II field parameter, θ^+, increases with increasing elastic mismatch, marginally increasing the stresses at the interface. The constraint effects associated with elastic mismatch and T-stress established in the limit of non-hardening are reproduced for moderately strain hardening material response. The constraint loss associated with compressive T-stress and higher elastic mismatch increases the resistance to crack extension in the opening mode.

Loss of constraint increases the resistance to both interface penetration and delamination. However, if interface failure is dominated by normal stresses across the interface, loss of constraint favours interface penetration, whereas for interfaces which fail due to shear stress, constraint loss favours delamination.

A crack within a graded interfacial zone between two elastically similar but plastically dissimilar elastic-perfectly plastic solids has been studied. Asymptotic stress fields under contained yielding were constructed for remote mode I loading. Due to the non-uniform yield stress the plastic zone shape is asymmetric and the extent of asymmetry depends upon the loading parameter $r_p/2l$. For low deformation levels the field is near mode I, with increasing load the asymmetry in plasticity increases and eventually saturates. A result of the asymmetry is that even under remote mode I loading the crack tip field is mixed-mode and the maximum hoop stress direction in the asymptotic field is inclined towards the material of higher yield strength. The constraint parameter, the mean stress, in the plane of maximum hoop stress decreases with increasing angle of inclination of the plane of maximum hoop stress. For crack extension on the plane of maximum hoop stress of the asymptotic field, increasing plastic mismatch and compressive T-stresses causes the direction of crack

propagation to be inclined more towards the material of higher yield strength and the toughness to be higher.

Using a statistical approach based on a weakest link model the effect of a gradient in yield strength and toughness on failure probability and crack extension direction was examined. In the statistical model the deformation level as measured by $r_p/2l$ plays an important role. At low $r_p/2l$ a crack in a graded zone is tougher than a crack in a homogeneous material of crack tip properties. However, for larger $r_p/2l$ the graded interface is less tough. The direction of crack propagation depends on both the toughness and yield strength mismatch. Yield strength mismatch favours crack extension towards the softer material whereas toughness mismatch drives the crack towards the less tough material. Thus, unlike in homogeneous solids the prediction of the maximum hoop stress direction in the asymptotic stress field and the average angle based on probabilistic arguments may give very different crack extension directions. Cleavage failure in En32 grade steel when subjected to a non-uniform temperature field confirms the predominant volume effect as the crack consistently initiates towards the hotter side (the side of lower yield strength).

Bibliography

Abboud, J. H., West, D. R. F., Rawlings, R. D., 1994. Functionally gradient layers of Ti-Al based alloys produced by laser alloying and cladding. Material Science and Technology 10(5), pp. 414-419.

ABAQUS Manual. Hibbit, Karlsson and Sorenson Inc. Providence Rhode Island.

Standard method for plane strain fracture toughness testing of metallic materials. Vol 03 01. American Society for Testing and Materials. Philadelphia. pp. 487-511.

Becker, T. L., Canon, R. M., Ritchie, R. O., 2002. Statistical fracture modelling: crack path and fracture criteria with application to homogeneous and functionally graded materials. Engineering Fracture Mechanics 69, 1521-1555.

Beremin, F. M., 1983. A local criterion for cleavage fracture of a nuclear pressure vessel steel. Metallurgical Transactions A 14A, pp. 2277-2287.

Betegón, C., Hancock, J. W., 1991. A two parameter characterisation of elastic-plastic crack tip fields. Journal of Applied Mechanics 58, pp. 104-110.

Bezensek, B., 2003. Elastic-plastic crack problems in the ductile brittle transition. PhD Thesis in preparation. University of Glasgow.

Bilby, B. A., Cottrell, Cardew, G. E., Goldthorpe, M. R., Howard, I. C., 1986. A finite element investigation of the effect of specimen geometry on the fields of stress and strain at

the tips of stationary cracks. In 'Size Effects in Fracture' Institute of Mechanical Engineers, London, UK. pp. 37-46.

Bowen, P., Druce, S. G., Knott, J. F., 1987. Micromechanical Modelling of Fracture Toughness. Acta Metallurgica 35 (7), pp. 1735-1746.

Burstow, M. C., Howard, I. C., Ainsworth, R. A., 1998. The influence of constraint on crack tip stress fields in strength mismatched welded joints. Journal of the Mechanics and Physics of Solids 46(5), pp. 845-872.

Chao, Y. J., Sutton, M. A., Wu R., 1993. Determination of the asymptotic crack tip fields for a crack perpendicular to an interface between elastic-plastic materials. Acta Mechanica 100 (1-2), pp. 13-36.

Choules, B. D., Kokini, K., 1996. Architecture of functionally graded ceramic coatings against surface fracture. Journal of Engineering Materials and Technology-Transactions of the ASME 118(4), pp. 522-528.

Comninou, M., 1977. The interface crack. Journal of Applied Mechanics 44(4), pp. 631-636.

Comninou, M., 1978. The interface crack in shear field. Journal of Applied Mechanics 45(2), pp. 287-290.

Cook, T. S. and Erdogan, F., 1972. Stresses in bonded materials with a crack perpendicular to the interface. International Journal of Engineering Sciences 10, pp. 677-697.

Cotterell, B., 1965. On brittle fracture paths. International Jornal of Fracture 1, pp. 96-103.

Cotterell, B., Rice, J. R., 1980. Slightly curved or kinked cracks. International Journal of Fracture 16, pp. 155-169.

Delale, F., Erdogan, F., 1983. The crack problem for a non-homogeneous plane. Journal of Applied Mechanics 50(3), pp. 609-614.

Du, Z. Z., Hancock, J. W., 1991. The effect of non-singular stresses on crack tip constraint. Journal of the Mechanics and Physics of Solids 39, pp. 555-567

Dundurs, J., 1969. Edge-bonded dissimilar orthogonal elastic wedges. Journal of Applied Mechanics 36, pp. 650-652.

England, A. H., 1965. A crack between dissimilar media. Journal of Applied Mechanics 45(2), pp. 287-290.

Erdogan, F., Sih, G. C., 1963. On the crack extension in plates under plane loading and transverse shear. Journal of Basic Engineering 85, pp. 519-527.

Evans, A. G., Marshall, D. B., 1989. The mechanical behaviour of ceramic matrix composites. Acta Metallurgica 37 (10), pp. 2567-2583.

Freudenthal, A. M., 1968. Statistical approach to brittle fracture. In: H. Liebowitz, Editor. Fracture: an advanced treatise, Vol. ". Academic Press, New York, pp. 591-619.

Griffith, A. A., 1920. The phenomena of rupture and flow in solids. Philosophical Transactions, Series A 221, pp. 163-198.

Gu, Pei, Asasro, R. J., 1997. Crack deflection in functionally graded materials. International Journal of Solids and Structures 43 (24) pp. 3085-3098.

Hancock, J. W., Reuter, W. A., Parks, D. M., 1993. Constraint and toughness parametrized by T. ASTM Symposium on Constraint Effects in Fracture, American Society for Testing and Materials, Philadelphia, pp. 21-40.

Harlin, G., Willis, J. R., 1988. The influence of crack size on the ductile-brittle transition. Proceedings of Royal Society, London, A415, pp. 197-226.

He, M. Y., Hutchinson, J. H., 1989. Crack deflection at an interface between dissimilar elastic materials. International Journal of Solids and Structures 25 (9), pp. 1053-1067.

He, M. Y., McMeeking, R. M., Zhang, N. T., 1992. Small scale yielding at a crack normal to the interface between an elastic and a yielding material. Thin Films: Stresses and Mechanical Properties, Material Research Society 239, pp. 585-590.

He, M. Y., Heredia, F. E., Wissuchek, D. J., Shaw, M. C., Evans, A. G., 1993. The mechanics of crack growth in layered materials. Acta Metallurgica et Materialia 41 (4), pp. 1223-1228.

Hill, R., 1950. *The mathematical theory of plasticity*. Oxford University Press, Oxford.

Hutchinson, J. H., 1968a. Singular behaviour at the end of a tensile crack in a hardening material. Journal of the Mechanics and Physics of Solids 16, pp. 13-31.

Hutchinson, J. H., 1968b. Plastic stress and strain fields at a crack tip. Journal of the Mechanics and Physics of Solids 16, pp. 337-347.

Inglis, C. E., 1913. Stresses in a plate due to the presence of cracks and sharp corners. Transactions of the Institute of Naval Architects 55, pp. 219-241.

Irwin, G. R., 1957. Encyclopedia of Physics, S. Flugge (ed.) vol. springer, pp. 551-590.

Irwin, G. R., Kies, J. A. and Smith, H. C., 1958. Proceedings of ASTM, 5(8), pp. 640.

Irwin, G. R., 1961. Plastic zone near a crack and fracture toughness. Sagamore Research Conference Proceedings, 4.

Kim, Y. J., Lin, G. Y., Cornec, A., Schwalbe, K. H., 1997. Effect of elastic and plastic mismatching of interfacial crack-tip fields in contained yielding. *Mis-Matching of Interfaces and Welds*, edited by K. H. Schwalbe and M. Kovak, GKSS Research Center Publications, Geesthacht, FRG, pp135-148.

Kokini, K., Takeuchi, Y., 1994. Transient thermal fracture of an interface crack in the presence of a surface crack. Journal of Thermal Stresses 17 (1), pp. 63-74.

Kumar, V., German, M. D., Shih, C. F., An engineering approach for elastic-plastic fracture analysis. General Electric Company EPRI Research Project 1237-1, NP-1931.

Larsson, S. G., Carlsson, A. J., 1973. Influence of non-singular stress terms and specimen geometry on small scale yielding at crack tips in elastic-plastic material. International Journal of Fracture 19, pp. 263-278.

Leevers, P. S., Radon, J. C., 1983. In herent stress biaxiality in various fracture specimen geometries. International Journal of Fracture 19, pp. 942-955.

Lei, Y., O'Dowd, N. P., Busso, E. P., Webster, G. A., 1998. Weibull stress solutions for 2-D cracks in elastic and elastic-plastic materials. International Journal of Fracture 89, pp. 245-268.

Li., J., 1998. Elastic-plastic interfacial crack problems. PhD Thesis at University of Glasgow, U.K.

Li, J., Hancock, J. W., 1999. Mode I and mixed fields with incomplete crack tip plasticity. International Journal of Solids and Structures 36, pp. 711-725.

Lo, K. K., 1978. Analysis of branched cracks. Journal of Applied Mechanics 45, pp. 797-802.

Maccagno, T. M., Knott, J. F., 1991. The low temperature brittle fracture behaviour of steel in mixed modes I and mode II. Engineering Fracture Mechanics, 38 (2/3), pp. 111-128.

The MathWorks, Inc. Version 5.3.0.10183 (R11) 1999.

McClintock, F. A., 1971. Plasticity aspects of fracture. Fracture: an Advanced Treatise (ed. H. Liebowitz) 3, pp. 47. London: Academic Press.

McMeeking, R. A., Parks, D. M., 1979. On criteria for J-dominance of crack tip fields in large scale yielding. In Landes, J. (ed.). Elastic-Plastic Fracture, ASTM STP 668. American Society of Testing and Materials, Philadelphia, pp. 175-194.

Murakami, Y., 1987. *Stress Intensity Factor Handbook*, Vol. I. Pergammon Press, New York.

Nemat-Nasser, S., Obata, M., 1984. O stress field near a stationary crack tip. Mechanics of Materials 3, pp. 235-243.

O'Dowd, N. P., Shih, C. F., 1991. Family of crack tip fields characterised by a triaxiality parameter: Part I-Structure of fields. Journal of the Mechanics and Physics of Solids 39, pp. 939-963.

O'Dowd, N. P., Lei, Y., Buso, E. P., 2000. Prediction of cleavage failure probabilities using the weibull stress. Engineering Fracture Mechanics 67(2), pp.87-100.

Palaniswamy, K., Knauss, W. G., 1978. On the problem of crack extension in brittle solids under general loading. Mechanics Today 4, pp. 87-148.

Rashid M. M., Tvergaard, V., 2003. On the path of a crack near a graded interfaceunder large scale yielding. International Jornal of Solids and Structures 40(11), pp. 2819-2831.

Rice, J. R., Sih, G. C., 1965. Plane problems of cracks in dissimilar media. Journal of Applied Mechanics 32, pp. 418-423.

Rice, J. R., 1968. A path independent integral and the approximate analysis of strain concentration by notches and cracks. Journal of Applied Mechanics 35, pp. 379-386.

Rice, J. R., Rosengren, G. F., 1968. Plane strain deformation near a crack tip in a power law hardening material. Journal of the Mechanics and Physics of Solids 16, pp. 1-12.

Rice, J. R., Tracey, D. M., 1973. Computation fracture mechanics. In: Fenves, S. J. et al. (Eds), Numerical and computational methods in structural mechanics, Academic Press, New York, pp. 585-623.

Rice, J. R., 1974. Limitations to the small scale yielding approximation for crack tip plasticity. Journal of the Mechanic and Physics of Solids 22, pp. 17-26.

Rice, J. R., 1982. Elastic-plastic crack growth. Mechanics of Solids- The Rodney Hill 60th Anniversary Volume, Pergamon Press, Oxford, pp. 539-562.

Rice, J. R., 1988. Elastic fracture mechanics concepts of interfacial cracks. Journal of Applied Mechanics 55, pp. 418-423.

Ritchie, R. O., Knott, J. F., Rice, J. R., 1973. On the relationship between critical tensile stress and fracture toughness in mild steel. Journal of the Mechanics and Physics of Solids 21, pp. 395-410.

Rooke, D. P., Cartwright, D. J., 1976. *Compendium of stress intensity factors*. Her Majesty's Stationary Office, London.

Rousseau, C. E., Tippur, H. V., 2001. Compositionally graded materials with cracks normal to the elastic gradient. Acta Materialia 48, pp. 4021-4033.

Sham, T-L., 1991. The determination of the elastic T-term using higher order weight functions. International Journal of Fracture 48, pp. 81-102.

Sham, T-L., Li, J., Hancock, J. W., 1999. A family of plane strain crack tip stress fields for interface cracks in strength mismatched elastic-perfectly plastic solids. Journal of the Mechanics and Physics of Solids 47, pp. 1963-2010.

Sherry, A. H., France, C. C., Goldthorpe, M. R., 1995. Compendium of T-stress solutions for 2 and 3-dimensional cracked geometries. Fatigue and Fracture of Engineering Matrials and Structures 18 (1), pp. 141-155.

Shih, C. F., 1981. Relationship between the J-integral and crack opening displacement for stationary and extending cracks. Journal of the Mechanics and Physics of Solids 29, pp. 305-326.

Shih, C. F., 1983. Tables of Hutchinson-Rice-Rosengren singular field quantities. Technical Report, Material Research Laboratory, Brown University. Providence, Rhode Island.

Shih, C. F., German, M. D., 1981. Requirements for a oner parameter characterization of crack tip fields by HRR singularity. International Journal of Fracture 17(1), pp. 27-43.

Shih, C. F., Asaro, R. J., 1988. Elastic-plastic analysis of cracks on bimaterial interfaces: part1-small scale yielding. Journal of Applied Mechanics 56, 763-779.

Shih, C. F., 1991. Cracks on bimaterial interfaces: elasticity and plasticity aspects. Materials Cience and Engineering A143, pp. 77-90.

Stahle, P., Shih, C. F., 1992. Cracking in thin films and substrates. Thin Films: Stresses and Mechanical Properties, Material Research Society 239, pp. 567-572.

Sugimura, Y., Lim, P. G., Shih, C. F., Suresh, S., 1995. Fracture normal to a bimaterial interface: effects of plasticity on crcak-tip shielding and amplification. Acta Metallurgica et Materialia 43 (3), pp. 1157-1169.

Sumpter, J., 1993. An experimental investigation of the T-stress approach. In Hackett, E. M., Schwalbe, K. H. and Dodds, R. H. (ed.). Constraint effect in fracture, ASTM STP 1171. American Society for Testing and Materials, Philadelphia.

Sumpter, J., Hancock, J. W., 1994. Status review of the J plus T stress fracture analysis method. In 10th fracture conference on fracture, pp. 617-626.

Suresh, S., Shih, C. F., 1991. Combined mode I-mode II and mode III fracture of brittle materials. Scripta Metallurgica et Materialia 25, pp. 991-996.

Timoshenko, S. P., Goodier, J. N., 1970. *Theory of Elasticity*, 3rd edn. McGraw-Hill, New York.

Tsai, SW., A survey of macroscopic failure criteria for composite materials. Journal of Reinforced Plastics and Composites 3 (1), pp. 40-62.

Wang, Y-Y., Parks, D. M., 1992. Evaluation of the T-stress in surface -cracked plates using line-spring method. International Journal of Fracture 59, pp. 25-44.

Wells, A. A., 1961. Unstable crack propagation in metals: cleavage and fast fracture. Proceedings of the Crack Propagation Symposium 1, paper 84, Cranfield UK.

Wetherhold, R. C., Seelman, S., Wang, J. Z., 1996. The use of functionally graded materials to eliminate or control thermal deformation. Composites Science and Technology 56(9), pp. 1099-1104.

Williams, M. L., 1957. On the stress distribution at the base of a stationary crack. Journal of Applied Mechanics 24, pp. 109-114.

Williams, M. L., 1959, The stresses around a fault or crack in dissimilar media, *Bulletin of Seismological Society of America*, vol. 49, 1959, pp. 199-204.

Zak, A. R., Williams, M. L., 1963. Crack point stress singularities at a bi-material interface. Journal of Applied Mechanics, 30, pp. 142-143.

Zhu, X. K., Chao, Y. J., 2001. Constraint effects on crack-tip fields in elastic-perfectly plastic materials. Journal of the Mechanics and Physics of Solids, 49, pp. 363-399.

Zywicz, Z. and Parks, D. M., 1989. Elastic yield zone around an interfacial crack tip. Journal of Applied Mechanics, 56, pp. 577-584.

Zywicz, Z. and Parks, D. M., 1992. Small-scale yielding interfacial crack-tip fields. Journal of the Mechanics and Physics of Solids, 40, pp. 511-536.